Indoor Positioning and Tracking based on the Received Signal Strength

Von der Fakultät für Ingenieurwissenschaften,
Abteilung Elektrotechnik und Informationstechnik
der Universität Duisburg-Essen

zur Erlangung des akademischen Grades

Doktor der Ingenieurwissenschaften (Dr.-Ing.)

genehmigte Dissertation

von

Laith Ihsan Khalil
aus
Bagdad, Irak

Gutachter: Prof. Dr.-Ing. Andreas Czylwik
Gutachter: Prof. Dr.-Ing. Steven X. Ding
Tag der mündlichen Prüfung: 15.05.2017

Acknowledgements

First of all and always I thank almighty 'Allah' for making me live these great moments. I could never finish this work without the faith I have in Him and depending on Him.

This dissertation represents a part of my research work that has been accomplished at the Chair of Communication Systems (NTS) in the Faculty of Engineering at the University of Duisburg-Essen in Germany.

I would like to express my deep gratitude to Prof. Dr.-Ing. Andreas Czylwik for his assistance and guidance in preparation of this dissertation. I can never thank him enough for helping me pursue my goals. I am also grateful to Prof. Dr.-Ing. Steven X. Ding for his interest in my work and for being co-reviewer of the dissertation.

I am also thankful to Prof. Dr.-Ing. Thomas Kaiser and Prof. Dr.-Ing. habil. István Erlich for their support in preparation of this work.

I would like to thank my colleagues at NTS for the constructive discussions and for the friendly atmosphere in the department.

A special thanks is given to my parents, brothers and sisters for their prayers and support throughout this work. I am deeply obliged to their encouragement and unconditional support. I also would like to express my deepest appreciation to the great efforts and support provided by my wife Abeer. I am grateful to my children (Mustafa and Diema) for always bringing joy and happiness and being a source of inspiration. Thank you for being a wonderful family.

Many thanks go to all my friends - especially those in Duisburg - with whom I spent very nice days.

Finally, I would like to thank the Iraqi ministry of Higher Education and Scientific Research (MOHESR), and the German Academic Exchange Service - Deutscher Akademischer Austauschdienst - (DAAD) for their financial support to carry out this work.

Duisburg, June 2017
Laith Ihsan Khalil

Übersicht

Die Received Signal Strength Indicator (RSSI) -basierte Innenraumlokaliserung und Verfolgung (L&T, englisch für Location and Tracking) ist eine vielversprechende und anspruchsvolle Technologie, die es mobilen Nutzerin bzw. Knoten ermöglicht, ihre Position zu ermitteln. Die vorliegende Arbeit konzentriert sich auf die Herausforderungen sowie die Verbesserung der Positioniergenauigkeit RSSI-basierter L&T. Der Autor schlägt zur Lösung des Problems 4 Ansätze vor.

Im ersten Ansatz entwickelt der Autor eine L&T-Lösung durch die Verwendung eines linearen Kalman Filters (KF). Die erforderlichen Gleichungen zur Beschreibung des Kalman Filters wurden problemorientiert hergeleitet und präsentiert. Im zweiten Ansatz schlägt der Autor eine L&T Lösung auf Basis des iterativen, erweiterten Kalman Filters (IEKF) vor, um die Genauigkeit des Extended Kalman Filter (EKF) zu verbessern. Im dritten Ansatz überwindet der Autor die besonderen Implementierungsherausforderungen des EKF durch eine L&T Lösung basierend auf der Grundlage der Scaled Unscented Transformation (SUT). Der Autor nennt das resultierende Filter Scaled Unscented Kalman Filter (SUKF). Im vierten Ansatz, überwindet der Autor die Schwierigkeiten bei der Umsetzung des EKF durch eine L&T Lösung, die auf der Umsetzung der Spherical Simplex Unscented Transformation (SSUT) auf das KF basiert. Der Autor nennt das resultierende Filter Spherical Simplex Unscented Kalman-Filter (SSUKF).

Die vorgeschlagenen Lösungen mit den verbessern die Möglichkeit, RSSI L&T in drahtlosen Ortungssystemen zu etabieren. Die Beiträge führten zu einer

signifikanten Verbesserung der Positionierungsgenauigkeit, Zuverlässigkeit und Einfachheit der Implementierung.

Abstract

Received Signal Strength Indicator (RSSI)-based indoor Location and Tracking (L&T) is a promising and challenging technology that enables mobile users/nodes to obtain their location information. This dissertation focuses on overcoming the challenges as well as improving the positioning accuracy for the RSSI-based L&T. In particular, the author considers 4 L&T solutions.

In the first, the author develops a L&T solution by designing the Kalman Filter (KF) to work linearly within the positioning framework. To elaborate on this implementation, the equations of the KF are presented in a consistent manner with the implementation. In the second, the author designs a L&T solution based on the Iterated Extended Kalman Filter (IEKF) to improve the accuracy compared with the popular Extended Kalman Filter (EKF). In the third, the author overcomes the particular implementation challenges of the EKF by designing a L&T solution based on the implementation of the Scaled Unscented Transformation (SUT) to the KF. The author calls the resulting filter Scaled Unscented Kalman Filter (SUKF). In the forth, the author overcomes the implementation difficulties of the EKF by designing a L&T solution based on the implementation of the Spherical Simplex Unscented Transformation (SSUT) to the KF. The author calls the resulting filter the Spherical Simplex Unscented Kalman Filter (SSUKF).

The proposed solutions with their corresponding achievements enhance the role of RSSI-based L&T in wireless positioning systems. The contributions led to significant improvement in the positioning accuracy, reliability and the ease of implementation.

List of Symbols

G_r	Receiver antenna gain
G_t	Transmitter antenna gain
$L(d)$	WLAN path loss model
$L_{\mathrm{FS}}(.)$	Free space path loss model
N	Number of anchor nodes
$W^{(c)}$	Weights of the scaled sigma points associated with the the covariances $\mathbf{P}_{\mathrm{y}}$ and $\mathbf{P}_{\mathrm{xy}}$
$W^{(m))}$	Weights of the scaled sigma points associated with the mean $\bar{\mathbf{y}}$
W	Weights of the Sigma points
α_{PL}	Path loss constant
α	Positive scaling parameter
β_{PL}	Path loss exponent
β	Weighting factor
$\boldsymbol{\chi}$	Sigma point
$\boldsymbol{\xi}$	Transformed sigma point
ϵ_{sync}	Synchronization error
η	Noise component
$\hat{d}$	Estimated distance
$\hat{x}$	The x coordinate of the estimated mobile position
$\hat{y}$	The y coordinate of the estimated mobile position

λ	Measurements noise
$\mathcal{N}(0,\sigma)$	Normal distribution with 0 mean and σ standard deviation
$\mathrm{E}[\Delta\rho]$	Estimation mean distance error
$\hat{\mathbf{p}}$	The estimated mobile position
$\hat{\mathbf{r}}_{k,q}$	Quantized measurement
$\mathbf{p}_i$	The position of the ith grid point
$\mathbf{p}$	The real mobile position
$\mathbf{u}$	Optional control vector
$\mathbf{RSSI}_{ij}$	The received signal strength measurements at the ith location from j anchor nodes
$\mathbf{A}$	State transition matrix
$\mathbf{B}$	Control vector
$\mathbf{E}[\cdot]$	Expected value
$\mathbf{H}(\mathbf{x})$	Models matrix
$\mathbf{I}$	Identity matrix
$\mathbf{K}_k$	The Kalman gain
$\mathbf{P}_k^-$	The *a priori* estimate error covariance matrix
$\mathbf{P}_k$	The *a posteriori* estimate error covariance matrix
$\mathbf{P}_x$	Covariance of the random variable $\mathbf{x}$ that undergoes non-linear function
$\mathbf{P}_\mathrm{y}$	Predicted covariance of the random variable $\mathbf{y}$
$\mathbf{Q}$	State noise covariance matrix
$\mathbf{R}$	Measurements noise covariance matrix
$\mathbf{S}$	Set of sigma points
$\mathbf{Z}$	Spherical simplex point
$\bar{\mathbf{x}}$	Mean of the random variable $\mathbf{x}$
$\bar{\mathbf{y}}$	Mean of the random variable $\mathbf{y}$
$\hat{\mathbf{x}}_k^-$	The *a priori* estimate of $\mathbf{x}_k$
$\mathbf{e}$	Estimation error
$\mathbf{f}(\cdot)$	System state transition function

$\mathbf{g}(\cdot)$	Non-linear function
$\mathbf{h}(\cdot)$	Measurements to state function
$\mathbf{p}_{\text{BS}}$	Anchor nodes location
$\mathbf{r}$	RSSI measurements vector
$\mathbf{v}_k$	Measurements noise
$\mathbf{w}$	System state noise
$\mathbf{x}$	System state
$\mathbf{y}$	Random variable
$\mathbf{z}$	System measurements
ρ	Distance error
σ	Standard deviation
$c(\mathbf{x})$	Cost function
d_{BP}	Breakpoint distance
d	The separation distance between the sender and the receiver
$h_i(\mathbf{x})$	The ith model that relates the position $\mathbf{p}$ to the channel measurement z_i
i	Iteration variable
j	Iteration variable
l	Optional control dimension
m	Measurements dimension
n_d	Ranging error
n	System state dimension
p_{PL}	The receiver signal strength
r	RSSI measurement
t_k	Time at k index
t_{rx}	Received signal time
t_{tx}	Transmitted signal time
x_k	The x coordinate of the real mobile position at k time index
x_{BS}	The x coordinate of anchor node

y_k	The y coordinate of the mobile position at k time index
y_{BS}	The y coordinate of anchor node
z_i	The ith measurement
$v_{x,k}$	The x component of the mobile velocity at k time index
$v_{y,k}$	The y component of the mobile velocity at k time index

List of Abbreviations

AOA	Angle of Arrival
BS	Base Station
Cell-ID	Cell Identification
COO	Cell Of Origin
dB	Decibel
EKF	Extended Kalman Filter
EU	European Union
FCC	Federal Communication Commission
GLONASS	GLObal Navigation Satellite System
GNSS	Global Navigation Satellite System
GPS	Global Positioning System
GSM	Global System for Mobile Communications
HMMs	Hidden Markov Models
IEKF	Iterated Extended Kalman Filter
IR	Infrared Radiation

KF	Kalman Filter
KFMs	Kalman Filter Models
L&T	Location and Tracking
LBSs	Location Based Services
LLS	Linear Least-Squares
LOS	Line Of Sight
LS	Least-Squares Methods
MIMO	Multiple-Input Multiple-Output
MS	Mobile Station
NFC	Near Field Communication
NICs	Network Interface Cards
NLLS	Non Linear Least-Squares
NLOS	Non Line Of Sight
OFDM	Orthogonal Frequency-Division Multiplexing
PDF	Probability Density Function
RF	Radio Frequency
RFID	Radio Frequency Identification
RSS	Received Signal Strength
RSSI	Received Signal Strength Indicator
SPKF	Sigma Point Kalman Filter
SS-UKF	Spherical Simplex-Unscented Kalman Filter
SSUKF	Spherical Simplex Unscented Kalman Filter
SSUT	Spherical Simplex Unscented Transformation
SUKF	Scaled Unscented Kalman Filter

SUT	Scaled Unscented Transformation
TDOA	Time Difference of Arrival
TGn	High Throughput Task Group
TOA	Time of Arrival
UKF	Unscented Kalman Filter
UT	Unscented Transformation
WLAN	Wireless Local Area Network

Contents

1 Introduction to the Positioning and Tracking Problem

1.1 Location Information for Wireless Systems

Wireless communications is rapidly growing in all fields around the world and this trend is likely to continue in the future also [13b]. The communication infrastructure that provides the wireless services has been developed enormously towards higher capacity, higher range, higher flexibility and more advanced services [FF11]. The mobility that characterizes wireless communication users opens demands for location information in different fields such as rescue, emergency, automotive application, monitoring, and navigation [FF11]. The continuous demand for location information massively creates opportunities for business and encourage for new ideas and innovations for developing and providing new services and applications [FF11]. Moreover, the raising of the smart devices (smartphones, tablets, computers, etc.) and mobile context-aware programs put challenges and demands for location information [KJ15b].

The demand for location information has boosted research and development for both industry and academia towards positioning solutions for wireless communication technologies that can be integrated with the deployed, under deployment and next generation wireless communication infrastructure [FF11; KJ15a]. The result is a wide variety of integrated and built-in solutions that can combine

and interoperate with communication and location information [FF11]. Innovations involve proposing *Location and Tracking* (L&T) algorithms which can be implemented in dedicated or integrated communication protocols, error mitigation and cooperative positioning [FF11].

Historically, the wireless positioning is dated back to the year 1999, when the Federal Communication Commission (FCC) passed a mandate requiring cellular providers to generate accurate location estimates in order to improve the quality and reliability services and the implementation of Enhanced 911 (E911) [Com+99; Com+01]. A similar mandate is issued by the European Union (EU), to help emergency services locating people who call them using the pan-European emergency number 112 that can be dialled in all EU member states [03].

Today, the number of L&T applications is covering a wide range of different fields. Successful systems in various fields exist and are dealing with L&T such as the Curiosity robotic rover on Mars [Wal12; Gre15], and autonomous cars which are self driving vehicles that have the ability to perceive the surrounding environment and navigate themselves without human intervention [Jo+14]. Moreover, companies like Facebook, Twitter and Google integrate location information services for understanding user needs [Des12]. Furthermore, market analysts forecast that the revenues from the Location Based Services (LBSs) market worldwide will grow from 10.3 billion Euro in 2014 to about 34.8 billion Euro in 2020 [14].

In future, it is expected that location information will be one of the great demanding innovations with the coming internet-of-things, machine-to-machine and sensor network technologies to optimize the networking and enable smart, personalized and pervasive services [Des12; VF13]. By the year 2024, over 3.4 billion devices will be interconnected using machine-to-machine connections [Mac14]. The integration of Near Field Communication (NFC), which has L&T applications, in the world of mobile communications is foreseen within the year 2020 [Des12].

From all of the above, it is clear that location information becomes crucial in different applications for both academia and industry.

1.2 Motivation

In order to deliver adequate L&T services, real-time and accurate user's locations must be obtained. Hence, a growing interest in developing effective L&T solutions and systems is exist.

Global Navigation Satellite System (GNSS) like Global Positioning System (GPS), GLObal Navigation Satellite System (GLONASS), or soon Galileo brought new applications to mankind in variety of location based services such as car navigation, high precision street construction, and finding services and shops in unknown areas [HLW07; HH13]. For instance, explicit positioning sensors based on the GPS and cellular network based systems can work worldwide for L&T and achieve relatively good accuracy [Sun+05]. Recent trails have been reported that the GPS achieves average errors between 10 m and 67 m depending on factors such as topology [MKH06]. Unfortunately, these techniques cannot be used directly indoors, as the signals are usually too weak to be used for localization purposes [Ots+05]. Moreover, GPS requires a direct view of several satellites to provide the location information, which is impossible for indoor environment [PW09].

A number of commercial systems and prototypes have been developed for indoor localization to act as the counterpart of GNSS. Those systems use Infrared (IR) [M+09; Tao+15], Radio Frequency Identification (RFID) [BP00; Yan+13], Ultra-Wideband (UWB) [Kuh+10], ultrasound [Bar+08] and optical positioning [TM10; TM11]. Besides the expensive deployment costs of those systems, each system has further limitations.

Positioning techniques that rely on the existing signals and hardware as well as the deployed communication networks have advantages over developing new positioning systems. One major advantage is the lower investment cost where no new communication networks need to be implemented on a large scale. Moreover, mobile users will not have to replace their devices due to the compatibility issue with the new deployed hardware.

To develop an indoor localization system with relatively low implementation costs and software complexity, WLAN has been widely investigated to act as the replacement of GPS within indoor environments. The main operation of the WLAN positioning systems is to detect and analyse the signals of the widely deployed signals of the WLAN access points at the integrated WLAN cards in most recent mobile phones [Sor+15]. Although the main application of WLAN is to provide internet access, using those networks for L&T is promising due to the wide deployment [Hon+09; Sor+15].

In WLAN, wireless routers which are known also as access points are used to provide internet access to WLAN enabled devices. In addition to the internet access, the access points are configured to broadcast beacon packets which contain different types of information [AH15]. Those packets are received by wireless enabled devices and the information is extracted using Network Interface Cards (NICs) [AH15]. A WLAN enabled device can measure the *Received Signal Strength Indicator* (RSSI), called also as *Received Signal Strength* (RSS), from the access points surrounding it as a part of the NICs operation [Kha+14; Sor+15]. These systems do not require investments in their deployment or providing them with additional hardware. This makes it very appealing for commercialization over other measurement based localization approaches such as the *Time of Arrival* (TOA) or *Angle of Arrival* (AOA) approaches [Sor+15]. However, the RSSI-based L&T systems have relatively low accuracy.

The low investment costs and the relative low localization accuracy of the WLAN-based L&T systems motivate this work for proposing algorithms and techniques to improve the localization accuracy.

1.3 Criticism on the State of the Art

Two popular approaches to deal with the RSSI-based L&T systems within indoor environment are location fingerprinting and *Extended Kalman Filter* (EKF). Finger-

printing uses the obtained channel measurements to obtain the location based on pre-recorded radio map that associates the locations with the measurements. Location fingerprinting will be presented in section 2.4.1. The EKF approach uses the measurements obtained from path loss models to obtain the position depending on an approximation solution for the non-linearity which exists in the relationship between the measurements and the position. The EKF will be given in more details in section 4.4. In this section, the criticism of both location fingerprinting and EKF are introduced.

1.3.1 Criticism on Fingerprinting

Fingerprinting is a group of techniques that performs localization of a mobile node based on the received information from the surroundings of the mobile node [FF11]. Fingerprinting associates Location information in an environment with values of received signal parameters. Therefore, it is important to have good knowledge about the surroundings in order to obtain location information during the localization process [FF11].

Although fingerprinting is the most accurate positioning technique, it has serious shortcomings. That is, the site survey to collect the signal measurements is extremely time consuming, the required recalibration upon any changes that may influence the propagation conditions [FF11], and the exhaustive matching between the obtained measurements and the pre-stored information to find a best match.

1.3.2 Criticism on Extended Kalman Filter

The Extended Kalman Filter (EKF) has been introduced to variety of non-linear application including navigation for estimating the position, attitude and velocity of mobile targets. Examples of those applications are the navigation of aircrafts

(manned and unmanned) [MLV10; Leu+14], mobile robots [LTC12], satellite observation system [Li+09] and spacecraft navigation [Cha+15]. Historically, one of the first successful real-world application was in the navigation of the Apollo mission to the moon and back [Hoa63].

The EKF approximates the non-linearity using the first order term of the Taylor series expansion. These approximations are valid only if the higher order terms of the derivatives of the Taylor series expansion are very small that can be neglected. If this condition is violated, i.e., the higher order terms are not small to be neglected, the filter might become unstable [JU97; BH12]. Furthermore, if the current state estimate is poor, further errors in the following estimates are expected. This in turn causes further errors in the updated estimate, and so on and so forth, leading to filter divergence [BH12]. As a result, EKF is more likely to diverge in some situations [BH12].

In addition, the approximation involves calculating the derivation of the Jacobian matrices that is not a trivial task and sometimes the derivation is very difficult to be implemented [JUD95]. Moreover, the EKF ignores the "probabilistic uncertainty" of the system state , the state covariance, the system noise variable into consideration [Van04]. In other words, the linearization of the EKF does not use or benefit from the probability distribution information of the state and the covariance of the system.

1.4 Objectives and Contributions of the Dissertation

This dissertation is motivated by the demand of improving different aspects of positioning and tracking of a mobile node within indoor environments. The main objective of this dissertation is to propose techniques, design digital signal processing algorithms and test them to improve positioning accuracy and/or ease of implementation to enable a mobile node from locating and tracking itself using

relative information from the surroundings within indoor environment. In particular, the focus is to propose techniques and algorithms based on the *Received Signal Strength Indicator* (RSSI) measurements of the widely deployed WLAN and the knowledge of location of fixed anchor nodes for indoor positioning and location tracking. Recently, most smartphones are equipped with circuitry for measuring the power level of the RSSI which makes the proposed techniques and algorithm, and the presented implementation of the KF applicable.

In this dissertation, the author focuses on the IEEE 802.11n as the latest off the shelf WLAN which uses a bandwidth of 40 MHz and exploits diversity from three antennas yielding a comparable small standard deviation of the path loss. Older WLAN standards such as 802.11a/b/g may suffer from larger standard deviations, which yield less accurate positioning results. Furthermore, the IEEE 802.11n supports a range of up to 200 m [09]. The maximum range is reported to have even longer distance of up to 250 m [12]. However, range will vary depending on the environment and on the capability of the client and access point [Bel07]. It is considered that IEEE 802.11n supports better range than the the most recent WLAN IEEE 802.11ac [13a]. It is reported that the IEEE 802.11 ac has a maximum indoor range of 35 m [13a].

The complexity of the proposed techniques shall remain the same as the state of art for better performance-complexity trade-off.

According to the main objective, the following tasks are defined and accomplished in the dissertation:

1. A representation of wireless channel model for WLAN 802.11n.
2. A representation of WLAN 802.11n anchor nodes.
3. A representation of a mobile node which gather the RSSI measurements.
4. A representation of evaluation model that has different testing parameters.
5. Design of EKF for performance evaluation.
6. Design of trilateration solution that establish a set of linear equations out of non-linear equations to be solvable using a LLS approach.

7. Design new solutions which can be implemented in the mobile node for positioning and tracking.

The innovative contributions of this dissertation are:

1. Proposing a positioning framework based on novel implementation of the KF. The KF is designed to work linearly to refine the position estimates. The estimation performance of this framework is tested by simulation and compared with the state of the art EKF. The contributions of this part originate in one conference paper:
    - **Laith Khalil**, Andreas Waadt, Guido Bruck and Peter Jung, "Positioning Framework for WLAN IEEE 802.11 n Utilizing Kalman Filter on Received Signal Strength," in *10th Int. Wireless Communications and Mobile Computing Conference (IWCMC)*, Aug. 2014, pp. 1172-1176.
2. Proposing a positioning and tracking solution based on the *Iterated Extended Kalman Filter* (IEKF). This solution is tested on simulation data and compared with the EKF.
3. Proposing a positioning and tracking solution based on the *Scaled Unscented Kalman Filter* (SUKF). Comparative simulation results relative to EKF are presented. The contributions of this part originate in one conference paper:
    - **Laith Khalil** and Peter Jung,"Scaled Unscented Kalman Filter for RSSI-Based WLAN IEEE 802.11n Positioning and Tracking," in *9th Int. Conf. on Next Generation Mobile Applications, Services and Technologies (NGMAST)*, Sep. 2015, pp. 132-137.
4. Proposing a positioning and tracking solution based on the *Spherical Simplex Unscented Kalman Filter* (SSUKF). This solution is tested on simulation data and compared to EKF. The contributions of this part originate in one conference paper:
    - **Laith Khalil** and Peter Jung, "Spherical Simplex Unscented Kalman Filter for RSSI-Based WLAN IEEE 802.11n Positioning and Tracking,"

in *IEEE 26th Annual Int. Sym. on Personal Indoor and Mobile Radio Communications (PIMRC)*, 30 Aug.-2 Sept. 2015, pp. 2284-2288.

1.5 Dissertation Outline

In this dissertation, the author proposes techniques and algorithms in order to improve the performance for indoor L&T. The main contributions and chapters organizations of this dissertation are summarized as follows.

- **Chapter 2: Positioning background**
  This chapter starts explaining the most common ranging technique for distance estimation. Then, identity methods and trilateration are presented as common positioning techniques. Afterwords, wireless channel modelling for WLAN IEEE 802.11 n is explained for distance estimation. Finally, the performance evaluation model for positioning and tracking of a mobile node within WLAN IEEE 802.11 n environment is illustrated in detail.

- **Chapter 3: Positioning Framework for RSSI-Based WLAN IEEE 802.11n**
  Chapter 3 starts with designing a Linear Least-Squares estimator. Then the state space models are designed to enable the KF to work linearly. The LLS and the KF work within the proposed positioning framework. The simulation procedure and the results are presented as well in this chapter.

- **Chapter 4: Iterated Extended Kalman Filter for RSSI-based WLAN IEEE 802.11n positioning and tracking**
  In this chapter, the non-linear dynamic system modelling is designed. For comparison purpose, the EKF is designed. A new positioning and tracking solution based on the IEKF is proposed. A performance evaluation model to validate the proposed solutions throughout this dissertation is presented in this chapter. The simulation procedure for implementing the IEKF for performance evaluation is presented. Moreover, simulation results based on the performance evaluation model are presented.

- **Chapter 5: Sigma Points Kalman Filters for RSSI-based WLAN IEEE 802.11n positioning and tracking**
  This chapter starts designing the *Scaled Unscented Transformation* (SUT). The author proposes a new positioning and tracking solution based on the SUKF. The SUKF results from application of the SUT to the KF. The design and the implementation of SUKF is presented. This solution is tested and implemented using a simulation procedure. Furthermore, simulation results are presented based on a performance evaluation model.

  Moreover in this chapter, the author proposes a L&T solution based on the *Spherical Simplex Unscented Transformation* SSUT. The SSUT is designed to model the positioning problem. A new positioning and tracking solution based on the SSUKF is presented. The SSUKF results from application of the SSUT to the KF. The simulation procedure for the implementing and testing the algorithm is given. An evaluation of the proposed solution is illustrated using simulation results.

- **Chapter 6: Conclusion and Future work**
  Chapter 6 summarizes the main research challenges and gives recommendations for future expansion of this work

2 Positioning Background

2.1 Overview

This chapter presents some of the theoretical tools related to the proposed algorithms for indoor tracking applications. First, the problem of positioning throughout this dissertation is defined. Then, the commonly known techniques to measure distances from anchor nodes are presented. These techniques are known as ranging techniques. In addition, the popular positioning algorithms for estimating the position based on ranging measurements are presented. In particular they are fingerprinting, trilateration and proximity.

Moreover in this chapter, a review of the data fusion and estimation techniques are presented. Then, wireless channel modelling for obtaining distance estimates out of the measurements are given. In addition, state space models are presented which model the dynamics and measurements of a L&T system. Designing these models allow for implementation of different variations of the KF. Finally, the derivation of the KF is presented in a consistent matter with the implementation carried out in this dissertation.

2.2 Positioning Problem

The location estimation problem for a moving object in $2-\mathrm{D}$ plane can be conceived by referring to Fig. 2.1.

In this figure, the mobile node is following a trajectory (with or without prior knowledge), and this node tries to locate itself by using the received measured signals from a number of surrounding *reference points* or *anchor nodes*.

The mobile node continuously collects the RSSI measurements $\mathbf{r} \in \mathbb{R}^N$ from a number of anchor nodes surrounding it at certain time intervals, where

$$\mathbf{r} = \begin{bmatrix} r(1) & r(2) & \dots & r(N) \end{bmatrix}^T, \tag{2.1}$$

where N is the number of anchor nodes. The mobile node converts the RSSI measurements into distance measurements $\mathbf{z} \in \mathbb{R}^N$ using a path loss model, where

$$\mathbf{z} = \begin{bmatrix} z(1) & z(2) & \dots & z(N) \end{bmatrix}^T. \tag{2.2}$$

The mobile node uses the distance measurements with the knowledge of anchor nodes' positions to locate itself. The red dashed line in Fig 2.1 refers to the *maximum circle of trust*. If the mobile node moves outside the circle of trust, it may lose at least one of the received signals from the anchor nodes due to different parameters such as the noise shadowing. As such, the mobile node loses the ability to locate itself.

Then the task is to find the location information estimation $\hat{\mathbf{p}}$ for the mobile node in movement which is written as

$$\hat{\mathbf{p}} = [\hat{x}, \hat{y}], \tag{2.3}$$

where $\hat{x}$ and $\hat{y}$ are the estimated position coordinates, note that the superscript "hat" denotes estimation. The corresponding position estimation error is written

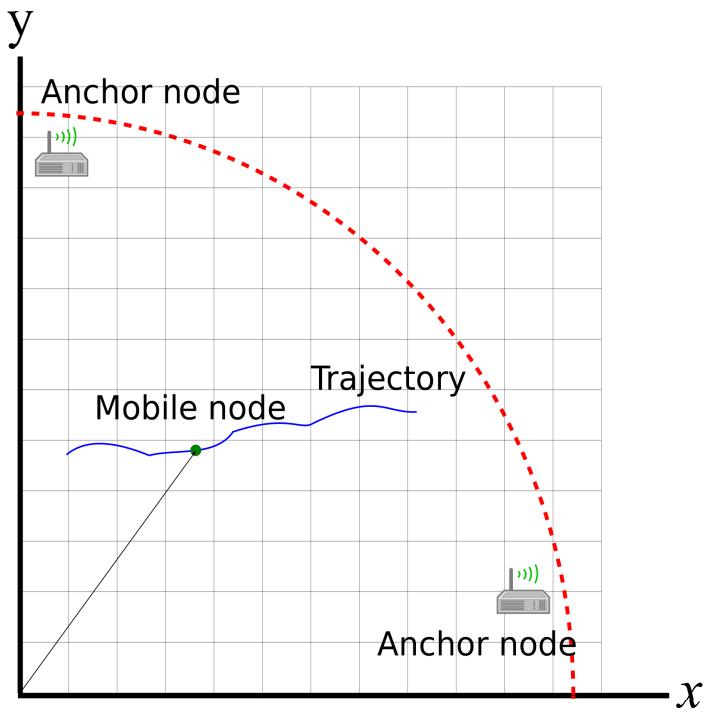

Figure 2.1: Position estimation problem for a moving device that is surrounded with a number of anchor nodes.

as

$$\mathbf{e} = [\mathbf{p} - \hat{\mathbf{p}}], \tag{2.4}$$

where

$$\mathbf{p} = [x, y], \tag{2.5}$$

is the real position. The estimation error comes from the fact that the measurements are corrupted by factors like noise and device inaccuracy.

2.3 Ranging

All the methods used to measure distances from anchor nodes to a mobile node can be referred to as ranging techniques. The most commonly used ranging techniques are the *Received Signal Strength Indicator* (RSSI), the *Time of Arrival* (Time of Arrival), and the *Angle of Arrival* (Angle of Arrival).

2.3.1 Received Signal Strength

The RSS or the RSSI is the measure of the magnitude voltage at receiver terminal [MR07]. It can be equivalently represented as squared magnitude of the signal strength, i.e., the measured power. The RSSI of Radio Frequency (RF) signals can be estimated by each receiver during normal communication. As such, the measurements do not require additional hardware or dedicated bandwidth [MR07]. These features make this technique relatively inexpensive and easy to be implemented and therefore it appeals researchers for distance estimation [MR07]. However, RSSI is a subject to noise and different propagation effects like the signal attenuation, scattering, multipath, shadowing and diffraction [Gol05].

The relation between the RSSI at the receiver and the signal strength at the transmitter can be modelled using a *propagation model* with propagation effects that depend on the propagation environment. Theoretical and empirical models are used to translate this relation into a distance estimate [Liu+07]. Examples of the propagation effects are the signal attenuation, scattering, diffraction and multipath effects [Gol05].

The propagation model in general, which is also called the *path loss model*, can be modelled using white Gaussian noise with standard deviation of σ as given, from [Gol05], as

$$p_{\mathrm{PL}} = \alpha_{\mathrm{PL}} - \beta_{\mathrm{PL}} \log(\frac{d}{d_0}) + \eta, \qquad \eta \sim \mathcal{N}(0, \sigma) \tag{2.6}$$

where p_{PL} is the received signal strength (e.g. measured in dBm), α_{PL} is a parameter that related to the transmitter signal strength, β_{PL} is path loss exponent, d is the distance separation between the sender and the receiver, and η is a Gaussian random variable with zero mean and σ standard deviation.

2.3.2 Time of Arrival

The TOA is a measurement of the time at which a signal arrives at the receiver side [MR07]. Two common approaches to the TOA are the one-way propagation time method and the round-trip propagation time method [MFA07]. The one-way propagation time measures the difference between the sending time of a signal at the transmitter and the receiving time of the signal at the receiver. This requires that both the sender and the receiver to be accurately synchronized, i.e., having the same local time [FF11]. In addition, a time stamp must be added by the sender to the signal in order to discern the distance by the receiver [MFA07]. These requirements add additional cost especially for a sophisticated synchronization mechanism [MFA07].

The time measured of the received signal t_{rx} can be modelled as the sum of the transmission time t_{tx}, the propagation delay and the synchronization error ϵ_{sync} as given [FF11]

$$t_{\text{rx}} = t_{\text{tx}} + \frac{d}{c} + \epsilon_{\text{sync}}, \tag{2.7}$$

where d is the distance between the sender and the receiver, c is the medium propagation speed. A major issue with this technique is to know the synchronization error which is often not possible to obtain. This can be considered as the major disadvantage of the TOA method [FF11].

For an asynchronous network, it is common to use the round-trip technique or the Time Difference of Arrival (TDOA) [MFA07; McC+00]. Round-trip propagation time measures the time difference between the time at which a signal is sent and the time at which the signal is returned from a receiver. The major error source is the time required from the receiver to process and send back the received signal. A more in depth study is provided in [McC+00]. Nevertheless, the TDOA will be presented in the following section.

2.3.3 Time Difference of Arrival

The TDOA is similar to TOA but is based on processing signals transmitted simultaneously by different terminals. The TDOA aims to get rid of the clock synchronization between the transmitter and the receiver [FF11]. As such, the TDOA aims to get rid of the clock synchronization error. For instance, if two Base Stations (BSs) BS_1 and BS_2 transmit two signals at the same time t_{tx} to a mobile station that has the distance d_1 to BS_1 and the distance d_2 to BS_2, then the TDOA t at the mobile station is [FF11]

$$t_{rx} = (t_{tx} + \frac{d_1}{c} + \epsilon_{\text{sync}}) - (t_{tx} + \frac{d_2}{c} + \epsilon_{\text{sync}}) = \frac{d_1 - d_2}{c}, \tag{2.8}$$

where c is the medium propagation speed and ϵ_{sync} is the synchronization error. Although the BSs and the MS do not need to be synchronized, the BSs need to be clock synchronized [FF11].

2.3.4 Angle of Arrival

The AOA is the measurement of angle of the signal arriving at the receiver rather than the distances in order to know the direction of transmission. This kind of information is complementary to RSSI and TOA [MR07]. The AOA can be divided into two subclasses [MFA07]: those making use of the receiver antenna's amplitude response and those making use of the receiver antenna's phase response.

The first category of measurement techniques use antenna anisotropy to derive the AOA measurements. A widely used approach is to use at least four stationary antennas with known anisotropic antenna patterns. By overlapping these patterns and comparing the received signal strength from each antenna yields the transmitter direction even when the signal strength changes.

The second category of measurement techniques derives the AOA measurements from the phase difference measurement of the arrival of signals. It requires an

antenna array or large receiver antenna relative to the wave length of the transmitted signal.

Both of the above categories require hardware that substantially increases the device cost and size. The accuracy of AOA is limited by the directivity of the antenna, shadowing and multipath reflections [MFA07].

2.4 Positioning Techniques

Based on different measurements in wireless communications, algorithms and techniques are used in order to estimate the mobile position from the obtained measurements. It has been discussed earlier, that the wireless channel measurements for position estimation are corrupted by noise. Various types of noise sources causing the channel measurements to present statistical behaviours that in some cases are difficult to model [FF11]. This will have an impact on the accuracy of any positioning system. Detailed error sources in wireless positioning can be found in [FF11].

In general, positioning techniques can be grouped into three categories based on the technique used to obtain the location information.

The first category is the location fingerprinting approach. This category is introduced in section 2.4.1.

The second category is called triangulation which includes techniques that use measurement techniques which are TOA, AOA and RSSI to estimate the position of a mobile node. These methods use trigonometry in order to combine data from several sources [FF11]. Trilateration is an example of this category which uses the ranging techniques for position estimation.

The third category is based on proximity-sensing. One popular example of this type is the Cell-ID [Liu+07]. This category will be introduced later in section 2.4.3.

2.4.1 Fingerprinting

Fingerprinting is considered the most accurate method to use the RSSI measurements for location estimation. Different techniques are developed to perform Fingerprinting. These techniques model the RSSI in areas of interest. This can be done by gathering RSSI measurements at reference grid points [FF11; AH15]. The vector of RSSI measurement values at a point is called the location fingerprinting of the point [AH15]. The gathered RSSI measurements are used to construct a propagation model, which is known as the *radio map* [AH15].

Fingerprinting is performed on two phases, an off-line phase and an on-line phase [FF11; AH15] as depicted in Fig. 2.2. The author follows [AH15] to give a simple explanation of the procedure.

During the off-line phase, an $m \times n$ radio map for the area of interest is constructed. The RSSI value $\mathbf{RSSI}_{ij}$ received from m surrounding anchor nodes are collected at n grid points $\mathbf{p}_i$, where

$$i = \{1, \ldots, n\},$$

and

$$j = \{1, \ldots, m\}.$$

The radio map is saved to a database to be used later during the on-line phase.

In on-line phase, a matching algorithm is used to compare RSSI measurements done by a mobile object at the present moment with pre-stored values in the radio map to find the grid point with minimum matching error.

The database can contain as much variety of measurements as possible from several systems such as GSM and WLAN if they are enabled at the mobile node [FF11]. Examples of the measurements variety are the RSSI, TOA and AOA.

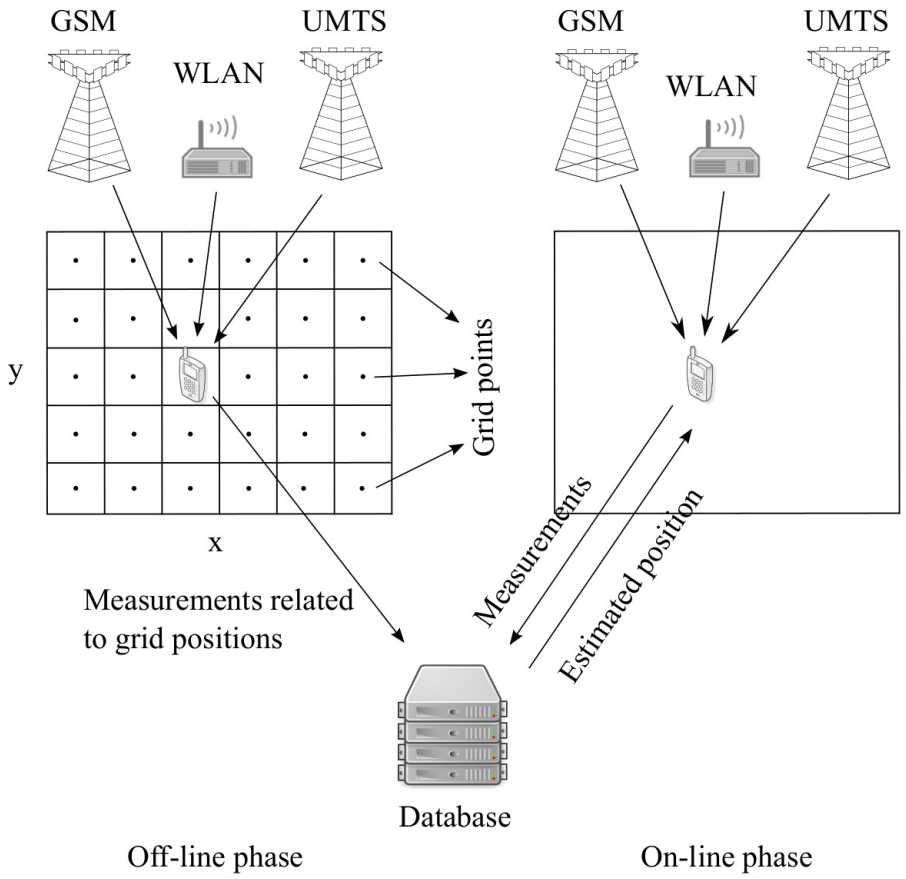

Figure 2.2: Fingerprinting method with two phases of operation. The off-line phase is on the left while the on-line phase is on the right. Inspired by [FF11].

The greater amount of information in the database requires more complex algorithms to manage the organization of those information as well as localization process [FF11].

Fingerprinting techniques are very dependent on the scenario [FF11]. If something that may influence the propagation conditions changes, for example a door opening in an indoor scenario, a re-calibration process (the off-line phase) must be done all over again [FF11].

2.4.2 Trilateration

Trilateration or lateration [FF11; RH05; MLM13] is the term used to describe the positioning technique that is based on the use of measured distances between the anchor nodes and a mobile station to determine it's absolute or relative position.

In order to enable 2-D positioning using this technique, distance measurements must be made with respect to received signals from at least three reference points or so-called anchor nodes [Fan90]. Similarly for 3-D positioning, 4 anchor nodes having non coplanar points are the minimum number of BSs to locate a mobile node [MH95].

In this method, each anchor node calculates the distances to the mobile nodes in interest according to the ranging techniques. The anchor node draws a circle around itself for each mobile node where the anchor node assumes that each mobile node should be at one of the points on the circumference of the corresponding circle [MR07]. The exact distances d_i, for $i = \{1, 2, \ldots, N\}$, between the n anchor nodes of locations $\mathbf{p}_{\mathrm{BS}_i}$ and the mobile node are the radii of the individual circles [MH99]. If the locations of the anchor nodes are defined as

$$\mathbf{p}_{\mathrm{BS}_i} = [x_{\mathrm{BS}_i}, y_{\mathrm{BS}_i}]^T \qquad i = \{1, 2, \ldots, N\}, \tag{2.9}$$

then the equation of any of these circles is written, from [MH99], as

$$d_i{}^2 = (x_{\mathrm{BS}_i} - x)^2 + (y_{\mathrm{BS}_i} - y)^2 \qquad i = \{1, \ldots, N\}. \tag{2.10}$$

The point of intersection of the circles is obtained by letting $i = \{1, 2, \ldots, N\}$ and solving for N non-linear equations [MH99]. In particular, the mobile node coordinates

$$\mathbf{p} = [x, y]^T, \tag{2.11}$$

is the point of intersection of several circles whose centers are the locations of N anchor nodes.

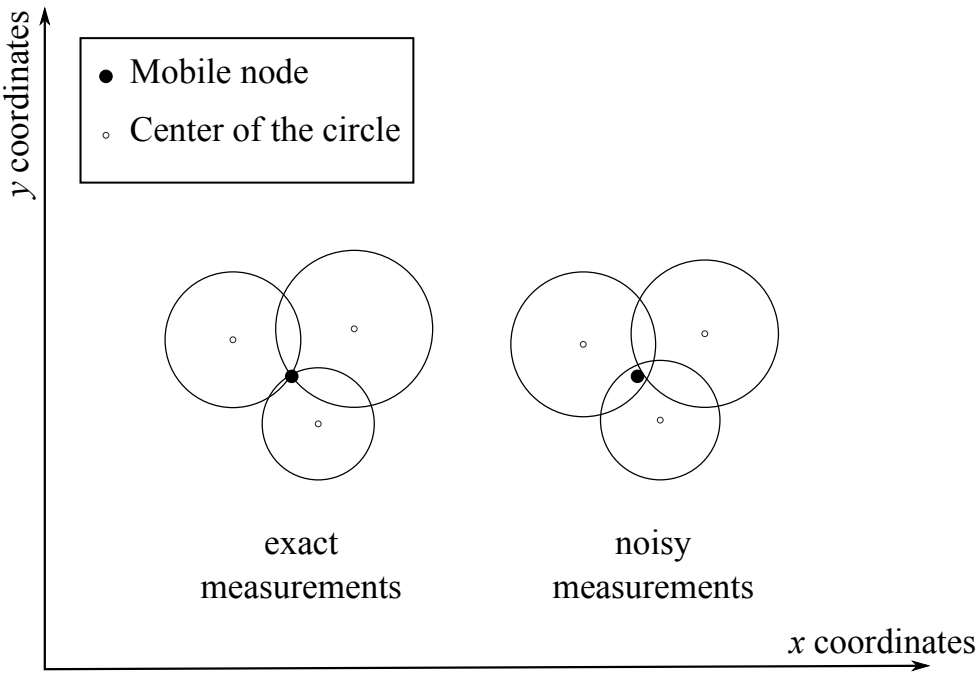

Figure 2.3: Positioning estimation using trilateration.

If the measurements are exact, i.e. without noise, it is possible to intersect the distances resulting in one point which the position of the mobile node [MR07]. However, due to the noisy behaviour of the measurements, it is not possible to determine a single estimate for the mobile node using this method [MR07]. In particular, the estimated distances are corrupted by noise and consequently do not intersect in one point as depicted in Fig. 2.3.

A simple approach to the non-intersecting circles problem is by intersecting of two circles and produce two points of interest then using the third one to select among two points [FF11]. More accuracy would be achieved if the three or more measurements are taken into consideration [FF11].

2.4.3 Proximity

The proximity techniques, not like other positioning techniques, do not rely on the distance or the angle of the communications link and present relative posi-

tion information. As such, the mobile position is identified according to the base station position once the mobile node is within the range of the base station.

This method is relatively easy for implementation where it can be implemented for different types of physical media [Liu+07]. This method is common in RFID and Infrared Radiation (IR) [Liu+07]. Another example is the Cell Identification (Cell-ID) or Cell Of Origin (COO) in cellular systems where the mobile cellular networks can identify the approximate position of a mobile handset by knowing which cell site the device is using at a given time [Liu+07; FF11]. In addition, these techniques can be used in hybrid solutions as well as for determining geographical constrains in positioning estimation [FF11]. However, this method is considered the least accurate among the positioning methods [FF11].

A simple algorithm for estimating the position of a mobile node based on the locations of all the BSs that the mobile can communicate with is the centroid method [FF11]. In this algorithm, the estimated position is the arithmetic mean of the coordinates of all the BSs detected by the mobile station. By assuming that the base stations are located at positions

$$\mathbf{p}_{\mathrm{BS}_i} = [x_{\mathrm{BS}_i}, y_{\mathrm{BS}_i}] \quad \text{for } i = \{1, 2, \ldots, N\}, \tag{2.12}$$

where N is the number of base stations. Then, the position of the mobile station

$$\mathbf{p} = [x, y], \tag{2.13}$$

can be simply calculated from

$$\mathbf{p} = \frac{1}{N} \sum_{1}^{N} \mathbf{p}_{\mathrm{BS}_i}. \tag{2.14}$$

2.5 Date Fusion and Estimation

In estimation theory and statistical inference, there are a number of approaches for estimating the parameter out of the observation. These approaches are categorized as Bayesian or non-Bayesian, depending on whether or not we consider the unknown parameter $\mathbf{x}$ from an observation $\mathbf{z}$ [WLW09].

In general, those approaches are categorized as non-Bayesian or Bayesian depending on how the unknown is treated form the existing measurements [WLW09].

The non-Bayesian approach treats the unknown $\mathbf{x}$ deterministically [WLW09]. In the context of L&T, this approach estimates the position of a MS by minimizing the resulting squared error between the actual measurements observed in the wireless channel and the expected measurements resulting from the estimated position [FF11]. Two common non-Bayesian estimators are the *Least-Squares Methods* (LS) estimator and the maximum likelihood estimator. The LS includes linear and non-linear estimations. While the *Linear Least-Squares* (LLS) presents closed form solution to the estimation problem, the *Non Linear Least-Squares* (NLLS) may not be solvable and therefore numerical optimization solutions must be provided [FF11].

In Bayesian estimation, statistical models for both $\mathbf{x}$ and $\mathbf{z}$ are used with the conditional density function $p(\mathbf{x}|\mathbf{z})$ to infer $\mathbf{x}$. The KF is an example of the Bayesian estimation. In the context of L&T, the position is determined as an estimator that minimizes the mean squared error between the actual measurements and the expected measurements [FF11]. The closed-form solution to the Bayesian framework is only possible with the assumption of *Gaussian* probabilistic models and the imposition of *linearity* to both the process and the measurement models [Cho14]. With these assumptions, the Bayesian solution is *optimal*, *tractable* and results in the *Kalman Filter* (KF) [Gel74]. However, the solution to the Bayesian framework with other assumptions (non-linear, non Gaussian) is

hard to obtain analytically [Cho14]. This can make the estimation process intractable [RAG04].

It should be mentioned here that the KF is an *estimator* for the problem of estimating the instantaneous state of a linear dynamic system by using measurements that are related linearly to the system state. Both the linear dynamic system and the measurements are corrupted by white noise [GA11]. The KF uses the knowledge about the system and measuring devices with a combination of all available measurements to produce an estimate of the desired variables in a way that the error is minimized statistically [May82]. Therefore, this filter is considered as *optimal recursive filter* [May82; GA11].

In the case of KF, the "filter" comes from the fact that the KF has a solution to the problem of *inferring* variables of interest that can not be determined directly out of the noisy measurements [May82]. In addition, the term "filter" in Kalman filtering means the *separation* of the variables of interest given by the system state from noise [GA11].

In L&T, the term "location", which is similar to "position", refers to the source of information that contains the 2 D or 3 D coordinates of a mobile node relative to its environment [FF11]. The process of obtaining the position information is called "localization" or "positioning". If the positioning process is related to time information, this process is referred to as "tracking" [FF11]. Relating position information to time information allows to obtain the mobile position at specific time [FF11]. In addition, this relationship allows for deriving other information such as speed and acceleration [FF11]. For instance, a moving object's *average speed* during an interval of time is found by dividing the distance by the time elapsed and the corresponding unit is the length per time unit such as meter per second [WHT10]. "Navigation" is a tracking solution that uses a map information to help users reaching their desired destinations [FF11].

For most general real-world systems (non-linear, non-Gaussian), the general form

of the recursive Bayesian filter is not tractable and therefore approximation solutions must be used [Hau05].

Numerous approximation solutions to the Bayesian estimation problem have been proposed over the last couple of decades in different fields. These solutions can be loosely grouped into the following main categories depending on the approach to approximate the integration [Van04; Mac12], some of them will be introduced in more details later in this dissertation:

1. Analytic approximations: To this group belong all the solutions that solve the filtering problem by linearization [Mac12].
    - Extended Kalman Filter (EKF) [WB; GA11]: The EKF applies the KF to the non-linear Gaussian systems by linearizing the system models using a first-order truncated Taylor series expansion around the current estimates. Due to it's good performance and relatively low complexity, this filter is still applied to a number of real world applications including L&T [Pet08; LH13; Hel+13; Ati+15]. The EKF will be given in detail in section 4.4.
    - Formulations of the KF that involve second order or higher order relationships in the non-linear process and/or measurement functions do exist [Ben81; Dau95] with extra implementation complexity [BH12].
2. Gaussian Sum Filters (GSF) [AS72]: The GSF approximate the *a posteriori* PDF by a weighted sum of Gaussian density functions, i.e., Gaussian mixture of densities (GM). EKF and other non-linear methods are then applied to each of those densities. Although GM solutions were applied to the L&T problems, those solutions require frequently reinitialization in high noise environment of each non-linear filter corresponding to each separate Gaussian density to minimize the conditional error covariance [AM79]. Novel techniques are still subject to research to reduce the computational burden, especially the weights and moments computations [BT10; CKV11; ZJ14].
3. Sequential Monte Carlo methods which are also known as "Particle Filters": These filters are popular to offer approximations to the non-linear/non-

Gaussian filter, and particularly multi-modal density function instead of uni-model ones [BH12]. The filters approximate the continuous probability function with discrete weights at sample points that are generally unevenly spaced [BH12]. These samples can be viewed as "particles" carried by the non-linear system dynamics. This is how the word "particles" is associated with the name of the filter [GA11]. Different variations of the particle filters exit and whole books are devoted to those variations [RAG04; Smi+13].

4. Deterministic sampling or so-called sigma-point approaches: This class of methods is based on sampling techniques for propagation of random variables through non-linear systems. This can be done by selecting a deterministic set of points that capture the moments of the density function while at the same time allow for direct transformation through the non-linear functions. The *Unscented Transformation* (UT) [JU97] and Stirling's interpolation approach to state estimation for non-linear systems [NPR00] are examples of this approach [PW09]. This recent and unfamiliar approach to the KF results in limited implementations such as to the outdoor location and tracking [PW08; PW09], and to underwater navigation [Sta10].

2.6 WLAN Channel Models

Wireless channel models which are also called *propagation models* have traditionally focused on predicting the average received signal strength at given distance from the transmitter, as well as the variability of the signal strength in close spatial proximity to a particular location [Rap02]. For instance, propagation models are used to estimate the radio coverage area of given transmitter [Rap02].

In channel models, the variation of the received signal strength over distance is due to path loss and shadowing [Gol05]. Path loss model is the average reduction of the signal power of an electromagnetic wave as it travels through space [Gol05]. Shadowing is caused by obstacles in the transmission path between the transmitter and the receiver that attenuate the received signal through

absorption, scattering, diffraction, signal reflection, as well as the location, motion, and material composition of surrounding objects [Gol05]. Some of these factors can vary in an unpredictable manner over time due to environmental dynamics and user movement [Gol05]. For instance, the travel of signals can have a Line Of Sight (LOS) transmission path as well as a path that is blocked by obstacles such as walls and furnitures.

In contrast to the wired channels which are predictable, radio channels are extremely random and do not offer easy analysis [Vij10]. As a result, determining *deterministic* propagation models can become rather complex by considering various propagation effects of the electromagnetic waves [Rap02]. Typically, wireless channel modelling is done *statistically* using measurements [Rap02].

The propagation models that predict the mean signal strength for an arbitrary transmitter-receiver separation distance are called *large-scale* propagation models [Rap02]. These models describe the signal strength over large transmitter-receiver separation distances. On the contrary, propagation models that describe the rapid changes of the received signal over very short distances are called *small-scale* fading models.

In the context of positioning, the channel models are used to estimate the distance at the receiver from the transmitter. For this purpose, a set of channel models is proposed by the High Throughput Task Group (TGn) [Erc04], to provide sufficient channel models for WLAN IEEE 802.11n. These models are consistent with numerous experimentally determined results as well as published results reported in the literature and are usable for both 2 GHz and 5 GHz [Erc04]. Furthermore, the models are advanced Multiple-Input Multiple-Output (MIMO) models that describe the LOS and Non Line Of Sight (NLOS) components of a MIMO channel, the effect of the Doppler components of the channel as well as the expected signal correlation across the antenna arrays [PO08].

The TGn channel models consist of six channel models that were proposed for different environments (Models A-F). The channel models A to C represent small

Table 2.1: Path loss model parameters, reconstructed from [Erc04].

Model	d_{BP} (m)	Slope before d_{BP}	Slope after d_{BP}	Shadow fading before d_{BP}	Shadow fading after d_{BP}
A	5	2	3.5	3	4
B	5	2	3.5	3	4
C	5	2	3.5	3	5
D	10	2	3.5	3	5
E	20	2	3.5	3	6
F	30	2	3.5	3	6

environments, while the models D to F represent larger environments [PO08]. These models are given, from [Erc04], as

$$\begin{aligned} L(d) &= L_{\mathrm{FS}}(d) && d \leq d_{\mathrm{BP}} \\ L(d) &= L_{\mathrm{FS}}(d_{\mathrm{BP}}) + 35\log_{10}(\frac{d}{d_{\mathrm{BP}}}) && d > d_{\mathrm{BP}} \end{aligned}, \tag{2.15}$$

where the first equation gives the free space path loss for distances less than d_{BP}, which is known as the breakpoint and d is the transmitter receiver separation distance. The second equation gives the path loss for distances larger than d_{BP}. Both equations are expressed in decibels, or dB. The term $L_{\mathrm{FS}}(.)$ refers to the free space path loss model which is given, from [Pro98], as

$$L_{\mathrm{FS}}(d) = -10\log_{10} G_t G_r (\frac{c}{4\pi d f})^2, \tag{2.16}$$

where G_t and G_r are the transmit and receive antenna gains respectively, c is the speed of light, and f is the carrier frequency in Hz. For unity antenna gains ($G_t = G_r = 1$) and frequency of 2.4 GHz, equation (2.16) can be written, from [PO08], as

$$L_{\mathrm{FS}}(d) = 40.04\,\mathrm{dB} + 2 \cdot 10\log_{10}\frac{d}{\mathrm{m}}. \tag{2.17}$$

Note that the slope is 2 for the path loss expression in (2.17). For distances larger than d_{BP}, the path loss expression has a slop of 3.5 as can be seen from (2.15).

Table 2.1 contains model mapping to a particular environment. In this table, the

shadow fading values show that for any transmitter/receiver configuration, the propagation environment can differ resulting that the received signal having an average strength differing from (2.15) [PO08].

With shadow fading added to (2.15), the equations can be written, from [PO08], as

$$\begin{aligned} L(d) &= L_{\mathrm{FS}}(d) + n_\sigma & d &\leq d_{\mathrm{BP}} \\ L(d) &= L_{\mathrm{FS}}(d_{\mathrm{BP}}) + 35\log_{10}(\frac{d}{d_{\mathrm{BP}}}) + n_\sigma & d &> d_{\mathrm{BP}} \end{aligned}, \tag{2.18}$$

where n_σ is the random noise mentioned above. Note that the value for σ differs before and after the breaking point as shown in Table 2.1.

Small-scale fading are caused fluctuations of the received signal in amplitude, phase or delays of multipath signals [Rap02]. In WLAN 802.11n which uses Orthogonal Frequency-Division Multiplexing (OFDM), the small-scale fading results in flat fading over all the subcariers of the signal [PO08]. The author of this dissertation ignores the small-scale fading by assuming that the OFDM band is sufficiently large that the overall power average regarding frequency selective fluctuation is unaffected to a large extent.

2.7 State-Space Models

In order to allow a system to use the noisy measurements for location estimation, those noisy (uncertain) measurements need to be represented. Probability theory provides representation for the uncertain measurements and can manipulate these measurements in a consistent manner [Van04; Gil+09]. In general, the measurement data can be either a time-series or a sequence generated by 1-dimensional spatial process [Mur02].

According to [Mur02], different "classical" approaches to time-series prediction are available which use linear models [Ham94] or non-linear models such as de-

cision trees [MCH02]. For discrete date, n-gram models [Jel97] or variable-length Markov models [RST96; McC96] are used widely [Mur02].

According to [Mur02], the state-space models are better than time-series modeling approach where the state-space models do not suffer from finite-window effects, can easily handle discrete and multi-variate inputs and outputs, and they can easily incorporate prior knowledge compared to the classical modeling approaches.

Moreover, the most common used probabilistic models of time-series prediction are the Hidden Markov Models (HMMs) and the Kalman Filter Models (KFMs) [GH00; Mur02]. HMMs represent information about the past through a single discrete random variable which is the hidden state [GH00; Mur02]. If there are n possible states, then $x_k \in \{1, \ldots, o\}$ [Mur02]. On the other side, KFMs represent information about the past through a real-valued hidden state vector [GH00; Mur02], where the state $\mathbf{x}_k$ are continuous random variables $\mathbf{x}_k \in \mathbb{R}^n$ [Mur02]. Note that the term "state-space models" is used widely in literature to describe the KFMs [GH00; Mur02; Van04; Cho14]. In this dissertation however, the author uses the term as well to express the KFMs.

From L&T prospective, it is found by the author that the KFMs fit well into the problem of estimating the location information over the HMMs. This is due to the fact that a KFM holds in its state all the possible values that the mobile object, which needs to be tracked, can take. Therefore, solving for the system state will lead to predict the set of all values for the system of interest.

The state-space models [Mur02; WB] can be written as a set of state and observation models. The dependency between the predicted state (future state) and the present state is specified through the dynamic equations of the system and the noise model. In particular, the dynamic nature of $\mathbf{x}_k \in \mathbb{R}^n$ is written as

$$\mathbf{x}_{k+1} = \mathbf{f}(\mathbf{x}_k, \mathbf{u}_k, \mathbf{w}_k), \tag{2.19}$$

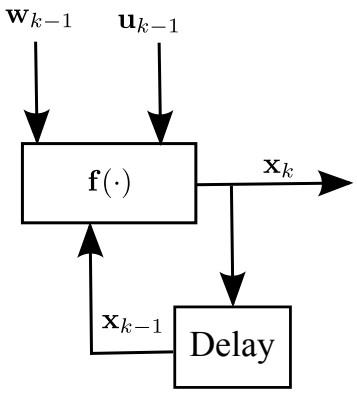

Figure 2.4: State dynamics of a discrete time system.

which is called also the system *process* model [Mur02]. k is the time index of the samples. The function $\mathbf{f}$, possibly non-linear, relates the previous state $\mathbf{x}_{k-1} \in \mathbb{R}^n$ to the current state $\mathbf{x}_k$. The vector $\mathbf{u}_k \in \mathbb{R}^l$ is an optional deterministic control input. For instance in the context of L&T, this optional vector is the acceleration update. The vector of random variables $\mathbf{w}_k \in \mathbb{R}^n$ represents the process uncertainty that derives the dynamic system through the function $\mathbf{f}$. For instance, the acceleration is considered as a control input in a L&T problem. Nevertheless, the state dynamics are depicted in Fig. 2.4. In the observation model, the observation $\mathbf{z}_k$ is related to the system state $\mathbf{x}_k$ and the measurement noise $\mathbf{v}_k$ as given

$$\mathbf{z}_k = \mathbf{h}(\mathbf{x}_k, \mathbf{v}_k), \tag{2.20}$$

where the function $\mathbf{h}$, possibly non-linear, relates the state space to the measurements $\mathbf{z}_k \in \mathbb{R}^m$. The measurements space is the set of all possible observations. The vector of random variables $\mathbf{v}_k \in \mathbb{R}^m$ represents the observation or measurement noise corrupting the state through the function $\mathbf{f}$. Note that the functions $\mathbf{f}(\cdot)$ and $\mathbf{h}(\cdot)$, as well as the value of n and m will be defined later in the dissertation according to the design of the state-space models.

The models presented here will be designed to work linearly as will be presented later in section 3.5. Moreover, the models will be designed to work in a non-linear fashion as will be presented later in section 4.2.

In the context of L&T, the state-space approach to model a moving object involves the state of the object like position, speed and acceleration [FF11; Cho14]. This state is a numerical quantity which is represented by a *vector* [Cho14]. The state includes the complete information about the object in its space where the state $\mathbf{x}$ is defined on the set of all values the object can take [Cho14].

By considering the positioning problem presented in section 2.2, the state $\mathbf{x}_k \in \mathbb{R}^4$ of the mobile node can be expressed, from [FF11; Cho14], as

$$\mathbf{x}_k = [x_k, y_k, v_{x,k}, v_{y,k}]^T, \tag{2.21}$$

where the x_k and $v_{x,k}$ are the position and velocity along the x-axis, y_k and $v_{y,k}$ are the position and velocity along the y-axis, and the superscript T denotes the transpose of the vector. The state $\mathbf{x}_k$ may also be expressed as

$$\mathbf{x}_k = [x_k, y_k]^T, \tag{2.22}$$

where the speed components can be derived from the position if needed.

2.8 The Discrete Kalman Filter

The KF is an *estimator* for estimating the *state* of a *linear dynamic system* that is corrupted by white noise by using *measurements* that are linearly related to the state and corrupted by white noise [GA11]. The KF is considered as optimal recursive filter [May82; BH12].

While the term "filter" in the context of KF is introduced earlier in chapter 1, the word *Optimal* means that the filter minimizes error by some mean and usually there are many ways of defining *optimal*, depending on the criteria chosen to evaluate the performance [May82; BH12]. One aspect of this optimality is that the KF incorporates all available measurements that can be provided to it regardless of their precision, to estimate the current value of the variables of interest, with

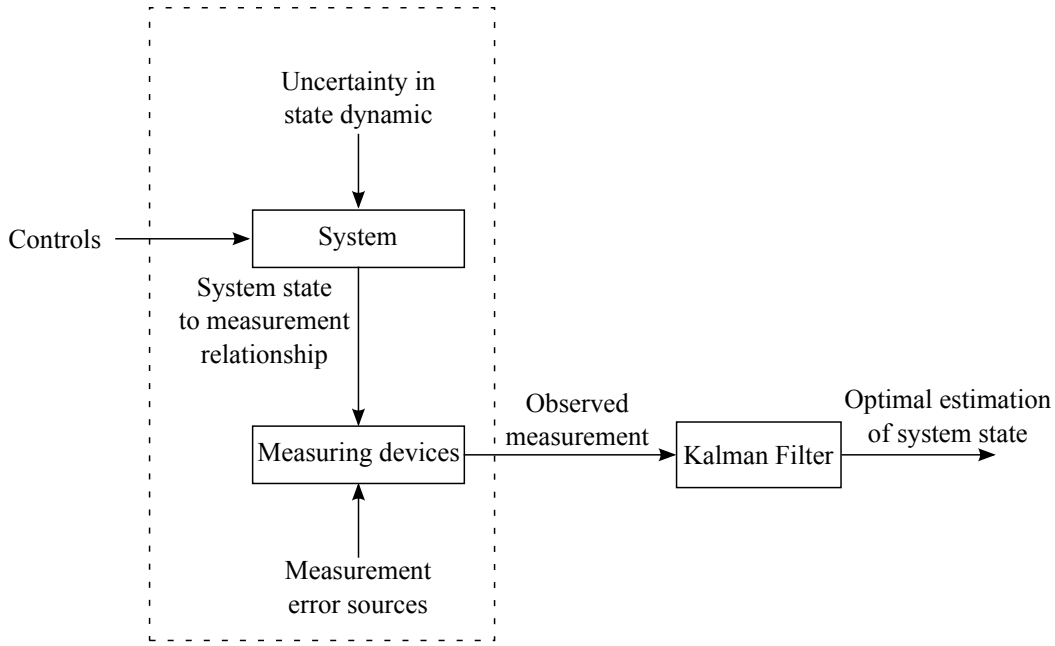

Figure 2.5: Typical Kalman Filter application, inspired by [Rib04].

use of: 1) Knowledge of the system and measurement device dynamics, 2) The statistical description of the system noises, measurement errors, and uncertainty in the dynamic models, and 3) Information about the initial conditions for the variables of interest [May82].

If KF is applied to a system dynamic with non-Gaussian noise and the measurements-to-system function having non-Gaussian noise, the KF can be shown to be the best minimum error variance filter out of the class of linear unbiased filters [May82].

The word "recursive" in the previous description is a mode of operation, in which the results of the previous step are used to help obtaining the desired current step results [May82].

A typical situation in which the KF can be used is depicted in Fig. 2.5, where a system is driven by some known controls, and measuring devices provide the measurements.

In what follows, the computational origins of the KF are presented. This will be done by presenting a re-ordered set of equations that is consistent with their implementation. The equations and their derivation that are presented in this section are based on the literature in [Lac; WB; BH12]. However, the equations presented in this section are rearranged. This filter targets systems that have linear state dynamic and linear relationship between the measurements and the system state. Therefore, the system state dynamic of (2.19) is written in linear form as

$$\mathbf{x}_k = \mathbf{A}\mathbf{x}_{k-1} + \mathbf{B}\mathbf{u}_{k-1} + \mathbf{w}_{k-1}, \tag{2.23}$$

where $\mathbf{A}_{k-1} \in \mathbb{R}^{n\times n}$ is the time-variant matrix which relates the current state $\mathbf{x}_k \in \mathbb{R}^n$ to the previous state $\mathbf{x}_{k-1} \in \mathbb{R}^n$ and $\mathbf{B} \in \mathbb{R}^{n\times l}$ relates the optional control $\mathbf{u} \in \mathbb{R}^l$ to the state $\mathbf{x}$. The measurement function of (2.20) is written in linear form as

$$\mathbf{z}_k = \mathbf{H}\mathbf{x}_k + \mathbf{v}_k, \tag{2.24}$$

where $\mathbf{H} \in \mathbb{R}^{m\times n}$ is the matrix which relates the measurements $\mathbf{z}_k$ to the state $\mathbf{x}_k$.

It is assumed that an initial estimate of the state is known at time t_k and this estimate is based on all the knowledge about the process prior to t_k. This prior, or so called *a priori*, estimate will be denoted as $\hat{\mathbf{x}}_k^-$ where the "hat" denotes estimate and the minus points out that the estimate is the "best" estimate prior to the cooperation with the measurements at t_k. The time t_k is obtained as

$$t_k = k \cdot T_s, \qquad k = \{0, 1, 2, \dots\} \tag{2.25}$$

where k is an integer and T_s is the sampling period. The *a priori* estimation error is

$$\mathbf{e}_k^- \equiv \mathbf{x}_k - \hat{\mathbf{x}}_k^-. \tag{2.26}$$

The estimate of the *a priori* state is obtained from (2.23) as

$$\hat{\mathbf{x}}_k^- = \mathbf{A}_k\hat{\mathbf{x}}_{k-1} + \mathbf{B}\mathbf{u}_{k-1}. \tag{2.27}$$

noting that the noise $\mathbf{w}_{k-1}$ has zero mean. $\hat{\mathbf{x}}_{k-1}$ represents the *a posteriori* state estimate which was updated based on the measurements obtained at t_{k-1}.

The *a priori* estimate error covariance matrix is then obtained from

$$\begin{aligned}\mathbf{P}_k^- &= \mathrm{E}[(\mathbf{e}_k^- \mathbf{e}_k^{-T}] \\ &= \mathrm{E}[\mathbf{x}_k - \hat{\mathbf{x}}_k^-)(\mathbf{x}_k - \hat{\mathbf{x}}_k^-)^T].\end{aligned} \tag{2.28}$$

The estimated *a posteriori* error corresponding to the *a posteriori* (updated) estimate can be defined as

$$\mathbf{e}_{k-1} \equiv \mathbf{x}_{k-1} - \hat{\mathbf{x}}_{k-1}, \tag{2.29}$$

and the associated *a posteriori* error covariance matrix is defined as

$$\begin{aligned}\mathbf{P}_{k-1} &= \mathrm{E}[\mathbf{e}_{k-1}\mathbf{e}_{k-1}^T] \\ &= \mathrm{E}[(\mathbf{x}_{k-1} - \hat{\mathbf{x}}_{k-1})(\mathbf{x}_{k-1} - \hat{\mathbf{x}}_{k-1})^T].\end{aligned} \tag{2.30}$$

In order to predict the *a priori* error covariance matrix $\mathbf{P}_k^-$ from the *a posteriori* error covariance matrix $\mathbf{P}_{k-1}$, the expression for the *a priori* error $\mathbf{e}_k^-$ of (2.26) is written by substituting the values of $\mathbf{x}_k$ and $\hat{\mathbf{x}}_k$ from (2.23) and (2.27) respectively as

$$\begin{aligned}\mathbf{e}_k^- &= \mathbf{A}_{k-1}\mathbf{x}_{k-1} + \mathbf{w}_{k-1} - \mathbf{A}_{k-1}\hat{\mathbf{x}}_{k-1} \\ &= \mathbf{A}_{k-1}\mathbf{e}_{k-1} + \mathbf{w}_{k-1},\end{aligned} \tag{2.31}$$

and the resulting of (2.31) is substituted in (2.28) which results in

$$\begin{aligned}\mathbf{P}_k^- &= \mathrm{E}[(\mathbf{A}_{k-1}\mathbf{e}_{k-1} + \mathbf{w}_{k-1})(\mathbf{A}_{k-1}\mathbf{e}_{k-1} + \mathbf{w}_{k-1})^T] \\ &= \mathbf{A}_{k-1}\mathbf{P}_{k-1}\mathbf{A}_{k-1}^T + \mathbf{Q}_{k-1},\end{aligned} \tag{2.32}$$

where

$$\mathbf{Q}_{k-1} = \mathrm{E}[\mathbf{w}_{k-1}\mathbf{w}_{k-1}^T], \tag{2.33}$$

and noting that $\mathbf{w}_{k-1}$ and $\mathbf{e}_k$ have zero cross correlation.

The next step in deriving the equations of the KF is to improve the *a priori* estimate by finding an equation that computes the *a posteriori* state estimate $\hat{\mathbf{x}}_k$ as a linear function of the *a priori* state estimate $\hat{\mathbf{x}}_k^-$ and a weighted difference between the exact measurement $\mathbf{z}_k$ and the measurement prediction $\mathbf{H}_k\hat{\mathbf{x}}_k^-$ as given

$$\hat{\mathbf{x}}_k = \hat{\mathbf{x}}_k^- + \mathbf{K}_k(\mathbf{z}_k - \mathbf{H}_k\hat{\mathbf{x}}_k^-), \tag{2.34}$$

where $\mathbf{K}_k$ is chosen to be the *gain*, which will be derived later, and the term $(\mathbf{z}_k - \mathbf{H}_k\hat{\mathbf{x}}_k^-)$ is called the measurement innovation [WB].

The $n \times m$ matrix $\mathbf{K}_k$ is chosen to produce optimal estimate update. The optimization can be done by finding the expression for the error covariance matrix associated with the *a posteriori* estimate, differentiating with respect to $\mathbf{K}_k$, setting the result equal to zero and solving for $\mathbf{K}_k$.

The optimization approach minimizes the individual terms of the diagonal of $\mathbf{P}_k$ which represents the estimation error variances for the elements of the state being estimated. To clarify the optimization problem of the error estimation, equation (2.30) is written as

$$\mathbf{P}_k = \begin{bmatrix} \mathrm{E}[e_{1_k}e_{1_k}^T] & \mathrm{E}[e_{1_k}e_{2_k}^T] & \dots & \mathrm{E}[e_{1_k}e_{n_k}^T] \\ \mathrm{E}[e_{2_k}e_{1_k}^T] & \mathrm{E}[e_{2_k}e_{2_k}^T] & \dots & \mathrm{E}[e_{2_k}e_{n_k}^T] \\ \vdots & \vdots & \ddots & \vdots \\ \mathrm{E}[e_{n_k}e_{1_k}^T] & \mathrm{E}[e_{n_k}e_{2_k}^T] & \dots & \mathrm{E}[e_{n_k}e_{n_k}^T] \end{bmatrix}, \tag{2.35}$$

note that the subscript numbers represent the element numbers of the estimation error vector $\mathbf{e}_k$. In the above representation, the sum of the diagonal elements of the matrix is the *trace of a matrix*. In this case, the trace is the sum of the mean square errors. Therefore, minimizing the trace will minimize the mean square estimation error of the state variable $\mathbf{x}_k$.

To get into the optimization process, equation (2.29) is considered for time index k as

$$\mathbf{e}_k \equiv \mathbf{x}_k - \hat{\mathbf{x}}_k. \tag{2.36}$$

By substituting (2.34) into (2.36), then the result into (2.30), it yields

$$\mathbf{P}_k = \mathrm{E}\{[\mathbf{x}_k - \hat{\mathbf{x}}_k^- - \mathbf{K}_k(\mathbf{z}_k - \mathbf{H}_k\hat{\mathbf{x}}_k^-)][\mathbf{x}_k - \hat{\mathbf{x}}_k^- - \mathbf{K}_k(\mathbf{z}_k - \mathbf{H}_k\hat{\mathbf{x}}_k^-)]^T\}. \tag{2.37}$$

Substitute for $\mathbf{z}_k$ from (2.24) into (2.37) results

$$\begin{aligned}\mathbf{P}_k = \mathrm{E}\{&[(\mathbf{x}_k - \hat{\mathbf{x}}_k^-) - \mathbf{K}_k(\mathbf{H}_k\mathbf{x}_k + \mathbf{v}_k - \mathbf{H}_k\hat{\mathbf{x}}_k^-)] \\ &[(\mathbf{x}_k - \hat{\mathbf{x}}_k^-) - \mathbf{K}_k(\mathbf{H}_k\mathbf{x}_k + \mathbf{v}_k - \mathbf{H}_k\hat{\mathbf{x}}_k^-)]^T\}.\end{aligned} \tag{2.38}$$

Taking expectation of the above expression and noting that

$$\begin{aligned}&\mathrm{E}[\mathbf{v}_k] = 0, \\ &\mathrm{E}[\mathbf{v}_k\mathbf{v}_k^T] = \mathbf{R}_k, \\ &\mathrm{E}\{[\mathbf{x}_k - \mathbf{x}_k^-][\mathbf{x}_k - \mathbf{x}_k^-]^T\} = \mathbf{P}_k^-,\end{aligned}$$

result in

$$\mathbf{P}_k = (\mathbf{I} - \mathbf{K}_k\mathbf{H}_k)\mathbf{P}_k^-(\mathbf{I} - \mathbf{K}_k\mathbf{H}_k)^T + \mathbf{K}_k\mathbf{R}_k\mathbf{K}_k^T. \tag{2.39}$$

Here equation (2.39) is a general expression for the error covariance matrix, and it applies for any gain $\mathbf{K}_k$ whether it is optimal or otherwise.

To proceed further in finding the particular $\mathbf{K}_k$ that minimizes the estimation error, we need to recall two matrix differentiation formulas that are needed for the differential approach. They are

$$\frac{d[\mathrm{trace}(\mathbf{AB})]}{d\mathbf{A}} = \mathbf{B}^T, \tag{2.40}$$

$$\frac{d[\mathrm{trace}(\mathbf{ACA})]}{d\mathbf{A}} = 2\mathbf{AC}. \tag{2.41}$$

Expanding the general form for $\mathbf{P}_k$, equation (2.39), results

$$\mathbf{P}_k = \mathbf{P}_k^- - \mathbf{K}_k\mathbf{H}_k\mathbf{P}_k^- - \mathbf{P}_k^-\mathbf{H}_k^T\mathbf{K}_k^T + \mathbf{K}_k(\mathbf{H}_k\mathbf{P}_k^-\mathbf{H}_k^T + \mathbf{R}_k)\mathbf{K}_k^T. \tag{2.42}$$

Differentiating the trace of $\mathbf{P}_k$ with respect to $\mathbf{K}_k$, noting that the trace of $\mathbf{P}_k\mathbf{H}_k^T\mathbf{K}_k^T$ is equal to the trace of $\mathbf{K}_k\mathbf{H}_k\mathbf{P}_k^-$, it yields

$$\frac{d(\text{trace}\,\mathbf{P}_k)}{d\mathbf{K}_k} = -2(\mathbf{K}_k\mathbf{P}_k^-)^T + 2\mathbf{K}_k(\mathbf{H}_k\mathbf{P}_k^-\mathbf{H}_k^T + \mathbf{R}_k). \tag{2.43}$$

Setting the derivative to zero and solving for optimal gain, yields

$$\mathbf{K}_k = \mathbf{P}_k^-\mathbf{H}_k^T(\mathbf{H}_k\mathbf{P}_k^-\mathbf{H}_k^T + \mathbf{R}_k)^{-1}. \tag{2.44}$$

The particular $\mathbf{K}_k$ that minimizes the mean square estimation error is called the *Kalman gain*.

The covariance matrix associated with the optimal estimation can now be computed by substituting the optimal gain expression, that is (2.44), into the general expression for the error covariance matrix given in (2.42). Three different equations yield the same results and can be obtained from this substitution. After some simplification, the result is

$$\begin{aligned}\mathbf{P}_k &= \mathbf{P}_k^- - \mathbf{P}_k^-\mathbf{H}_k^T(\mathbf{H}_k\mathbf{P}_k^-\mathbf{H}^T + \mathbf{R}_k)^{-1}\mathbf{H}_k\mathbf{P}_k^- \\ &= \mathbf{P}_k^- - \mathbf{K}_k\mathbf{H}_k\mathbf{P}_k^- \\ &= (\mathbf{I} - \mathbf{K}_k\mathbf{H}_k)\mathbf{P}_k^-,\end{aligned} \tag{2.45}$$

which updates the error covariance matrix. Equations (2.27), (2.32), (2.44), (2.34), and (2.45) represent the KF recursive equations. The block diagram that illustrates the relationship of the KF to a system with its measurements model is depicted in Fig. 2.6.

Based on all previous information, the operation of the KF can be divided into two modes which are *prediction* and *correction* [WB].

In prediction mode, the KF estimates the state of the system and obtains noisy measurements as a form of feedback. The equations that perform prediction are called *time update equations* [WB], i.e., equations (2.27) and (2.32). These equations

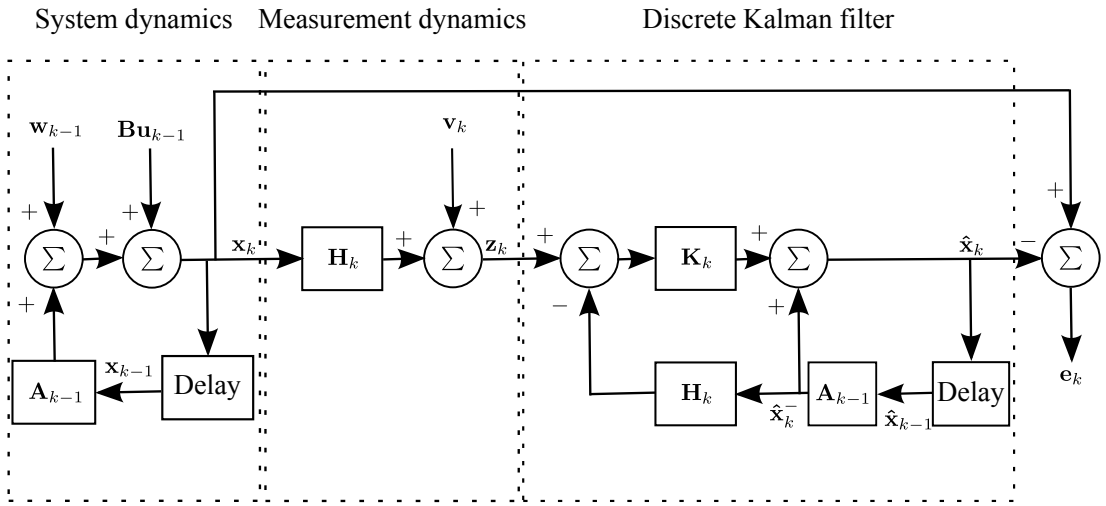

Figure 2.6: Block diagram represents the relationship of a discrete-time system to a discrete-time Kalman Filter, inspired by [GA11].

are responsible for time forwarding of the *a posteriori* state estimate $\hat{\mathbf{x}}_{k-1}$ to obtain the *a priori* state estimate $\hat{\mathbf{x}}_k^-$, and forwarding the *a posteriori* error covariance estimate $\mathbf{P}_{k-1}$ to obtain the *a priori* error covariance estimate $\mathbf{P}_k^-$ for the next time step.

In correction mode of operation, the new obtained measurements are incorporated with the *a priori* estimate to obtain an improved *a posteriori* estimate. The equations that perform correction are called also *measurements update equations* [WB]. Those equations are: 2.34, 2.44 and 2.45.

3 Positioning Framework for RSSI-Based WLAN IEEE 802.11n

3.1 Overview

In this chapter, a positioning framework for RSSI-Based WLAN IEEE 802.11n L&T is designed. In the beginning, a simulation model for validating the proposed L&T solutions through this dissertation is presented. Then, a Linear Least-Squares estimator is developed for positioning purposes. The positioning framework for RSSI-Based WLAN IEEE 802.11n L&T is then designed which is extended to accuracy improvement technologies and is applicable to smartphones and similar devices. Furthermore, a KF implementation is presented which brings advantages over the most common approach "Extended Kalman Filter" in terms of several aspects. The implementation includes the desig of the Kalman Filter models and initializing. The main advantage of this technique is the ability to work on the position estimates to improve their accuracy. This approach is helpful in systems that provide only position estimates where channel measurements are not available for developers.

The validation of the proposed L&T solution is done using a simulation procedure that is presented as well. The simulation is done using Monte Carlo sim-

ulation. Finally, comparative results are presented and discussed. This chapter encompasses the research published in [Kha+14].

3.2 Performance Evaluation Model

For performance evaluation, the author defines a test model for L&T of a mobile node within the WLAN IEEE 802.11n environment. This model is used for testing and evaluating the proposed L&T algorithms throughout this dissertation.

In this model, it is assumed that the mobile node locates itself using information provided by a number of surrounding anchor nodes. The mobile node continuously collects the RSSI measurements $\mathbf{r}_k$ from a number of anchor nodes surrounding it at certain time intervals, where

$$\mathbf{r}_k = \begin{bmatrix} r_k(1) & r_k(2) & \dots & r_k(N) \end{bmatrix}^T, \tag{3.1}$$

and $N \in \{3, 4, 6\}$ is the number of anchor nodes with coordinates

$$\mathbf{p}_{\mathrm{BS}_i} = \begin{bmatrix} x_{\mathrm{BS}_i} \\ y_{\mathrm{BS}_i} \end{bmatrix}, \quad \text{for} \quad i = \{1, 2, \dots, N\}. \tag{3.2}$$

The anchor nodes are equally spaced and located on a circle of a radius of 70 m as shown basically in Fig 3.1. This selection comes from the fact that the WLAN IEEE 802.11n is expected to support distances up to 200 m [09] or even longer distances of up to 250 m [12]. It is reported that it can support distances greater than 90 m within an indoor environment [Low11]. The author selects the *circle of trust* to have a diameter of 150 m. A mobile station that moves outside this circle is expected to drop the connection to at least one of the surrounding anchor nodes and will therefore lose the ability to estimate its position as explained earlier in sec. 2.7.

The coordinates of the anchor nodes are given in table 3.1.

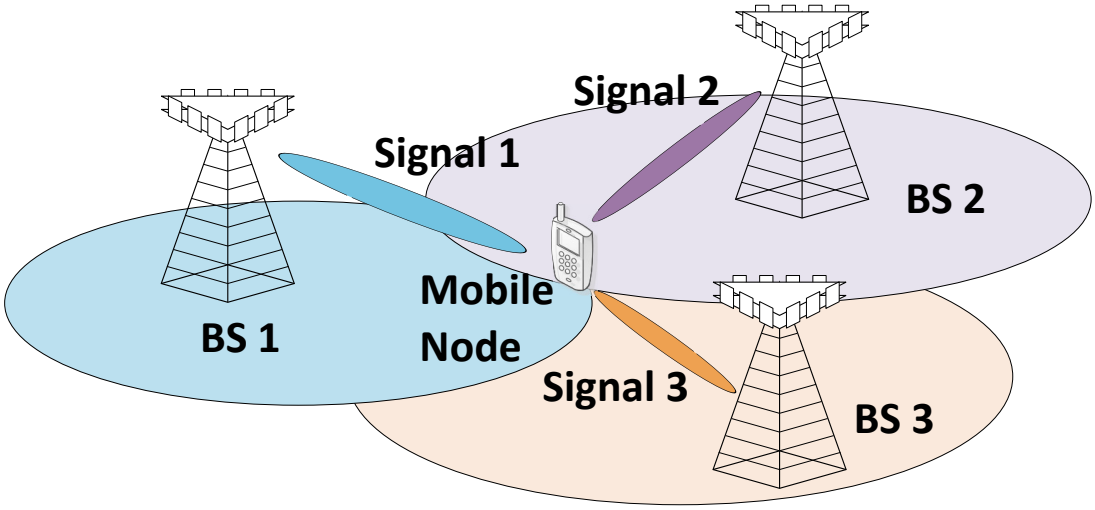

Figure 3.1: Positioning based on distance measurements.

Table 3.1: Anchor nodes coordinates.

3 Anchor Nodes		4 Anchor Nodes		6 Anchor Nodes	
x	y	x	y	x	y
-60.62	-35.00	-70.00	0.00	-60.62	35.00
60.62	-35.00	0.00	-70.00	-60.626	-35.00
0.00	70.00	70.00	-0.00	0.00	-70.00
		0.00	70.00	60.62	-35.00
				60.62	35.00
				0.00	70.00

The measurement vector $\mathbf{r}_k$ is converted to a distance vector, denoted as

$$\mathbf{z}_k = \begin{bmatrix} z_k(1) & z_k(2) & \dots & z_k(N) \end{bmatrix}^T, \tag{3.3}$$

based on one of the High Throughput Task Group (TGn) channel models [Erc04]. TGn proposed sufficient channel models for WLAN IEEE 802.11 n that can be used in both small and large indoor environments. These models are presented in section 2.6.

The proposed positioning algorithms are implemented in the mobile node to use the distances vector $\mathbf{z}_k$ and the anchor nodes' coordinates $\mathbf{p}_{\text{anc}_i}$, where i is an element of $\{1, \dots, N\}$, in different ways accordingly to locate and track the mobile node.

In order to evaluate the proposed L&T algorithms and to define the movement patterns of a mobile node, a motion model is needed for these purposes. In general, pedestrian motion models are rather complex and governed by decision models, choice of destination, and interaction with other people [Ant05; KPV10]. In this dissertation, the pedestrian motion model is described by linear differential equations, to be followed, in which the acceleration u is random and uniformly distributed, i.e.

$$f(u) = \begin{cases} \frac{1}{0.5-(-0.5)} & -0.5\,\frac{\text{m}}{\text{s}^2} \leq u \leq 0.5\,\frac{\text{m}}{\text{s}^2} \\ 0 & \text{otherwise} \end{cases} \tag{3.4}$$

In the above equation, the interval $[-0.5\,\frac{\text{m}}{\text{s}^2}, 0.5\,\frac{\text{m}}{\text{s}^2}]$ is selected to ensure that the speed is mostly not exceeding 1.5 m/s which is assumed to be the maximum pedestrian speed.

By knowing that the acceleration u^x_{k-1} of the x coordinate at time index $k-1$ is the change of velocity with time [WHT10], i.e.

$$u^x_{k-1} = \frac{\Delta v}{\Delta t} = \frac{v^x_k - v^x_{k-1}}{t_k - t_{k-1}} \quad , \tag{3.5}$$

the speed v_k^x of x coordinate at time index k can be obtained from the speed v_{k-1}^x of x coordinate at time index $k-1$ by writing (3.5) as which results in

$$v_k^x = v_{k-1}^x + Tu_{k-1}^x, \tag{3.6}$$

where

$$T = t_k - t_{k-1}, \tag{3.7}$$

the displacement of the x coordinate, i.e. $x_k - x_{k-1}$, is then calculated from the area of a trapezoid [Mor14] between the speed v_{k-1} at time t_{k-1} and the speed v_k at time t_k, i.e.

$$x_k - x_{k-1} = \frac{1}{2}T(v_k^x + v_{k-1}^x). \tag{3.8}$$

Substituting (3.6) into (3.8) yields

$$x_k = x_{k-1} + Tv_{k-1}^x + \frac{1}{2}T^2u_{k-1}^x. \tag{3.9}$$

A similar formula for the speed v_k^y of the y coordinate can be written as

$$v_k^y = v_{k-1}^y + Tu_{k-1}^y, \tag{3.10}$$

with similar formula of the position y_k of the y coordinate as

$$y_k = y_{k-1} + Tv_{k-1}^y + \frac{1}{2}T^2u_{k-1}^y. \tag{3.11}$$

In the motion model, the mobile node starts to move from the center of simulation area $(0, 0)$ driven by the random acceleration which leads to random velocity and position at each time instant of the mobile node. For performance evaluation purpose, 100 random traces are adopted in which each trace is repeated 100 times to have different measurement noise conditions so that a total of 10000 random traces are generated. All the generated traces end before exceeding the circle of 75 m which is the *circle of trust*.

To demonstrate how the mobile node moves according to the proposed motion

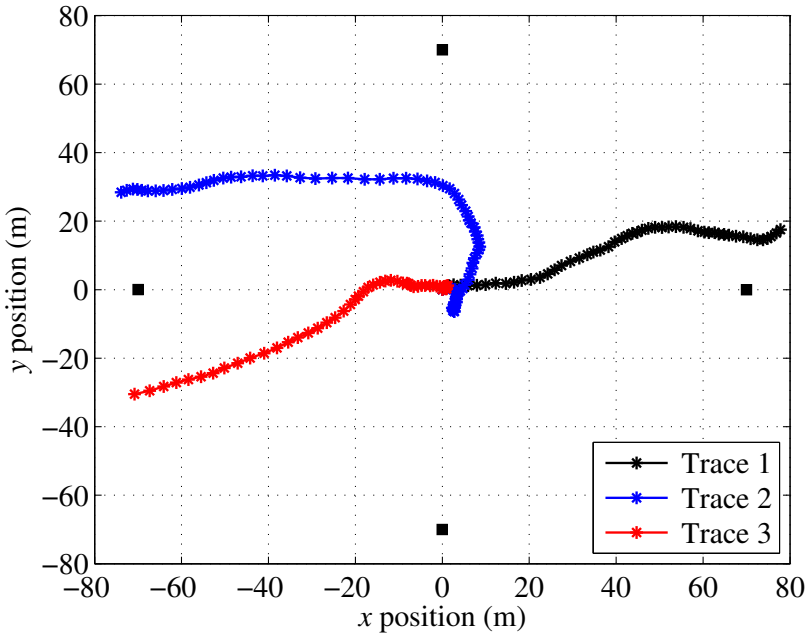

Figure 3.2: Three movement traces of a mobile node surrounded with four anchor nodes.

model, Figure 3.2 is given. In this figure, three different traces are generated according to the proposed model.

3.3 Linear Least-Square Estimator Design

In the context of wireless positioning, LS can be used to approximate a set of wireless channel measurements in order to estimate the position of a certain MS [FF11]. The estimated position is obtained through minimizing the sum of the squares of the errors between a *model* that relates the position to the wireless measurements and the actual wireless channel measurements [FF11]. In the beginning, the equations of the LLS estimator [FF11] is presented with respect to a model. To obtain the model, the author proposes trilateration and a linearized system of equations [Waa+10a]. Once the model is known, the position can be estimated using LLS method.

By considering the positioning problem of section 2.2, the mobile node with coordinates

$$\mathbf{x} = [x, y]^T, \tag{3.12}$$

receives the distance measurements

$$\mathbf{z} = [z_1, z_2, \ldots, z_N]^T, \tag{3.13}$$

from N BSs. Let $h_i(\mathbf{x})$ be the model that relates the position coordinates $\mathbf{x}$ to the distance measurement z_i obtained from the ith BS such that

$$z_i = h_i(\mathbf{x}) + \eta_i, \qquad i = \{1, 2, \ldots, N\} \tag{3.14}$$

where η_i is ith measurement noise component added to the model. Equation (3.14) can be rewritten in matrix formulation as follows

$$\mathbf{z} = \mathbf{H}(\mathbf{x}) + \boldsymbol{\eta}, \tag{3.15}$$

where

$$\mathbf{H}(\mathbf{x}) = \begin{bmatrix} h_1(\mathbf{x}) \\ h_2(\mathbf{x}) \\ \cdots \\ h_N(\mathbf{x}) \end{bmatrix}, \qquad \boldsymbol{\eta} = \begin{bmatrix} \eta_1 \\ \eta_2 \\ \cdots \\ \eta_N \end{bmatrix}. \tag{3.16}$$

Now the goal is to find an estimate of the unknown $\mathbf{x}$, which is denoted by $\hat{\mathbf{x}}$. According to LS, this estimation is done by minimizing the sum of squares of $z_i - h_i(\mathbf{x})$ such that the cost function $c(\mathbf{x})$ is minimized. The cost function is written as

$$c(\mathbf{x}) = \sum_{i=1}^{N} \eta_i^2 = \sum_{i=1}^{N} [z_i - h_i(\mathbf{x})]^2 = [\mathbf{z} - \mathbf{H}(\mathbf{x})]^T [\mathbf{z} - \mathbf{H}(\mathbf{x})]. \tag{3.17}$$

The estimated position $\mathbf{x}$ is determined as argument that minimize the cost function $c(\mathbf{x})$, i.e.,

$$\hat{\mathbf{x}} = \arg \min_{\mathbf{x}} \{c(\mathbf{x})\}. \tag{3.18}$$

The solution to (3.18) can be obtained by letting the cost function $c(\mathbf{x})$ achieve its

minimum value which is done when its derivatives with respect to $\mathbf{x}$ are equal to zero as given

$$\frac{dc(\mathbf{x})}{d\mathbf{x}} = \frac{d}{d\mathbf{x}}[(z_1 - h_1(\mathbf{x}))^2 + (z_2 - h_2(\mathbf{x}))^2 + \cdots + (z_n - h_n(\mathbf{x}))^2] = 0, \tag{3.19}$$

with further manipulation

$$\begin{aligned} \frac{dc(\mathbf{x})}{d\mathbf{x}} &= -2[(z_1 - h_1(\mathbf{x}))\frac{dh_1(x)}{d\mathbf{x}} + (z_2 - h_2(\mathbf{x}))\frac{dh_2(\mathbf{x})}{d\mathbf{x}} \\ &\quad + \cdots + (z_n - h_n(\mathbf{x}))\frac{dh_n(\mathbf{x})}{d\mathbf{x}}] = 0. \end{aligned} \tag{3.20}$$

Equation (3.20) can be written in matrix formulation as

$$\frac{dc(\mathbf{x})}{d\mathbf{x}} = -2[\mathbf{z}^T - \mathbf{H}(\mathbf{x})^T]\frac{d\mathbf{H}(\mathbf{x})}{d\mathbf{x}} = 0. \tag{3.21}$$

If the model is non-linear, numerical optimization might be required [FF11] to get a solution for $\mathbf{x}$. The *Linear Least-Squares* (LLS) assumes that the model of (3.14) or (3.15) is linear, i.e.,

$$\begin{bmatrix} z_1 \\ z_2 \\ \vdots \\ z_N \end{bmatrix} = \begin{bmatrix} h_{11} & h_{12} \\ h_{21} & h_{22} \\ \vdots & \vdots \\ h_{N1} & h_{2N} \end{bmatrix} \begin{bmatrix} x \\ y \end{bmatrix} + \begin{bmatrix} \eta_1 \\ \eta_2 \\ \vdots \\ \eta_N \end{bmatrix}, \tag{3.22}$$

or

$$\mathbf{z} = \mathbf{H}\mathbf{x} + \boldsymbol{\eta}. \tag{3.23}$$

The linearity simplifies the mathematical formulation of the LS, which is given in (3.21), in the sense that it is possible to get a closed-form solutions for the parameters that minimizes the cost function $c(\mathbf{x})$. By comparing (3.15) and (3.23), we have

$$\mathbf{H}(\mathbf{x}) = \mathbf{H}\mathbf{x}. \tag{3.24}$$

Substituting (3.24) into (3.21) results

$$\frac{dc(\mathbf{x})}{d\mathbf{x}} = -2[\mathbf{z}^T - \mathbf{x}^T\mathbf{H}^T]\frac{d\mathbf{H}\mathbf{x}}{d\mathbf{x}} = 0, \tag{3.25}$$

with further manipulation

$$\mathbf{z}^T\mathbf{H} = \mathbf{x}^T\mathbf{H}^T\mathbf{H}. \tag{3.26}$$

Transposing both sides of (3.26), we have

$$\mathbf{H}^T\mathbf{H}\mathbf{x} = \mathbf{H}^T\mathbf{z}, \tag{3.27}$$

with further manipulation, the $\mathbf{x}$ can be obtained as

$$\mathbf{x} = (\mathbf{H}^T\mathbf{H})^{-1}\mathbf{H}^T\mathbf{z} \tag{3.28}$$

In order to define the model, the trilateration technique which is introduced in section 2.4.2 is considered for this purpose.

Trilateration establishes a set of N non-linear equations. Several solution methods are proposed to deal with the non-linear equations such as the minimum path discovery [Mas06] and the linearized system of equations [MH95; Waa+10a]. The later establishes a set of linear equations out of the non-linear equations obtained from (2.10).

By considering section 2.4.2, the following equation

$${d_i}^2 = (x_{\mathrm{BS}_i} - x)^2 + (y_{\mathrm{BS}_i} - y)^2 \qquad i = \{1, \ldots, N\}, \tag{3.29}$$

is constructed for each surrounding anchor node. As a result, N non-linear equations are generated which need to be solved for location estimation.

Due to the noise, every ranging result is the estimation $\hat{d}_i$ of the exact distance d_i between the mobile node and the ith anchor node. The estimation $\hat{d}_i$ is generally error prone. The ranging error of the distance between the mobile node and the

ith anchor node can be given as

$$n_{d_i} = \hat{d}_i - d_i. \tag{3.30}$$

The author proposes the linearized system of equations solution which is first presented as ideal case, i.e. without noise, in [MH95] and later presented with noise in [Waa+10a] to establish a set of linear equations that can be solved using LLS.

This solution can be obtained by subtracting (3.29) for BS_i from the adjacent equivalent expression for BS_{i+1}. By rewriting (3.29) in matrix vector form and introducing ranging error n_{d_i} which is defined in (3.30), we have

$$\hat{d}_i^2 - 2n_{d_i}\hat{d}_i + {n_{d_i}}^2 = |\mathbf{x} - \mathbf{p}_{\mathrm{BS}_i}|^2. \tag{3.31}$$

Subtracting adjacent quadratic equations (i) and $(i+1)$ yields N equations

$$\hat{d}_{i+1}^2 - \hat{d}_i^2 - n_{\Delta d^2,i,i+1} = |\mathbf{x} - \mathbf{p}_{\mathrm{BS}_{i+1}}|^2 - |\mathbf{x} - \mathbf{p}_{\mathrm{BS}_i}|^2, \tag{3.32}$$

which are linear with the unknown variable $\mathbf{x}$. The term $n_{\Delta d^2,i,i+1}$ contains the noise differences as given

$$n_{\Delta d^2,i,i+1} = -2n_{d_{i+1}}\hat{d}_{i+1} + 2n_{d_i}\hat{d}_i + n_{d_{i+1}}^2 - n_{d_i}^2. \tag{3.33}$$

The set of N equations of (3.32) can be written as follows

$$\mathbf{H} \cdot \mathbf{x} = \mathbf{b} - \mathbf{n}_{\Delta d^2}, \tag{3.34}$$

where

$$\mathbf{H} = \begin{bmatrix} x_{\mathrm{BS}_2} - x_{\mathrm{BS}_1} & y_{\mathrm{BS}_2} - y_{\mathrm{BS}_1} \\ \vdots & \vdots \\ x_{\mathrm{BS}_N} - x_{\mathrm{BS}_N - 1} & y_{\mathrm{BS}_N} - y_{\mathrm{BS}_N - 1} \\ x_{\mathrm{BS}_1} - x_{\mathrm{BS}_N} & x_{\mathrm{BS}_1} - x_{\mathrm{BS}_N} \end{bmatrix}, \tag{3.35}$$

the **b** vector

$$b_i = \begin{cases} \dfrac{d_{i+1}^2 - d_i^2 - x_{\mathrm{BS}_{i+1}}^2 + x_{\mathrm{BS}_i}^2 - y_{\mathrm{BS}_{i+1}}^2 + y_{\mathrm{BS}_i}^2}{2} & i < N \\ \dfrac{d_1^2 - d_N^2 - x_{\mathrm{BS}_1}^2 + x_{\mathrm{BS}_N}^2 - y_{\mathrm{BS}_1}^2 + y_{\mathrm{BS}_N}^2}{2} & i = N \end{cases}, \tag{3.36}$$

and the noise vector

$$\mathbf{n}_{\Delta d^2} = \begin{cases} -2n_{d_{i+1}}\hat{d}_{i+1} + 2n_{d_i}\hat{d}_i + n_{d_{i+1}}^2 - n_{d_i}^2 & , \quad i < N \\ -2n_{d_1}\hat{d}_1 + 2n_{d_i}\hat{d}_i + n_{d_1}^2 - n_{d_i}^2 & , \quad i = N \end{cases}. \tag{3.37}$$

A solution to (3.34) can be done by neglecting the error component and solving for the position. This equation can be solved using the LLS method which is presented in section 3.3 as given

$$\hat{\mathbf{x}} = (\mathbf{H}^T\mathbf{H})^{-1}\mathbf{H}^T\mathbf{b}. \tag{3.38}$$

Here, the LS method will produce identical results with the maximum likelihood estimator if the measurements have a Gaussian distribution which is the case in our assumptions. The position estimation using trilateration which is formulated using linearized system of equation is summarized in Algorithm 3.1.

Algorithm 3.1 Position estimation using trilateration and linearized system of equation.

1: **procedure** LINEARIZED SYSTEM OF EQUATION FORMULATION
2: Obtain the measurements **d**;
3: Formulate (3.35) and (3.36);
4: **end procedure**
5: **procedure** LINEAR LEAST-SQUARES IMPLEMENTATION
6: Obtain the estimated position $\hat{\mathbf{x}}$ from (3.38).
7: **end procedure**

3.4 Framework Structure

The positioning framework for IEEE 802.11n is designed and implemented in MATLAB. The functional architecture of the framework is shown in Fig. 3.3 which consists of 4 layers as given

1. *Measurement layer*

   The measurement layer contains the operations needed to measure the RSSI values $\mathbf{r} \in \mathbb{R}^N$. These values are expressed in *Decibel* (dB). In the design, a set of 200 values is chosen to represent different RSSI values. After measurements, the RSSI values go to the quantization layer. A large set of measurements had been taken into consideration due to the measurement errors which in turns produce estimated position errors.

2. *Quantization layer*

   This layer converts the RSSI measurements $\mathbf{r}$ to quantized values $\hat{\mathbf{r}} \in \mathbb{R}^N$ after receiving these values from the measurement layer. In the design, a set of 200 values is defined to represent the quantized values with quantization level of 1 dB.

3. *Estimation*

   As depicted in Fig. 3.3, the estimation layer consists of further two subfunctions for converting the received power to *distance estimates* and to convert those estimates into *position estimates*.

   The quantized RSSI measurements $\hat{\mathbf{r}}$ are converted to *distance estimates* $\hat{\mathbf{d}} \in \mathbb{R}^N$ according to a channel model proposed by the *High Throughput Task Group* (TGn) [Erc04]. Six models have been proposed for different environments. The TGn models are presented in section 2.6. The author chooses the model F out of the six channel models. This model is intended for indoor large environment and has the biggest shadow noise of 6 dB standard

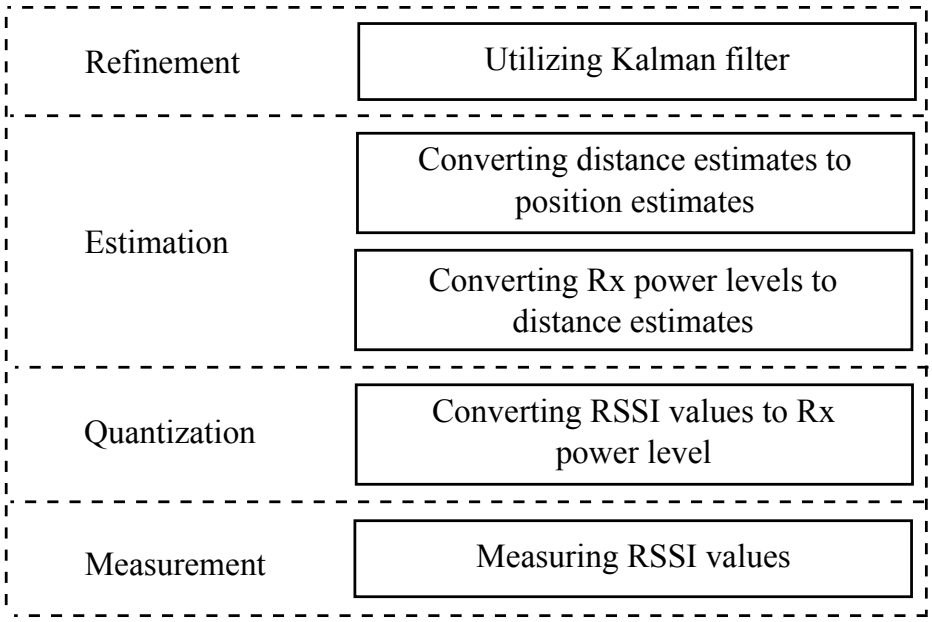

Figure 3.3: Positioning framework for IEEE 802.11 n system, inspired by [Kot+03].

deviation among other models. This noise influences the RSSI and hence the position estimates.

Generally, propagation model is a result of reflections, diffractions, and multi-path effects. In addition, other parameters such as walls, building structure, obstacles and moving objects have influence on the propagation model. These factors make using of propagation model for localization almost impossible. Figure 3.4 compares measurements having 6 dB standard deviation noise with the path loss model F in its ideal case, i.e. without noise.

The LLS estimator, which is presented in section 3.3, is used to convert distance estimates $\hat{\mathbf{d}}$ into *position estimates* $\hat{\mathbf{x}}$ based on the knowledge of the locations of the surrounding anchor nodes.

4. *Refinement*

This layer enables refinement of the position estimates. In this layer, the KF which is designed in section 3.6 is implemented so that the position mea-

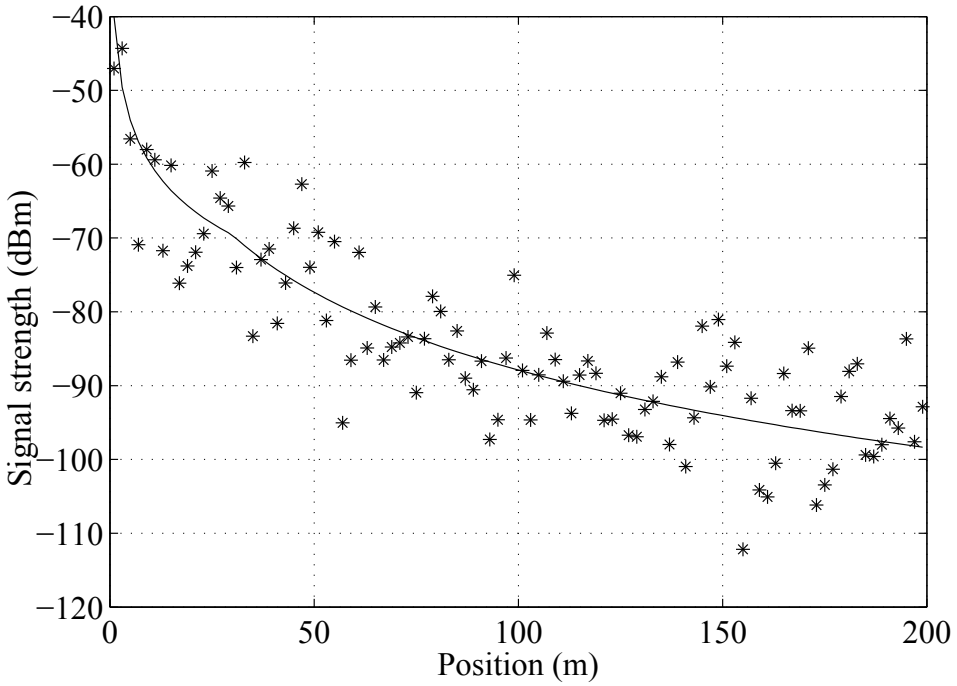

Figure 3.4: WLAN IEEE 802.11n propagation model with measurements having 6 dB standard deviation noise.

surements are combined with expected estimates for better results. The KF is implemented to work with the position estimates in order to obtain improved position estimates. As such, this layer does not rely directly on the distance estimates in the estimation layer. Therefore, further data fusion, replacing, and removing or changing the KF can be done without additional setup to the KF. In addition, different position accuracy improvement techniques intended for linear systems can be used in this layer as alternative to the designed KF without further changing in other layers.

3.5 Linear State Space Models Design

By referring to positioning problem given in section 2.2, it is desired to design the state-space models that are presented in section 2.7.

Based on the proposed motion model of section 3.2, it is possible to write the system state dynamics equation for the state to be estimated. More specifically, the equations (3.6), (3.9), (3.10), and (3.11) are used to design the state dynamics in matrix form as

$$\begin{bmatrix} x_k \\ y_k \\ v_k^x \\ v_k^y \end{bmatrix} = \begin{bmatrix} 1 & 0 & T & 0 \\ 0 & 1 & 0 & T \\ 0 & 0 & 1 & 0 \\ 0 & 0 & 0 & 1 \end{bmatrix} \begin{bmatrix} x_{k-1} \\ y_{k-1} \\ v_{k-1}^x \\ v_{k-1}^y \end{bmatrix} + \begin{bmatrix} \frac{1}{2}T^2 & 0 & 0 & 0 \\ 0 & \frac{1}{2}T^2 & 0 & 0 \\ 0 & 0 & T & 0 \\ 0 & 0 & 0 & T \end{bmatrix} \begin{bmatrix} u_{k-1}^x \\ u_{k-1}^y \\ u_{k-1}^x \\ u_{k-1}^y \end{bmatrix} + \begin{bmatrix} w_{k-1}^1 \\ w_{k-1}^2 \\ w_{k-1}^3 \\ w_{k-1}^4 \end{bmatrix}, \quad (3.39)$$

or

$$\mathbf{x}_k = \mathbf{A}\mathbf{x}_{k-1} + \mathbf{B}\mathbf{u}_{k-1} + \mathbf{w}_{k-1}, \quad (3.40)$$

where $\mathbf{x}_k \in \mathbb{R}^4$ is the process state vector at time t_k. $\mathbf{A} \in \mathbb{R}^{4x4}$ is the matrix relating the state $\mathbf{x}_{k-1} \in \mathbb{R}^4$ of the previous time step t_{k-1} to the state $\mathbf{x}_k$ of the current time state k which is written as

$$\mathbf{A} = \begin{bmatrix} 1 & 0 & T & 0 \\ 0 & 1 & 0 & T \\ 0 & 0 & 1 & 0 \\ 0 & 0 & 0 & 1 \end{bmatrix}. \quad (3.41)$$

$\mathbf{B} \in \mathbb{R}^{4\times4}$ is the matrix relating the acceleration vector $\mathbf{u}_{k-1} \in \mathbb{R}^4$ of the previous time step t_{k-1} to the state $\mathbf{x}_k$ of the current time state k which is written as

$$\mathbf{B} = \begin{bmatrix} \frac{1}{2}T^2 & 0 & 0 & 0 \\ 0 & \frac{1}{2}T^2 & 0 & 0 \\ 0 & 0 & T & 0 \\ 0 & 0 & 0 & T \end{bmatrix}, \quad (3.42)$$

and $\mathbf{u}_{k-1} \in \mathbb{R}^4$ is the acceleration vector which is randomly generated according

to section 3.2 and is written as

$$\mathbf{u}_{k-1} = \begin{bmatrix} u_{k-1}^{x} \\ u_{k-1}^{y} \\ u_{k-1}^{x} \\ u_{k-1}^{y} \end{bmatrix}. \tag{3.43}$$

$\mathbf{w}_{k-1} \in \mathbb{R}^4$ is the process uncertainty vector with covariance matrix $\mathbf{Q}_{k-1}$ that has the following structure

$$\mathbf{E}[\mathbf{w}_{k-1}{\mathbf{w}_{i-1}}^T] = \begin{cases} \mathbf{Q}_{k-1}, & i = k \\ 0, & i \neq k \end{cases} \tag{3.44}$$

where the covariance matrix $\mathbf{Q}_{k-1}$ is obtained from the calculated variances of the state x_{k-1} after operating the KF. Nevertheless, determining the matrix will follow in section 3.6. The measurements are assumed to hold the position estimate $\hat{\mathbf{x}}_{\mathrm{tr}_k} \in \mathbb{R}^2$ which are obtained from Algorithm 3.1, i.e,

$$\begin{bmatrix} z_k^1 \\ z_k^2 \end{bmatrix} = \begin{bmatrix} \hat{x}_{\mathrm{tr}_k} \\ \hat{y}_{\mathrm{tr}_k} \end{bmatrix} \tag{3.45}$$

or

$$\mathbf{z}_k = \hat{\mathbf{x}}_{\mathrm{tr}_k}, \tag{3.46}$$

where $\mathbf{z}_k \in \mathbb{R}^2$ is the measurement vector at time t_k and the subscript "tr" denotes to trilateration. The state to measurement equation is then written as

$$\begin{bmatrix} z_k^1 \\ z_k^2 \end{bmatrix} = \begin{bmatrix} 1 & 0 \\ 0 & 1 \end{bmatrix} \begin{bmatrix} x_k \\ y_k \end{bmatrix} + \begin{bmatrix} v_k^1 \\ v_k^2 \end{bmatrix}, \tag{3.47}$$

or

$$\mathbf{z}_k = \mathbf{H} \begin{bmatrix} x_{k-1} \\ y_{k-1} \end{bmatrix} + \mathbf{v}_k, \tag{3.48}$$

where $\mathbf{H} \in \mathbb{R}^{2\times 2}$ is the matrix relates the measurements $\mathbf{z}_k$ to the state $\mathbf{x}_k$ which

is written as

$$\mathbf{H} = \begin{bmatrix} 1 & 0 \\ 0 & 1 \end{bmatrix}. \tag{3.49}$$

$\mathbf{v}_k \in \mathbb{R}^2$ is the measurements state noise vector which has known covariance matrix $\mathbf{R}_k$ with the following structure

$$\mathbf{E}[\mathbf{v}_k \mathbf{v}_i{}^T] = \begin{cases} \mathbf{R}_k, & i = k \\ 0, & i \neq k \end{cases}, \tag{3.50}$$

However, the determining of the matrix will follow in section 3.6. The random noise variables $\mathbf{w}_k$ and $\mathbf{v}_k$ have zero mean and are independent of each other, i.e.

$$\mathbf{E}[\mathbf{w}_{k-1} \mathbf{v}_i{}^T] = 0, \quad \text{for all } k \text{ and } i. \tag{3.51}$$

3.6 Kalman Filter Implementation Design

The models given in (3.40) and (3.48) form the fundamental of the KF design. In addition, the covariance matrix $\mathbf{Q}$ of the model of (3.40) and the covariance matrix $\mathbf{R}$ of (3.48) are essential to be declared. Moreover, the error covariance matrix $\mathbf{P}_0$ and the *zeroth* state $\hat{\mathbf{x}}_0$ need to be initialized. Then, an update of the position estimate can be done based on the information provided to the filter.

The author assumes that the covariances $\mathbf{Q}$ and $\mathbf{R}$ are not changing throughout the operation of the KF and therefore the subscript "k" is dropped from both matrices. For convenience, the calculation process of the measurement noise covariance $\mathbf{R}$ is proceeding the calculation of the state uncertainty covariance $\mathbf{Q}$.

The measurement noise covariance is associated with the noisy measurements of the position,i.e.

$$\mathbf{R} = \begin{bmatrix} E[v_1 v_1] & E[v_1 v_2] \\ E[v_2 v_1] & E[v_2 v_2] \end{bmatrix}. \tag{3.52}$$

Assuming that the individual noises v_1 and v_2 are uncorrelated, the variances $\sigma^2_{v_1}$ and $\sigma^2_{v_2}$ of the relating coordinates x and y respectively can be calculated from the estimated position using the developed Algorithm 3.1, resulting as

$$\mathbf{R} = \begin{bmatrix} \sigma^2_{v_1} & 0 \\ 0 & \sigma^2_{v_2} \end{bmatrix}. \tag{3.53}$$

Based on the simulation results of x_k and y_k, both $\sigma^2_{v_1}$ and $\sigma^2_{v_2}$ are found to be equal to $1558\,\mathrm{m}^2$.

The state uncertainty covariance matrix $\mathbf{Q}$ is impossible to be determined prior to the operation of the KF since there is no prior knowledge available of the process output. Therefore, the $\mathbf{Q}$ is approximately initialized so that the KF can work in an *off-line* mode of operation. In this mode, the main and the only concern is to measure the matrix $\mathbf{Q}$ for an *on-line* mode of operation of the KF.

The covariance matrix $\mathbf{Q}$ is associated with the state uncertainty, i.e.

$$\mathbf{Q} = \begin{bmatrix} E[w_1 w_1] & E[w_1 w_2] & E[w_1 w_3] & E[w_1 w_4] \\ E[w_2 w_1] & E[w_2 w_2] & E[w_2 w_3] & E[w_2 w_4] \\ E[w_3 w_1] & E[w_3 w_2] & E[w_3 w_3] & E[w_3 w_4] \\ E[w_4 w_1] & E[w_4 w_2] & E[w_4 w_3] & E[w_4 w_4] \end{bmatrix}. \tag{3.54}$$

During the offline-mode, the variance $\sigma^2_{w_1}$ for the position's coordinate x, the variance $\sigma^2_{w_2}$ for the position's coordinate y, the variance $\sigma^2_{w_3}$ for the velocity of the x coordinate and the variance $\sigma^2_{w_4}$ for the velocity of the y coordinate are initialized, resulting in

$$\mathbf{Q} = \begin{bmatrix} \sigma^2_{w_1} & 0 & 0 & 0 \\ 0 & \sigma^2_{w_2} & 0 & 0 \\ 0 & 0 & \sigma^2_{w_3} & 0 \\ 0 & 0 & 0 & \sigma^2_{w_4} \end{bmatrix}. \tag{3.55}$$

From the *off-line* mode, new variances $\sigma^2_{w_1}$, $\sigma^2_{w_2}$, $\sigma^2_{w_3}$ and $\sigma^2_{w_4}$ can be obtained. These variances used to update the covariance matrix $\mathbf{Q}$ for the *on-line* mode of oper-

ation for the KF. According to simulations, the values of the *off-line* mode and the *on-line* have similar output results of the KF. Nevertheless, the values of the *off-line* mode as well as the *on-line* mode are given in Table 3.2.

Table 3.2: Process noise covariance values.

off-line mode		on-line mode	
Sigma	Value	Sigma	Value
$\sigma^2_{w_1}$	366.5 m^2	$\sigma^2_{w_1}$	196 m^2
$\sigma^2_{w_2}$	366.5 m^2	$\sigma^2_{w_2}$	196 m^2
$\sigma^2_{w_3}$	366.5 $\frac{\mathrm{m}^2}{\mathrm{s}^2}$	$\sigma^2_{w_3}$	35 $\frac{\mathrm{m}^2}{\mathrm{s}^2}$
$\sigma^2_{w_4}$	366.5 $\frac{\mathrm{m}^2}{\mathrm{s}^2}$	$\sigma^2_{w_4}$	35 $\frac{\mathrm{m}^2}{\mathrm{s}^2}$

To complete initializing the KF, the error covariance matrix $\mathbf{P}_{k-1}$ can be initialized for $k = 1$ as

$$\mathbf{P}_{k-1} = \mathbf{Q}, \tag{3.56}$$

and the *zeroth* state $\hat{\mathbf{x}}_0$ is initialized. The initial value for $\hat{\mathbf{x}}_0$ can be obtained from the LLS presented in Algorithm 3.1 as

$$\hat{\mathbf{x}}_0 = \begin{bmatrix} \hat{\mathbf{x}}_{\mathrm{tr}_0} \\ 0 \\ 0 \end{bmatrix}, \tag{3.57}$$

where the subscript "tr" refers to trilateration and the velocities v_k^x and v_k^y of the *zeroth* state $\hat{\mathbf{x}}_0$ are initialized to zero.

After completing the inizialization of the KF, the equations of the KF [GA11; BH12] can be implemented. By referring to the system dynamic model given in (3.40), the *a priori* estimation of the state is obtained as

$$\hat{\mathbf{x}}_k^- = \hat{\mathbf{x}}_{k-1} + \mathbf{B}\mathbf{u}_{k-1}, \tag{3.58}$$

where $\hat{\mathbf{x}}_k^-$ refers to the state prediction estimate at time t_1 based on the measurements obtained at previous time t_0.

The measurements $\mathbf{z}_k$ which are obtained from (3.46) are then used to correct the prediction of (3.58) to produce the *a posteriori* state estimate as

$$\hat{\mathbf{x}}_k = \hat{\mathbf{x}}_k^- + \mathbf{K}_k[\mathbf{z}_k - \mathbf{H}(\hat{\mathbf{x}}_k^-)], \tag{3.59}$$

where $\mathbf{K}_k$ is the Kalman gain which is calculated as

$$\mathbf{K}_k = \mathbf{P}_k^- \mathbf{H}^T (\mathbf{H}\mathbf{P}_k^- \mathbf{H}^T + \mathbf{R})^{-1}, \tag{3.60}$$

where $\mathbf{P}_k^-$ is the *a priori* estimation error covariance matrix which is calculated as

$$\mathbf{P}_k^- = \mathbf{A}_{k-1}\mathbf{P}_{k-1}\mathbf{A}_{k-1}^T + \mathbf{Q} \tag{3.61}$$

where $\mathbf{P}_k$ is the *a posteriori* estimation error covariance matrix. The *a posteriori* estimation error covariance is then updated using the following

$$\mathbf{P}_k = (\mathbf{I} - \mathbf{K}_k\mathbf{H})\mathbf{P}_k^-. \tag{3.62}$$

The equations (3.58), (3.61), (3.60), (3.59) and (3.62) are repeated once new measurements $\mathbf{z}$ are obtained. Repeating the calculation ensures the expected precision and the real time operation of the system. The KF implementation is summarized in Algorithm 3.2.

3.7 Simulation Procedure

The simulations, which are based on the model presented in section 3.2, are carried out according the steps that follow. Note that steps 1-5 are inspired by [Waa+10b]. Nevertheless, the simulation steps are:

1. The distances d_i between the mobile node and ith anchor node are calculated for $i = 1, \ldots, N$.

Algorithm 3.2 Kalman Filter Implementation Design Algorithm for the positioning problem

1: Initialize the **A** matrix as in (3.41).
2: Initialize the **H** matrix as in (3.49).
3: Initialize the measurement noise matrix **R** as in (3.53).
4: Initialize and update the process noise matrix **Q** as in (3.55).
5: Initialize the error estimation covariance $\mathbf{P}_0$ as in (3.56).
6: Initialize the system state $\hat{\mathbf{x}}_0$ as in (3.57) based on Algorithm 3.1.
7: **for** $k = 1$ to ∞ **do**
8: Obtain the measurements $\mathbf{z}_k$ from Algorithm 3.1 as in (3.46);
9: Compute the *a priori* state $\hat{\mathbf{x}}_k^-$ as in (3.58);
10: Calculate the *a priori* estimation error matrix $\mathbf{P}_k^-$ as in (3.61);
11: Calculate the Kalman gain $\mathbf{K}_k$ as in (3.60);
12: Calculate the *a posteriori* state $\hat{\mathbf{x}}_k$ as in (3.59);
13: Calculate the *a posteriori* estimation error covariance matrix $\mathbf{P}_k$ as in (3.62);
14: Extract the position information $\hat{x}_k$,$\hat{y}_k$ from the state $\hat{\mathbf{x}}_k$;
15: **end for**

2. According to the distance, the RSSI vector $\mathbf{r}_k$ is calculated in the mobile node for the anchor nodes.
3. A zero mean Gaussian random variable $\eta(0, \sigma^2)$ is generated and added to the RSSI value according to the model F of the TGn channel models. In this model, the Gaussian random variable η is added only to the RSSI measurements for distances larger than the breakpoint distance d_{BP} as presented in section 2.6. As a result, the error prone vector $\mathbf{r}_k \in \mathbb{R}^N$ is generated from

$$\hat{\mathbf{r}}_k = \mathbf{r}_k + \eta(0, \sigma^2) \tag{3.63}$$

where $\hat{\mathbf{r}}_k$ is defined in (3.1).
4. The error prone measurement $\hat{\mathbf{r}}_k$ is quantized, yielding the quantized measured $\hat{\mathbf{r}}_{k,q}$.
5. The estimated distance $\hat{d}_i$ is extracted from $\hat{\mathbf{r}}_{k,q}$ according to the model F of the TGn channel models presented in section 2.6.
6. Trilateration is used to formulate a set of equations of circles out of the estimated distances and the locations of the anchor nodes. The equation of circles is given in section 2.4.2.

7. The linearized system of equations is used to formulate the equation of circles into one equation which is solvable using the LLS method. That is, to formulate (3.35) and (3.36).
8. The LLS method is used to estimate the mobile position $\hat{\mathbf{x}}_{\text{tr}}$.
9. KF is used for position accuracy improvement. Here, the system measurements hold the estimated position $\hat{\mathbf{x}}_{\text{tr}}$ and the system state holds the position refinement $\hat{\mathbf{p}}$.
10. The position coordinates $\hat{x}$ and $\hat{y}$ are extracted from the system state $\hat{\mathbf{x}}$.
11. The distance error ρ is calculated as

$$\rho = |\hat{\mathbf{p}} - \mathbf{p}|\,, \tag{3.64}$$

where $\mathbf{p}$ is the real mobile node position.
12. The simulation steps 3-11 are carried out for different traces according to the performance evaluation model. A detailed explanation for the this model is given in section 3.2.
13. The simulation steps 3-12 are repeated for 100 iterations to simulate different noise conditions.
14. The mean distance error $E(\Delta\rho)$ is conducted by averaging all the obtained values of the distance error ρ.
15. The simulation steps 3-14 are carried out for different numbers of anchor nodes $N \in \{3, 4, 6\}$.

3.8 Results

In this section, the simulation results for the proposed algorithm are presented. The results are obtained according to the evaluation performance model which is presented in section 3.2 and the simulation procedure of section 3.7.

Figures 3.5, 3.6, and 3.7 depict the error distance ρ for $3, 4$ and 6 anchor nodes respectively according to different distances d to the network's center of coordi-

nate $(0, 0)$ for the proposed KF implementation compared with the LLS estimator. The KF is implemented in the *refinement layer* of the framework presented in Fig. 3.3 while the LLS estimator is implemented in the *estimation layer* of the framework.

The error distance ρ is obtained according to section 3.2, where 100 random traces representing different traces in which each is repeated 100 times to represent different noise condition resulting in 10000 random traces. Each trace contains a number of positions that the mobile node is following during its movement. The error distance ρ is then obtained by measuring the distance between the estimated position $\hat{\mathbf{p}}$ with the real position $\mathbf{p}$ of the mobile node. As such, ρ can be defined to be the distance estimation error as

$$\rho_k = \sqrt{(x_k - \hat{x}_k)^2 + (y_k - \hat{y}_k)^2}, \tag{3.65}$$

where x_k and y_k are the real coordinates of the mobile node at time index k and $\hat{x}_k$ and $\hat{y}_k$ are the estimated coordinates at time index k. The distance d is measured from the network's center of coordinates $(0, 0)$ and has the maximum value of 75 m in order not to exceed the diameter of the *circle of trust* of 150 m described earlier in section 2.2.

The estimated mean error distance values $\mathrm{E}[\Delta\rho]$ for $3, 4$ and 6 anchor nodes are calculated for each technique. In case of the LLS estimator, the mean error distance values are 29.48 m, 26.56 m and 22.11 m for $3, 4$ and 6 anchor node respectively. Compared with the LLS estimator, the KF showed significant improvement of the mean error distance of 19.01 m with 35.51 % improvement, 17.28 m with $34, 93$ % improvement and 14.40 m with $34, 87$ % improvement for $3, 4$ and 6 anchor nodes respectively. The mean error distance values are summarized in Table 3.3.

From Figs. 3.5, 3.6, 3.7, and the comparative values of the mean error distance, it is clear that the KF implementation reduces the estimation error considerably compared with the LLS estimator.

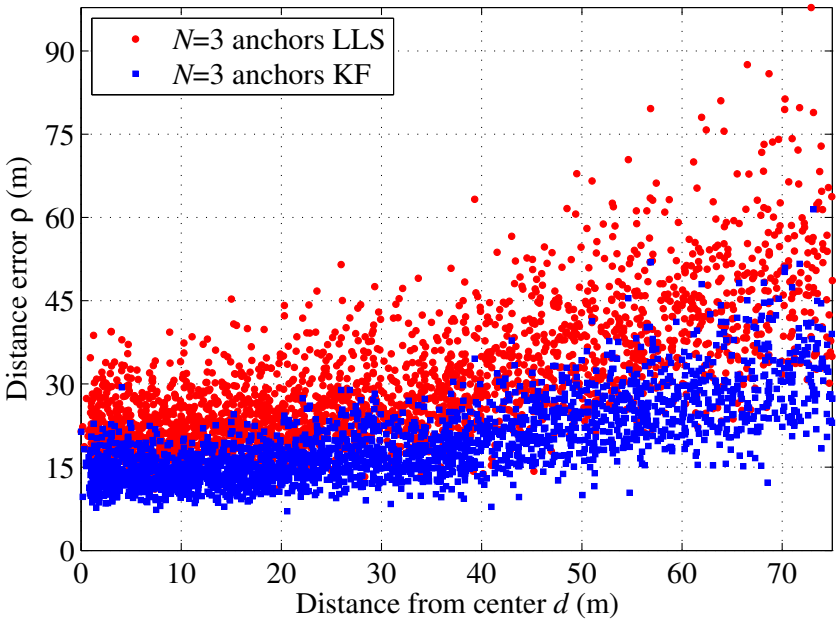

Figure 3.5: Error distance ρ for distances d that shows the advantages of the proposed KF implementation compared to the LLS using 3 anchor nodes.

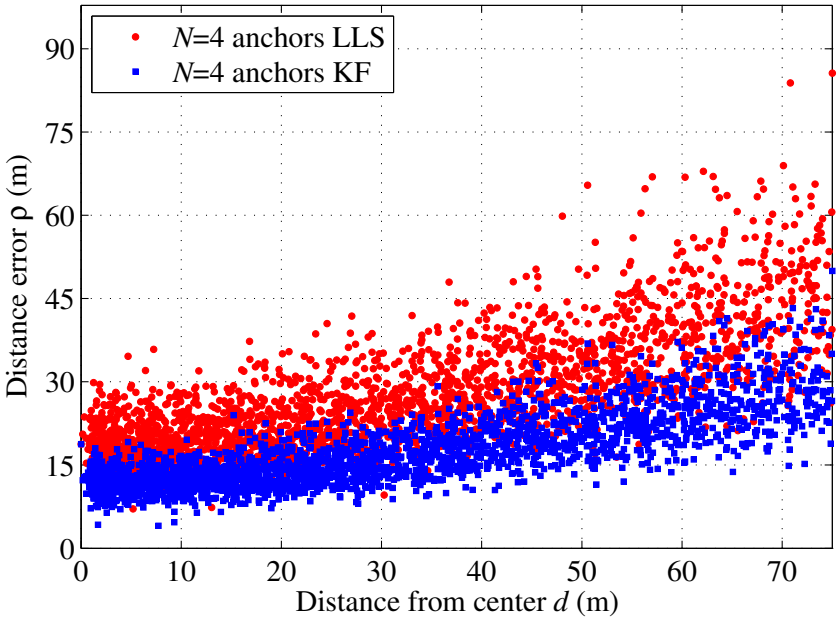

Figure 3.6: Error distance ρ for distances d that shows the advantages of the proposed KF implementation compared to the LLS using 4 anchor nodes.

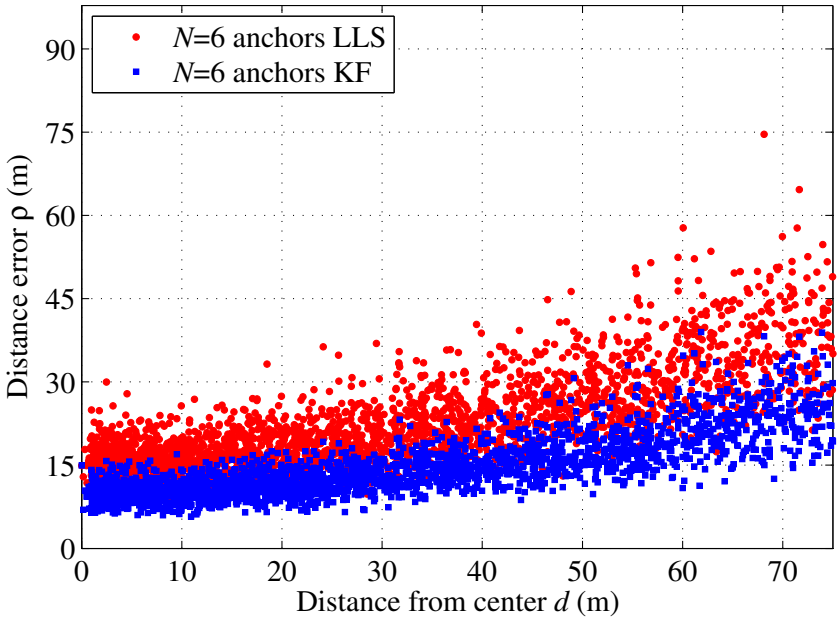

Figure 3.7: Error distance ρ for distances d that shows the advantages of the proposed KF implementation compared to the LLS using 6 anchor nodes.

To compare the proposed KF implementation with the EKF, figures 3.8, 3.9 and 3.10 are given. The EKF is considered as a popular technique as pointed out in section 1.3.2. However, the EKF will be presented in details in section 4.4. Nevertheless, the results of the EKF are based on the performance evaluation model of section 3.2 and the simulation procedure that will be presented in section 4.5.2.

The estimated mean error distance $\mathrm{E}[\Delta\rho]$ values for $3, 4$ and 6 anchor nodes of the EKF are calculated for performance comparison. The values are 21.91 m, 20.21 m and 16.57 m for $3, 4$ and 6 anchor node respectively. The obtained error values can be found in Table 3.3 for convenience. Based on these results, the proposed KF implementation has 13.23 %, 14.49 %, 13.09 % improvement for $3, 4, 6$ anchor nodes respectively compared with the EKF.

To show the distribution of the error distance of the KF over the distance d, figures 3.11, 3.12, and 3.13 are given. From Fig. 3.11 which has 65 % of the error distance values below 20 m for the case of 3 anchor nodes, it can be seen that the

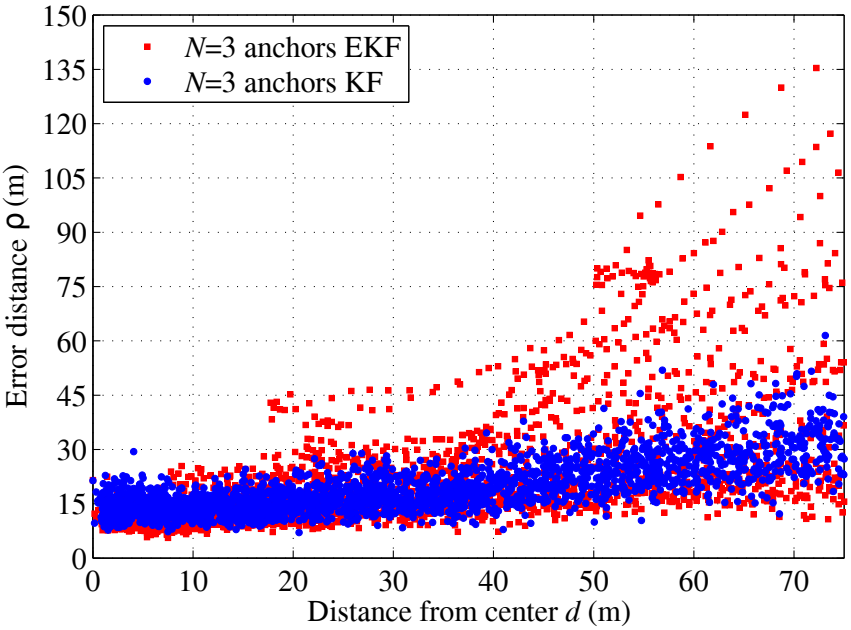

Figure 3.8: Error distance ρ for distances d for the KF implementation compared to the EKF using 3 anchor nodes.

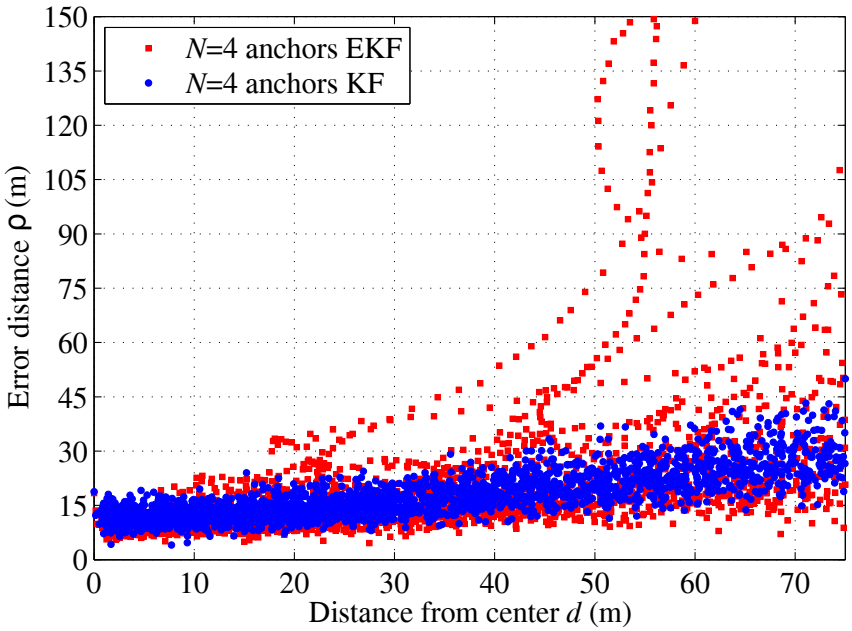

Figure 3.9: Error distance ρ for distances d for the KF implementation compared to the EKF using 4 anchor nodes.

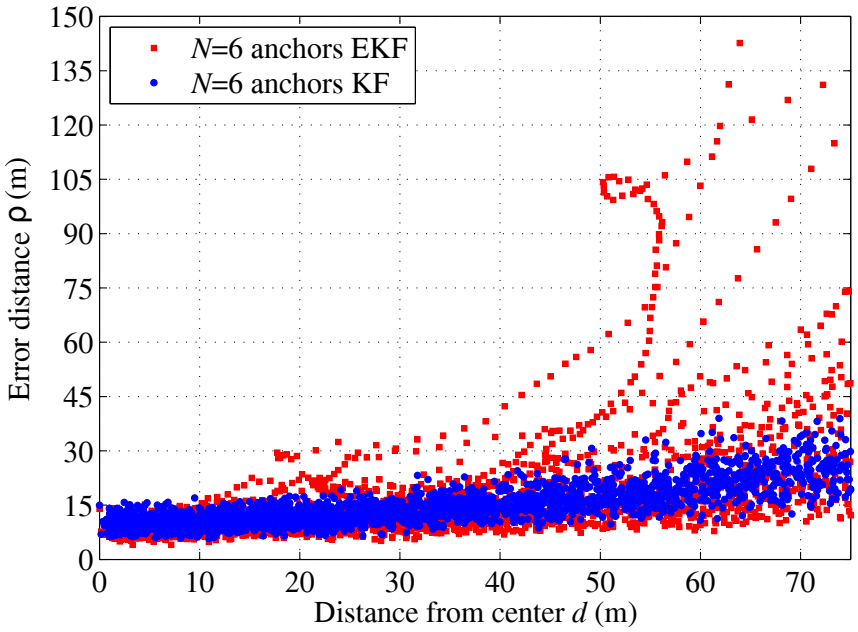

Figure 3.10: Error distance ρ for distances d for the KF implementation compared to the EKF using 6 anchor nodes.

largest probability occurs at the distance of 12 m. Larger distance error are obtained in larger distances from the network center. By considering Fig. 3.12 which shows the results for 4 anchor nodes with a probability of 70 % for distances below 20 m. The largest probability occurs at a distance error of 8 m. Figure 3.13 shows the results for 6 anchor nodes with a probability of 79 % for distance errors below 20 m. The largest probability occurs at the distance of 6 m. For comparison purpose, the error distribution of the popular EKF will be presented in Figs. 4.9, 4.10 and 4.11 of chapter 4.

From the simulation results above, it can be concluded that the proposed KF implementation has better estimation accuracy than the EKF in all the testing conditions.

Table 3.3: Mean error distance $E[\Delta\rho]$ for each test case.

Method	Mean error distance $E[\Delta\rho]$ (m)		
	3 Anchor nodes	4 Anchor nodes	6 Anchor nodes
LLS	29.48	26.56	22.11
EKF	21.915	20.21	16.57
KF	19.01	17.28	14.40

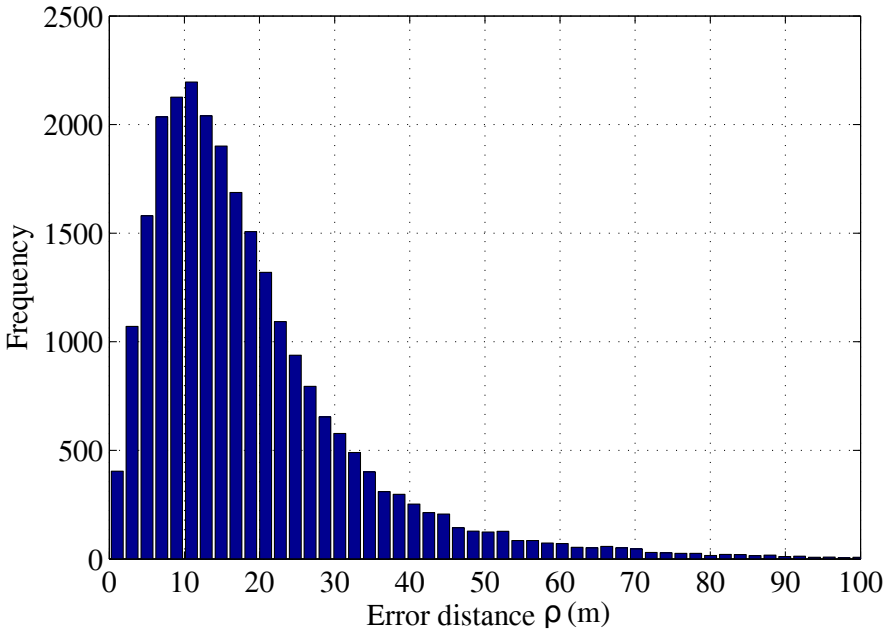

Figure 3.11: Error distance ρ distribution for distances d in the case of 3 anchor nodes for the proposed KF implementation.

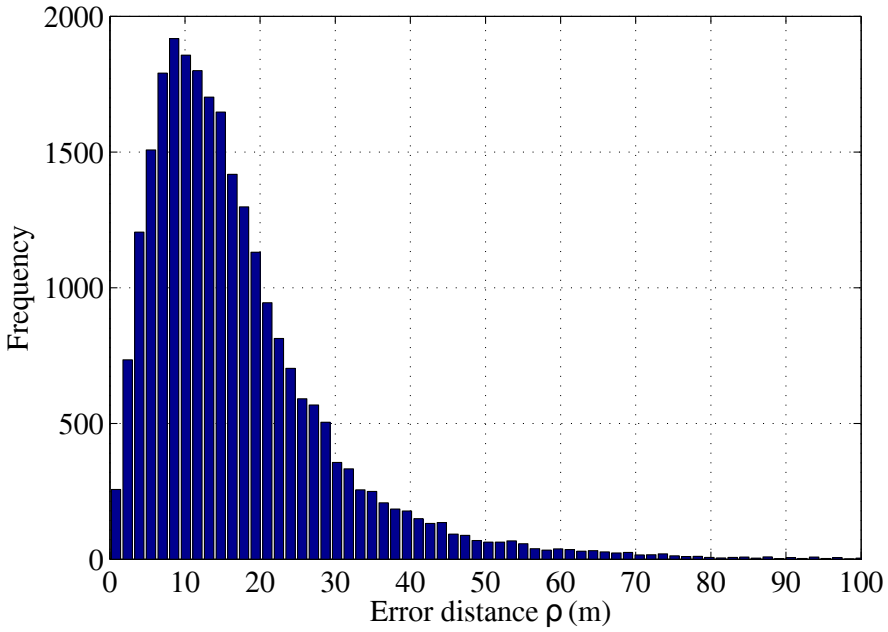

Figure 3.12: Error distance ρ distribution for distances d in the case of 4 anchor nodes for the proposed KF implementation.

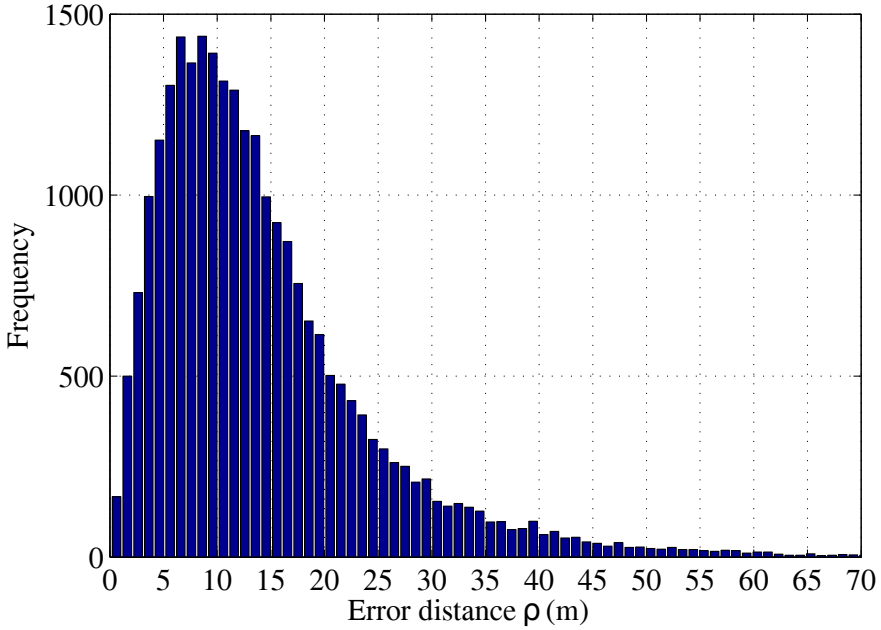

Figure 3.13: Error distance ρ distribution for distances d in the case of 6 anchor nodes for the proposed KF implementation.

4 IEKF for RSSI-Based WLAN IEEE 802.11n Positioning and Tracking

4.1 Overview

Some of the successful applications of the KF are with the non-linear dynamics and (or) the non-linear measurements [BH12]. In particular when the evolving state has a non-linear relationship with the previous state and (or) the measurements have a non-linear relationship with the system state. A block diagram that illustrates the application of the non-linearity of the system dynamics function and the measurements function to the KF is depicted in Fig. 4.1.

In this chapter, the state-space models are designed according to the positioning problem given in section 2.2. One of the solutions for solving the non-linearity in the designed models is linearization. In general, these non-linear models are only solvable using the KF [GA11].

The most popular linearization approach to approximate the non-linearity so that the non-linearity becomes solvable with the KF is the EKF. The EKF is designed for L&T based on the designed models. The EKF is then used for comparative

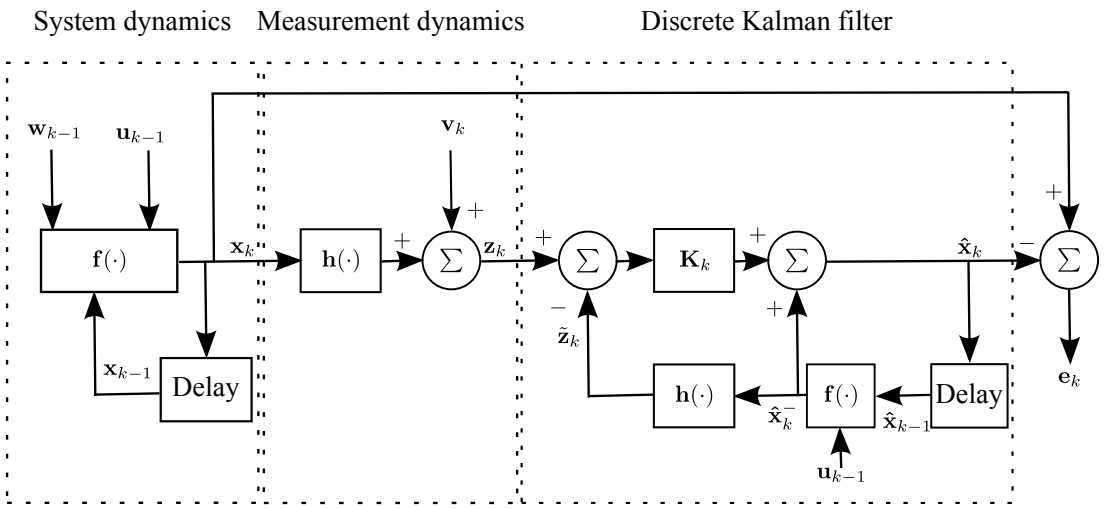

Figure 4.1: Non linear Kalman Filter.

evaluation with all the proposed techniques through this dissertation. An algorithmic implementation of the EKF for L&T is proposed.

In addition in this chapter, the author proposes the IEKF for L&T application. Unlike the EKF which linearizes about the *a priori* state estimate, the IEKF linearizes about the most recent *a posteriori* state estimate. The algorithmic implementation of this filter is proposed. In addition, the simulation environment for testing the proposed filter is explained. Finally in this chapter, comparative results of the filter implementation are illustrated.

4.2 Non-Linear State-Space Models Design

By considering the positioning problem presented in section 2.2, it is desired to design the state-space models that are introduced earlier in section 2.7.

By referring to the proposed motion model of section 3.2, it is possible to write the system state dynamics equation in which the state is desired to be estimated. In particular, the equations (3.6), (3.9), (3.10) and (3.11) are used to design the state

dynamics in matrix form as

$$\begin{bmatrix} x_k \\ y_k \\ v_k^x \\ v_k^y \end{bmatrix} = \begin{bmatrix} 1 & 0 & T & 0 \\ 0 & 1 & 0 & T \\ 0 & 0 & 1 & 0 \\ 0 & 0 & 0 & 1 \end{bmatrix} \begin{bmatrix} x_{k-1} \\ y_{k-1} \\ v_{k-1}^x \\ v_{k-1}^y \end{bmatrix} + \begin{bmatrix} \frac{1}{2}T^2 & 0 & 0 & 0 \\ 0 & \frac{1}{2}T^2 & 0 & 0 \\ 0 & 0 & T & 0 \\ 0 & 0 & 0 & T \end{bmatrix} \begin{bmatrix} u_{k-1}^x \\ u_{k-1}^y \\ u_{k-1}^x \\ u_{k-1}^y \end{bmatrix} + \begin{bmatrix} w_{k-1}^1 \\ w_{k-1}^2 \\ w_{k-1}^3 \\ w_{k-1}^4 \end{bmatrix}, \quad (4.1)$$

or

$$\mathbf{x}_k = \mathbf{A}\mathbf{x}_{k-1} + \mathbf{B}\mathbf{u}_{k-1} + \mathbf{w}_{k-1}, \quad (4.2)$$

where $\mathbf{x}_k \in \mathbb{R}^4$ is the process state vector at time t_k. $\mathbf{A} \in \mathbb{R}^{4\times4}$ is the matrix relating the state $\mathbf{x}_{k-1} \in \mathbb{R}^4$ of the previous time step t_{k-1} to the state $\mathbf{x}_k$ of the current time state k which is written as

$$\mathbf{A} = \begin{bmatrix} 1 & 0 & T & 0 \\ 0 & 1 & 0 & T \\ 0 & 0 & 1 & 0 \\ 0 & 0 & 0 & 1 \end{bmatrix}, \quad (4.3)$$

$\mathbf{B} \in \mathbb{R}^{4\times4}$ is the matrix relating the control vector $\mathbf{u}_{k-1} \in \mathbb{R}^4$ of the previous time step t_{k-1} to the state $\mathbf{x}_k$ of the current time state k which is written as

$$\mathbf{B} = \begin{bmatrix} \frac{1}{2}T^2 & 0 & 0 & 0 \\ 0 & \frac{1}{2}T^2 & 0 & 0 \\ 0 & 0 & T & 0 \\ 0 & 0 & 0 & T \end{bmatrix}, \quad (4.4)$$

and $\mathbf{u}_{k-1} \in \mathbb{R}^4$ is the acceleration vector which is randomly generated as presented in section 3.2 and is written as

$$\mathbf{u}_{k-1} = \begin{bmatrix} u_{k-1}^x \\ u_{k-1}^y \\ u_{k-1}^x \\ u_{k-1}^y \end{bmatrix}. \quad (4.5)$$

$\mathbf{w}_{k-1} \in \mathbb{R}^4$ is the state process uncertainty vector with known covariance matrix $\mathbf{Q}_k$ with the following structure

$$\mathbf{E}[\mathbf{w}_{k-1}{\mathbf{w}_{i-1}}^T] = \begin{cases} \mathbf{Q}_{k-1}, & i = k \\ 0, & i \neq k \end{cases} \tag{4.6}$$

However, the procedure of determining the matrix $\mathbf{Q}_k$ will be followed in section 4.3.

The measurements $\mathbf{z}_k \in \mathbb{R}^N$ at time t_k are the distances $\mathbf{d}_k \in \mathbb{R}^N$ measured from the mobile node to the surrounding anchor nodes which are expressed as

$$\begin{bmatrix} z_k^1 \\ \vdots \\ z_k^N \end{bmatrix} = \begin{bmatrix} d_k^1 \\ \vdots \\ d_k^N \end{bmatrix}. \tag{4.7}$$

The state to measurement function (2.20) is then given by

$$\begin{bmatrix} z_k^1 \\ \vdots \\ z_k^N \end{bmatrix} = \begin{bmatrix} \sqrt{(x_{\mathrm{BS}_1} - x_k)^2 + (y_{\mathrm{BS}_1} - y_k)^2} \\ \vdots \\ \sqrt{(x_{\mathrm{BS}_N} - x_k)^2 + (y_{\mathrm{BS}_N} - y_k)^2} \end{bmatrix} + \begin{bmatrix} v_k^1 \\ \vdots \\ v_k^N \end{bmatrix}, \tag{4.8}$$

or

$$\mathbf{z}_k = \mathbf{h}(\mathbf{x}_k) + \mathbf{v}_k, \tag{4.9}$$

where $\mathbf{v}_k \in \mathbb{R}^N$ is the measurements state noise vector with known covariance matrix $\mathbf{R}_k$ that has the following structure

$$\mathbf{E}[\mathbf{v}_k{\mathbf{v}_i}^T] = \begin{cases} \mathbf{R}_k, & i = k \\ 0, & i \neq k \end{cases}, \tag{4.10}$$

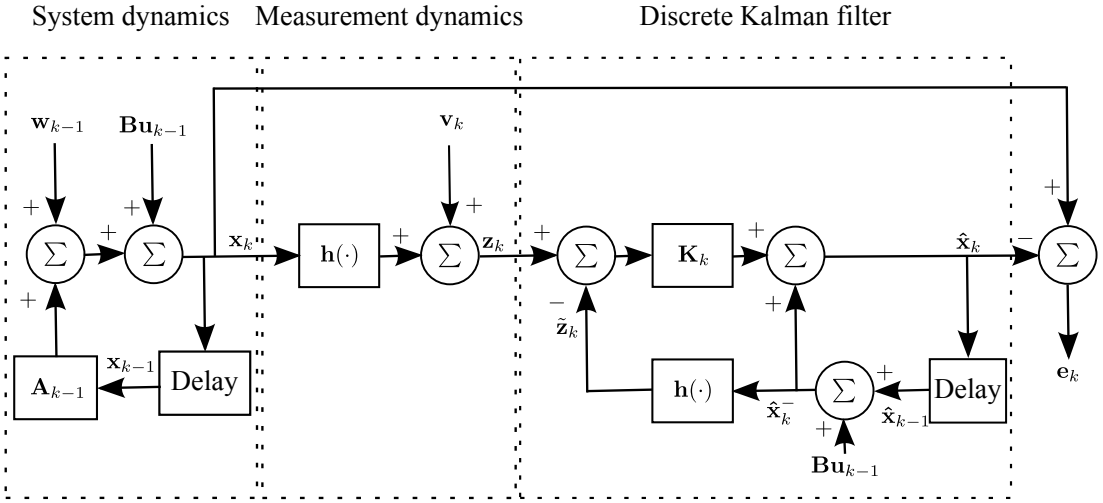

Figure 4.2: The designed state-space models application to the Kalman Filter application.

The noise components of $\mathbf{w}_{k-1}$ and $\mathbf{v}_k$ are independent of each other, i.e.

$$\mathbf{E}[\mathbf{w}_{k-1}\mathbf{v}_i] = 0, \quad \text{for all } k \text{ and } i. \tag{4.11}$$

Nevertheless, the procedure for determining the matrix $\mathbf{R}_k$ will be followed in section 3.2. A block diagram that illustrates the application of the designed state-space models to the KF is depicted in Fig. 4.2.

4.3 Noise Covariance Matrices Calculation

To proceed with the design process of the EKF, the uncertainty covariance matrix $\mathbf{Q}$ of the model of (4.1) and the noise covariance $\mathbf{R}$ of the model of (4.9) need to be determined.

The author assumes that the matrices $\mathbf{Q}$ and $\mathbf{R}$ are not changing during the operation of the EKF and therefore the subscript "k" is dropped from both matrices. For the sake of simplicity, the calculation process of the measurement noise

covariance matrix **R** will proceed the calculation of the uncertainty covariance matrix **Q**.

The measurement noise covariance matrix **R** is associated with the noisy sensor measurements, that is

$$\mathbf{R} = \begin{bmatrix} E[v_1 v_1] & E[v_1 v_2] & \dots & E[v_1 v_N] \\ E[v_2 v_1] & E[v_2 v_2] & \dots & E[v_2 v_N] \\ \vdots & \vdots & \ddots & \vdots \\ E[v_N v_1] & E[v_N v_2] & \dots & E[v_N v_N] \end{bmatrix}. \tag{4.12}$$

By assuming no bias in the sensors, the variance $\sigma_{v_i}^2$ of the measurement noise of the sensors $i = 1, 2, \dots, N$ can be calculated from the obtained measurement data prior to the working of the EKF. As such, the state noise covariance can be written as

$$\mathbf{R} = \begin{bmatrix} \sigma_{v_1}^2 & 0 & \dots & 0 \\ 0 & \sigma_{v_2}^2 & \dots & 0 \\ \vdots & \vdots & \ddots & \vdots \\ 0 & 0 & \dots & \sigma_{v_N}^2 \end{bmatrix}. \tag{4.13}$$

Based on the simulation results, the sigmas $\sigma_{v_1}^2, \sigma_{v_2}^2, \dots, \sigma_{v_N}^2$ are found to be equal to $358.779\,\mathrm{m}^2$.

The covariance matrix **Q** is associated with the state uncertainty, i.e.

$$\mathbf{Q} = \begin{bmatrix} E[w_1 w_1] & E[w_1 w_2] & E[w_1 w_3] & E[w_1 w_4] \\ E[w_2 w_1] & E[w_2 w_2] & E[w_2 w_3] & E[w_2 w_4] \\ E[w_3 w_1] & E[w_3 w_2] & E[w_3 w_3] & E[w_3 w_4] \\ E[w_4 w_1] & E[w_4 w_2] & E[w_4 w_3] & E[w_4 w_4] \end{bmatrix}. \tag{4.14}$$

Assuming that the individual uncertainties w_1, w_2, w_3 and w_4 are not correlated,

the state uncertainty covariance matrix can be written as

$$\mathbf{Q} = \begin{bmatrix} \sigma_{w_1}^2 & 0 & 0 & 0 \\ 0 & \sigma_{w_2}^2 & 0 & 0 \\ 0 & 0 & \sigma_{w_3}^2 & 0 \\ 0 & 0 & 0 & \sigma_{w_4}^2 \end{bmatrix}. \tag{4.15}$$

The state uncertainty covariance matrix $\mathbf{Q}$ is impossible to be calculated prior to the operation of the EKF since there is no prior knowledge of the output of the filter. As such, the matrix $\mathbf{Q}$ is approximately initialized to let the EKF work in the *off-line* mode of operation. In this mode, the main target is to measure the matrix $\mathbf{Q}$ for the *on-line* mode of operation for the EKF.

For the *off-line* mode of operation, the values $\sigma_{w_1}^2$, $\sigma_{w_2}^2$, $\sigma_{w_3}^2$ and $\sigma_{w_4}^2$ can be initialized. The values are calculated based on the expected results of the filter and they are given in Table 4.1. Then new variances values $\sigma_{w_1}^2$, $\sigma_{w_2}^2$, $\sigma_{w_3}^2$ and $\sigma_{w_4}^2$ are caluclated for the *on-line* mode from the simulations and are given in Table 4.1. Nevertheless, it should be mention that the values of the *off-line* mode and *on-line* mode have similar output results of the filter according to simulations.

Table 4.1: Process noise covariance values.

off-line mode		on-line mode	
Sigma	Value	Sigma	Value
$\sigma_{w_1}^2$	366.5 m^2	$\sigma_{w_1}^2$	95 m^2
$\sigma_{w_2}^2$	366.5 m^2	$\sigma_{w_2}^2$	95 m^2
$\sigma_{w_3}^2$	366.5 $\frac{\mathrm{m}^2}{\mathrm{s}^2}$	$\sigma_{w_3}^2$	0 $\frac{\mathrm{m}^2}{\mathrm{s}^2}$
$\sigma_{w_4}^2$	366.5 $\frac{\mathrm{m}^2}{\mathrm{s}^2}$	$\sigma_{w_4}^2$	0 $\frac{\mathrm{m}^2}{\mathrm{s}^2}$

4.4 Extended Kalman Filter Design

The Kalman Filter described in section 2.8 has addressed the estimation of the state $\mathbf{x} \in \mathbb{R}^n$ of a discrete time controlled process which is governed by a linear stochastic difference equation of a dynamical system and a linear state to measurements relationship. If the state dynamics and (or) the measurement relationship to the process is non-linear, the Kalman Filter in its original form is not be applicable anymore.

Linearizing the non-linearity in the models is considered as a solution to overcome this problem. The EKF [Sim96; GA11] linearizes the non-linear models of (2.19) and (2.20) at each time instant around the most recent state estimate which is the *a priori* state estimate $\hat{\mathbf{x}}_k^-$.

The EKF assumes that the function $\mathbf{f}(\cdot)$ and the function $\mathbf{h}(\cdot)$ of the state-space problem presented in section 2.7 are sufficiently differentiable at $\hat{\mathbf{x}}_k^-$ so that they can be represented by a Taylor series expansion, according to [GA11]

$$\mathbf{f}(\mathbf{x}_k) \equiv \mathbf{f}(\hat{\mathbf{x}}_k^-) + \mathbf{f}'(\hat{\mathbf{x}}_k^-)(\mathbf{x}_k - \hat{\mathbf{x}}_k^-) + \frac{\mathbf{f}''(\hat{\mathbf{x}}_k^-)}{2!}(\mathbf{x}_k - \hat{\mathbf{x}}_k^-)^2 + \ldots, \tag{4.16}$$

$$\mathbf{h}(\mathbf{x}_k) \equiv \mathbf{h}(\hat{\mathbf{x}}_k^-) + \mathbf{h}'(\hat{\mathbf{x}}_k^-)(\mathbf{x}_k - \hat{\mathbf{x}}_k^-) + \frac{\mathbf{h}''(\hat{\mathbf{x}}_k^-)}{2!}(\mathbf{x}_k - \hat{\mathbf{x}}_k^-)^2 + \ldots, \tag{4.17}$$

where the prime $'$ refers to the derivative of a function. Then, the EKF approximates the non-linearity of the functions $\mathbf{f}(\cdot)$ and $\mathbf{h}(\cdot)$ into linear equations using first order Taylor series expansions of (4.16) and (4.17).

By recalling the design of the state-space models in section 4.2, it can be clearly seen that the function $\mathbf{f}(\cdot)$ is linear and therefore no linearization procedure is required. However, the function $\mathbf{h}(\cdot)$ is non-linear.

Linearizing the function $\mathbf{h}(\cdot)$ of (4.9) about the *a priori* $\hat{\mathbf{x}}_k^-$ is done by obtaining the first order Taylor series expansion, from [GA11], as

$$\mathbf{h}(\mathbf{x}_k) \simeq \mathbf{h}(\hat{\mathbf{x}}_k^-) + \mathbf{H}_k[\mathbf{x}_k - \hat{\mathbf{x}}_k^-], \tag{4.18}$$

where $\mathbf{H}_k$ is the partial derivative of $\mathbf{h}$ with respect to $\mathbf{x}$ evaluated at $\hat{\mathbf{x}}_k^-$ as

$$\mathbf{H}_k = \frac{\partial \mathbf{h}}{\partial \mathbf{x}}|_{\mathbf{x}=\hat{\mathbf{x}}_k^-} = \frac{\partial}{\partial \mathbf{x}} \left[\begin{array}{c} \sqrt{(x_{\mathrm{BS}_1} - x_k)^2 + (y_{\mathrm{BS}_1} - y_k)^2} \\ \vdots \\ \sqrt{(x_{\mathrm{BS}_N} - x_k)^2 + (y_{\mathrm{BS}_N} - y_k)^2} \end{array} \right] \Bigg|_{\mathbf{x}=\hat{\mathbf{x}}_k^-}$$

$$= \left[\begin{array}{cc} \frac{\hat{x}_k^- - x_{\mathrm{BS}_1}}{\sqrt{(x_{\mathrm{BS}_1} - \hat{x}_k^-)^2 + (y_{\mathrm{BS}_1} - \hat{y}_k^-)^2}} & \frac{\hat{y}_k^- - y_{\mathrm{BS}_1}}{\sqrt{(x_{\mathrm{BS}_1} - \hat{x}_k^-)^2 + (y_{\mathrm{BS}_1} - \hat{y}_k^-)^2}} \\ \vdots & \vdots \\ \frac{\hat{x}_k^- - x_{\mathrm{BS}_N}}{\sqrt{(x_{\mathrm{BS}_N} - \hat{x}_k^-)^2 + (y_{\mathrm{BS}_N} - \hat{y}_k^-)^2}} & \frac{\hat{y}_k^- - y_{\mathrm{BS}_N}}{\sqrt{(x_{\mathrm{BS}_N} - \hat{x}_k^-)^2 + (y_{\mathrm{BS}_N} - \hat{y}_k^-)^2}} \end{array} \right]. \tag{4.19}$$

Substituting the approximation of (4.19) into the non-linear model of (4.9), according to [Sim96], results in

$$\mathbf{z}_k \approx \mathbf{h}(\hat{\mathbf{x}}_k^-) + \mathbf{H}_k(\mathbf{x}_k - \hat{\mathbf{x}}_k^-) + \mathbf{v}_k, \tag{4.20}$$

which can be written as

$$\mathbf{z}_k - \mathbf{h}(\hat{\mathbf{x}}_k^-) + \mathbf{H}_k\hat{\mathbf{x}}_k^- = \mathbf{H}_k\mathbf{x}_k + \mathbf{v}_k. \tag{4.21}$$

By assuming that

$$\tilde{\mathbf{z}}_k = \mathbf{h}(\hat{\mathbf{x}}_k^-), \tag{4.22}$$

then (4.21) can be written as

$$\mathbf{z}_k - \tilde{\mathbf{z}}_k = \mathbf{H}_k\mathbf{x}_k - \mathbf{H}_k\hat{\mathbf{x}}_k^- + \mathbf{v}_k. \tag{4.23}$$

By defining the prediction error as

$$\tilde{\mathbf{e}}_{x_k} = \mathbf{x}_k - \hat{\mathbf{x}}_k^-, \tag{4.24}$$

and the measurement residual as

$$\tilde{\mathbf{e}}_{z_k} = \mathbf{z}_k - \tilde{\mathbf{z}}_k, \tag{4.25}$$

then (4.21) can be written as

$$\tilde{\mathbf{e}}_{z_k} = \mathbf{H}_k \tilde{\mathbf{e}}_{x_k} + \mathbf{v}_k, \tag{4.26}$$

which is a linear function and can be considered as the measurement function of (2.24) of the discrete KF [WB].

After linearizing the non-linearity and determining the noise covariances as given in section 4.3, the EKF can be initialized. In particular, the error covariance matrix $\mathbf{P}_{k-1}$ can be initialized for $k = 1$ as

$$\mathbf{P}_{k-1} = \mathbf{Q}, \tag{4.27}$$

and the system state $\hat{\mathbf{x}}_0$ is initialized as

$$\hat{\mathbf{x}}_0 = \begin{bmatrix} \hat{\mathbf{x}}_{\text{tr}} \\ 0 \\ 0 \end{bmatrix}, \tag{4.28}$$

where $\hat{\mathbf{x}}_{\text{tr}}$ is the estimated position obtained from Algorithm 3.1 and the velocities v_k^x and v_k^y of the *zeroth* state $\hat{\mathbf{x}}_0$ are initialized to zero.

Recalling again the design of the system dynamics of (4.1), the *a priori* state estimation can be obtained as

$$\hat{\mathbf{x}}_k^- = \hat{\mathbf{x}}_{k-1} + \mathbf{B}\mathbf{u}_{k-1}. \tag{4.29}$$

The measurements $\mathbf{z}_k$ are then used to correct the prediction of (4.29) to produce

Algorithm 4.1 The Extended Kalman Filter (EKF) Implementation Algorithm

Obtain the location of the anchor nodes $\mathbf{P}_{\text{BS}}$.
Initialize the $\mathbf{A}$ matrix as in (4.3).
Initialize the measurement noise matrix $\mathbf{R}$ as in (4.13).
Initialize and then update the process noise matrix $\mathbf{Q}$ as in (4.15).
Initialize the error estimation covariance $\mathbf{P}_0$ as in (4.27).
Initialize the system state $\hat{\mathbf{x}}_0$ as in (4.28).
for $i = 1$ to $i = \infty$ **do**
    Obtain the measurements $\mathbf{z}_k$;
    Compute the partial derivative $\mathbf{H}_k$ as in (4.19);
    Compute the *a priori* state estimate $\hat{\mathbf{x}}_k^-$ as in (4.29);
    Obtain the measurements $\mathbf{z}_k = \{z_1, z_2, \ldots, z_N\}$;
    Compute the *a priori* error estimation $\mathbf{P}_k^-$ from as in (4.32);
    Compute the Kalman gain $\mathbf{K}_k$ as in (4.31);
    Compute the *a posteriori* state estimate $\hat{\mathbf{x}}_k$ as in (4.30);
    Compute the *a posteriori* error estimation matrix $\mathbf{P}_k$ as in (4.33);
end for

the *a posteriori* state estimate as

$$\hat{\mathbf{x}}_k = \hat{\mathbf{x}}_k^- + \mathbf{K}_k[\mathbf{z}_k - \mathbf{h}(\hat{\mathbf{x}}_k^-)], \tag{4.30}$$

where $\mathbf{K}_k$ is the Kalman gain which is calculated as

$$\mathbf{K}_k = \mathbf{P}_k^- \mathbf{H}^T (\mathbf{H}\mathbf{P}_k^- \mathbf{H}^T + \mathbf{R}_k)^{-1}, \tag{4.31}$$

where $\mathbf{P}_k^-$ is the *a priori* estimation error covariance matrix which calculated as

$$\mathbf{P}_k^- = \mathbf{A}_{k-1}\mathbf{P}_{k-1}\mathbf{A}_{k-1}^T + \mathbf{Q}. \tag{4.32}$$

The *a posteriori* estimation error covariance is then updated using

$$\mathbf{P}_k = (\mathbf{I} - \mathbf{K}_k\mathbf{H})\mathbf{P}_k^-. \tag{4.33}$$

Once new measurements are obtained, equations (4.19), (4.29), (4.32), (4.31) and (4.33) are repeated to obtain the position estimate $\hat{\mathbf{p}}$. The EKF implementation is summarized in Algorithm 4.1.

4.5 IEKF for RSSI-Based Indoor Positioning and Tracking

In the context of positioning, the widely used technique for track and estimate the position out of the RSSI measurements is the EKF. However, the EKF has several problems discussed in section 1.3.2.

In this section, the author proposes the IEKF to improve the estimation accuracy over the EKF. The IEKF shall be applied for the WLAN IEEE 802.11 n networks to exploit the RSSI measurements for L&T of a mobile node.

This section starts by presenting the design of the IEKF and gives the implementation algorithm. Next the simulation procedure is explained. Finally, comparable results are illustrated using a Monte-Carlo simulation in MATLAB.

4.5.1 Iterated Extended Kalman Filter Implementation Design

The *Iterated Extended Kalman Filter* IEKF [GA11] linearizes the non-linearity of (2.19) and (2.20) at each time instant about the most recent *a posteriori* state estimate $\hat{\mathbf{x}}_k$.

Based on the design of the state-space models presented in section 4.2, is it noticed that the function $\mathbf{f}(\cdot)$ is linear and therefore no linearization procedure is required. In contrast, the function $\mathbf{h}(\cdot)$ of (4.9) is non-linear and linearization procedure should be carried out.

Similar to the EKF, the IEKF approximates the non-linearity using the first order Taylor series expansion

$$\mathbf{h}(\mathbf{x}_k) \simeq \mathbf{h}(\hat{\mathbf{x}}_k) + \mathbf{H}_k[\mathbf{x}_k - \hat{\mathbf{x}}_k], \tag{4.34}$$

where $\mathbf{H}_k$ is the partial derivative of $\mathbf{h}$ with respect to $\mathbf{x}$ evaluated at $\hat{\mathbf{x}}_k$ as

$$\begin{aligned}\mathbf{H}_k = \frac{\partial \mathbf{h}}{\partial \mathbf{x}}\Big|_{\mathbf{x}=\hat{\mathbf{x}}_k} &= \frac{\partial}{\partial \mathbf{x}} \begin{bmatrix} \sqrt{(x_{\mathrm{BS}_1} - x_k)^2 + (y_{\mathrm{BS}_1} - y_k)^2} \\ \vdots \\ \sqrt{(x_{\mathrm{BS}_N} - x_k)^2 + (y_{\mathrm{BS}_N} - y_k)^2} \end{bmatrix} \Bigg|_{\mathbf{x}=\hat{\mathbf{x}}_k} \\ &= \begin{bmatrix} \frac{\hat{x}_k - x_{\mathrm{BS}_1}}{\sqrt{(x_{\mathrm{BS}_1} - \hat{x}_k)^2 + (y_{\mathrm{BS}_1} - \hat{y}_k)^2}} & \frac{\hat{y}_k - y_{\mathrm{BS}_1}}{\sqrt{(x_{\mathrm{BS}_1} - \hat{x}_k)^2 + (y_{\mathrm{BS}_1} - \hat{y}_k)^2}} \\ \vdots & \vdots \\ \frac{\hat{x}_k - x_{\mathrm{BS}_N}}{\sqrt{(x_{\mathrm{BS}_N} - \hat{x}_k)^2 + (y_{\mathrm{BS}_N} - \hat{y}_k)^2}} & \frac{\hat{y}_k - y_{\mathrm{BS}_N}}{\sqrt{(x_{\mathrm{BS}_N} - \hat{x}_k)^2 + (y_{\mathrm{BS}_N} - \hat{y}_k)^2}} \end{bmatrix}\end{aligned} \tag{4.35}$$

Substituting the approximation of (4.35) into the non-linear model of (4.9), results in

$$\mathbf{z}_k \approx \mathbf{h}(\hat{\mathbf{x}}_k) + \mathbf{H}_k(\mathbf{x}_k - \hat{\mathbf{x}}_k) + \mathbf{v}_k, \tag{4.36}$$

which can be written as

$$\mathbf{z}_k - \mathbf{h}(\hat{\mathbf{x}}_k) + \mathbf{H}_k\hat{\mathbf{x}}_k = \mathbf{H}_k\mathbf{x}_k + \mathbf{v}_k. \tag{4.37}$$

By assuming that

$$\tilde{\mathbf{z}}_k = \mathbf{h}(\hat{\mathbf{x}}_k), \tag{4.38}$$

then (4.37) can be written as

$$\mathbf{z}_k - \tilde{\mathbf{z}}_k = \mathbf{H}_k\mathbf{x}_k - \mathbf{H}_k\hat{\mathbf{x}}_k + \mathbf{v}_k. \tag{4.39}$$

By defining the prediction error as

$$\tilde{\mathbf{e}}_{x_k} = \mathbf{x}_k - \hat{\mathbf{x}}_k, \tag{4.40}$$

and the measurement residual as

$$\tilde{\mathbf{e}}_{z_k} = \mathbf{z}_k - \tilde{\mathbf{z}}_k, \tag{4.41}$$

then (4.21) can be written as

$$\tilde{\mathbf{e}}_{z_k} = \mathbf{H}_k \tilde{\mathbf{e}}_{x_k} + \mathbf{v}_k, \tag{4.42}$$

which is a linear function and can be considered as the measurement function of (2.24) of the discrete KF.

At this point, the linearization of the non-linearity is finished. The determination of the covariances matrices $\mathbf{R}$ and $\mathbf{Q}$ is done in the same method as presented in section 4.3.

In order to let the IEKF start working, the error covariance matrix $\mathbf{P}_{k-1}$ is initialized as

$$\mathbf{P}_{k-1} = \mathbf{Q}, \tag{4.43}$$

and the system state $\mathbf{x}_0$ is initialized as

$$\hat{\mathbf{x}}_0 = \begin{bmatrix} x_{\text{tr}} \\ 0 \\ 0 \end{bmatrix}, \tag{4.44}$$

where $\mathbf{x}_{\text{tr}}$ is the estimated position from Algorithm 3.1 and the velocities v_k^x and v_k^y of the *zeroth* state $\hat{\mathbf{x}}_0$ are initialized to zero.

Based on the initial state estimation $\hat{\mathbf{x}}_0$ and by recalling (4.2), the IEKF predict the estimation as

$$\hat{\mathbf{x}}_k^- = \hat{\mathbf{x}}_{k-1} + \mathbf{B}\mathbf{u}_{k-1}, \tag{4.45}$$

In addition, IEKF uses a recursion algorithm to improve the state estimate $\hat{\mathbf{x}}_k$. This algorithm uses successive evaluation of the partial derivative $\mathbf{H}_k$, the Kalman Gain $\mathbf{K}_k$, and the state estimate $\hat{\mathbf{x}}_k$. In this algorithm, the ith estimate of the state vector $\mathbf{x}_k$ is denoted by $\hat{\mathbf{x}}_k^{[i]}$, where $i = \{0, 1, 2, \dots\}$. Based on simulation, it is found by the author that the accuarcy is not improving for $i > 2$ and the best results are obtained when $i = 2$. The initial iteration value is the *a priori* estimate

$\hat{\mathbf{x}}_k^-$ from (4.45) as

$$\hat{\mathbf{x}}_k^{[0]} = \hat{\mathbf{x}}_k^-, \tag{4.46}$$

which is the zeroth iteration. Iteration proceeds for $i = \{1, 2\}$ as follows

$$\mathbf{H}_k^{[i]} = \frac{\partial \mathbf{h}}{\partial \mathbf{x}}|_{\mathbf{x}=\hat{\mathbf{x}}_k^{[i-1]}}, \tag{4.47}$$

$$\mathbf{K}_k^{[i]} = \mathbf{P}_k^- \mathbf{H}_k^{\mathrm{T}[i]} (\mathbf{H}_k^{[i]} \mathbf{P}_k^- \mathbf{H}_k^{[i]\mathrm{T}} + \mathbf{R}_k)^{-1}, \tag{4.48}$$

$$\hat{\mathbf{x}}_k^{[i]} = \hat{\mathbf{x}}_k^- + \mathbf{K}_k^{[i]} (\mathbf{z}_k - \mathbf{h}(\hat{\mathbf{x}}_k^{[i]})), \tag{4.49}$$

The final *a posteriori* estimation of the state $\hat{\mathbf{x}}_k^{[i]}$ for $i = 2$ is obtained from the last iteration, and the corresponding *a posteriori* estimation noise covariance is calculated using the following formula

$$\mathbf{P}_k = \mathbf{P}_k^- - \mathbf{K}_k^{[i]} \mathbf{H}_k^{[i]} \mathbf{P}_k^- \qquad i = 2. \tag{4.50}$$

The IEKF equations and their implementation are summarized in algorithm 4.2.

4.5.2 Simulation Procedure

The simulations of the implementation of the IEKF, which are based on the model presented in section 3.2, are carried out according to the following steps:

1. The simulation steps 1-8 of the simulation procedure given in section 3.7 are executed to obtain an initial system state $\hat{\mathbf{x}}_0$.
2. IEKF or EKF is used for L&T according to section 4.5.1 or section 4.4 respectively. Here, the system measurements hold the estimated distance $\hat{d}_i$ and the system state holds the position estimation $\hat{\mathbf{p}}$.
3. The estimated position $\hat{\mathbf{p}}$ is extracted from the the system state $\hat{\mathbf{x}}$.
4. The distance error ρ is calculated as given in (3.64).

Algorithm 4.2 Iterated Extended Kalman Filter Implementation Design Algorithm

1: Obtain the location of the anchor nodes $\mathbf{P}_{\mathrm{BS}}$.
2: Initialize the measurement noise matrix $\mathbf{R}$ as in (4.13).
3: Initialize and possibly tune the process noise matrix $\mathbf{Q}$ as in (4.15).
4: Initialize the error estimation covariance $\mathbf{P}_0$ as in (4.43).
5: Initialize the system state $\hat{\mathbf{x}}_0$ as in (4.44).
6: **for** $k = 1$ to ∞ **do**
7: Compute the partial derivative $\mathbf{H}_k$ as in (4.35);
8: Compute the *a priori* state estimate $\hat{\mathbf{x}}_k^-$ as in (4.45);
9: Obtain the measurements $\mathbf{z}_k = \{z_1, z_2, \ldots, z_N\}$;
10: **for** $i = 1$ to $i = 2$ **do**
11: Compute the partial derivative $\mathbf{H}_k^{[i]}$ as in (4.35);
12: Compute the Kalman gain $K_k^{[i]}$ as in (4.48);
13: Compute the *a posteriori* state estimate $\hat{\mathbf{x}}_k^{[i]}$ as in (4.49);
14: **end for**
15: Compute the *a posteriori* error estimation matrix $\mathbf{P}_k$ as in (4.50);
16: Extract the position information $\hat{x}_k$,$\hat{y}_k$ from the state $\hat{\mathbf{x}}_k^{[i]}$;
17: **end for**

5. The simulation steps 1-4 are carried out for different traces according to the performance evaluation model presented in section 3.2.
6. The simulation steps 1-5 are repeated for 100 iterations.
7. The mean distance error $E(\Delta\rho)$ is conducted by averaging all the obtained values of the distance error ρ.
8. The simulation steps 1-7 are executed for different numbers of anchor nodes $N \in \{3, 4, 6\}$.

4.5.3 Results

The simulation results for the proposed IEKF are depicted in Figs. 4.3, 4.4, and 4.5. The results are obtained based on the performance evaluation model which is presented in section 3.2 and the simulation procedure of section 4.5.2.

In the figures mentioned above, the IEKF is evaluated using the error distance ρ according to distance d from the network's center for $3, 4$, and 6 anchor nodes in

Table 4.2: Mean error distance for IEKF compared with EKF.

Method	Mean error distance $E[\Delta\rho]$ (m)		
	3 Anchor nodes	4 Anchor nodes	6 Anchor nodes
IEKF	16.06	13.44	11.11
EKF	21.915	20.21	16.57

comparison with the widely used method EKF. The error distance ρ is defined to be the distance estimation error between the estimated position $\hat{\mathbf{p}}$ and the real position $\mathbf{p}$ as expressed in (3.65). The error distance ρ is calculated for the positions that the mobile node follows in all the traces of the movement schemes presented in section 3.2. The distance d is the distance from the network's center to the radius of the *circle of trust* that has 150 m diameter as presented in section 2.2.

From Figs. 4.3, 4.4, 4.5, it can be seen that the IEKF did diverge as the EKF resulting in lower error distance comparing with the EKF.

In addition to the presented figures, the estimated mean error distance $E[\Delta\rho]$ values for the IEKF are calculated by averaging all the obtained error distance ρ values for $3, 4$ and 6 anchor nodes. The obtained values are 16.06 m, 13.44 m, 11.11 m for $3, 4, 6$ anchor nodes respectively. The IEKF shows $36,42\,\%$, $33,49\,\%$ and $32,95\,\%$ improvement compared to the EKF for $3, 4$ and 6 anchor node respectively. Nevertheless, the IEKF mean error distance values are given in Table 4.2.

In order to show the distribution of the IEKF error distance values according to the distances d, figures 4.6, 4.7 and 4.8 are presented. By considering Fig. 4.6 that has 71 % of the error distance values below 20 m for the case of 3 anchor nodes, the largest probability is obtained at the distance of 10 m. For the case of 4 anchor nodes, Fig. 4.7 with the probability of 82 % at distances lower than 20 m is presented. The largest error probability occurs at the distance of 9 m. For the case of 6 anchor nodes, Fig. 4.8 that has a probability of 91 % for distances below 20 m is depicted. The largest error probability occurs in this figure is the distance of 9 m.

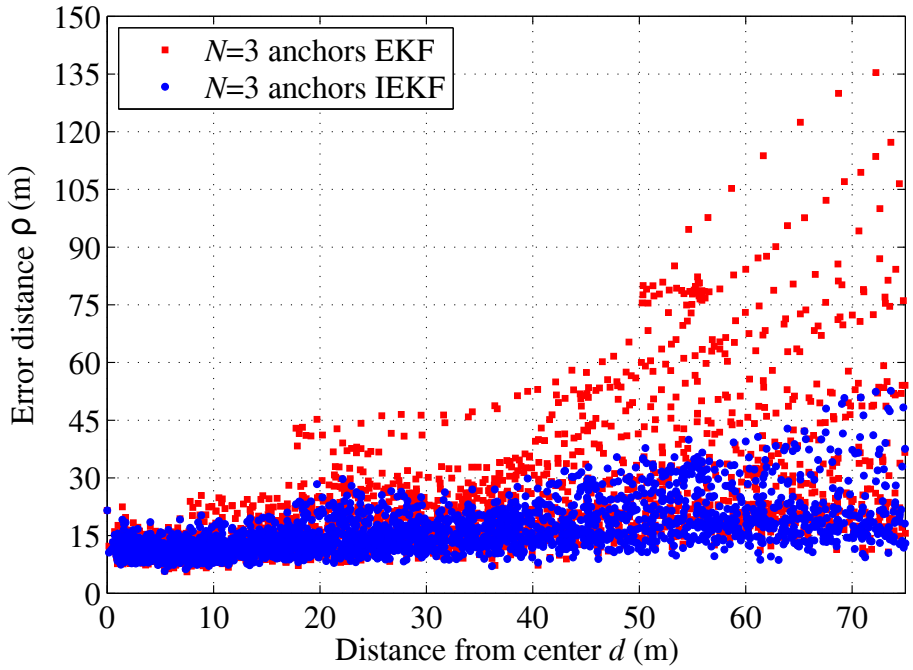

Figure 4.3: IEKF simulated error distance ρ according to distance d compared to the EKF using 3 anchor nodes.

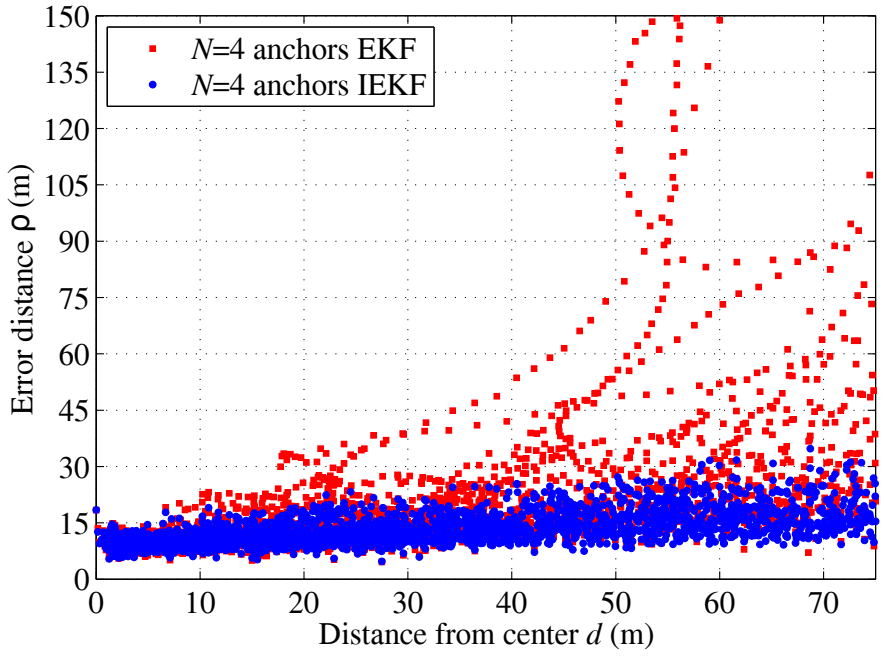

Figure 4.4: IEKF simulated error distance ρ according to distance d compared to the EKF using 4 anchor nodes.

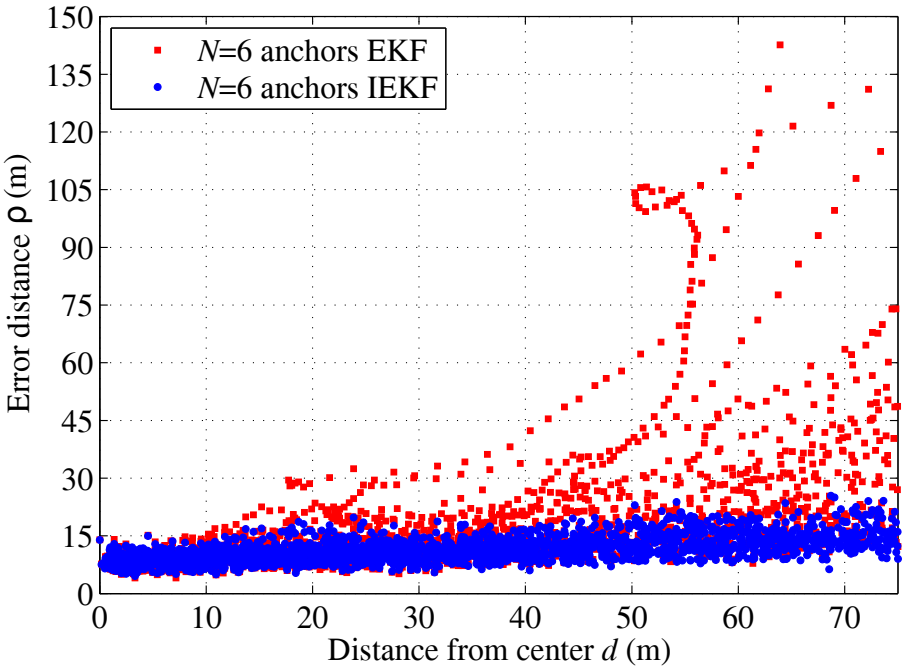

Figure 4.5: IEKF simulated error distance ρ according to distance d compared to the EKF using 6 anchor nodes.

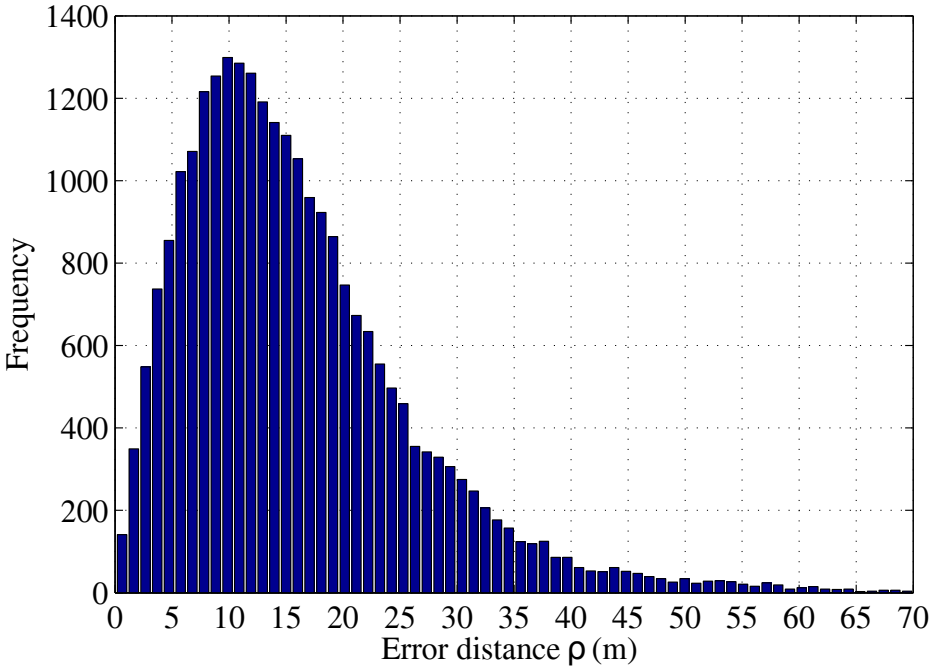

Figure 4.6: Error distance distribution for the IEKF in case of 3 anchor nodes.

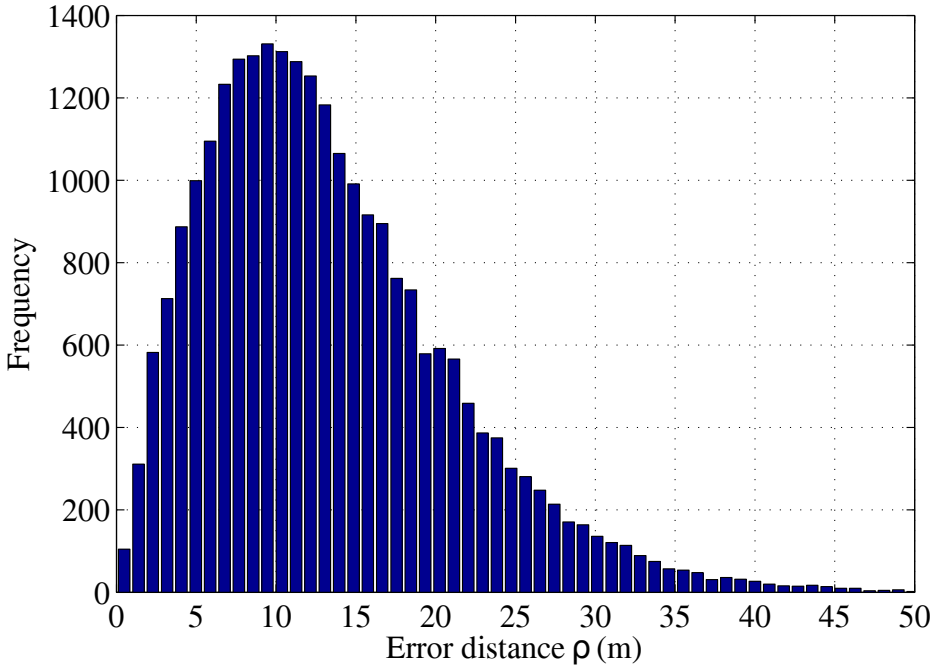

Figure 4.7: Error distance distribution for the IEKF in case of 4 anchor nodes.

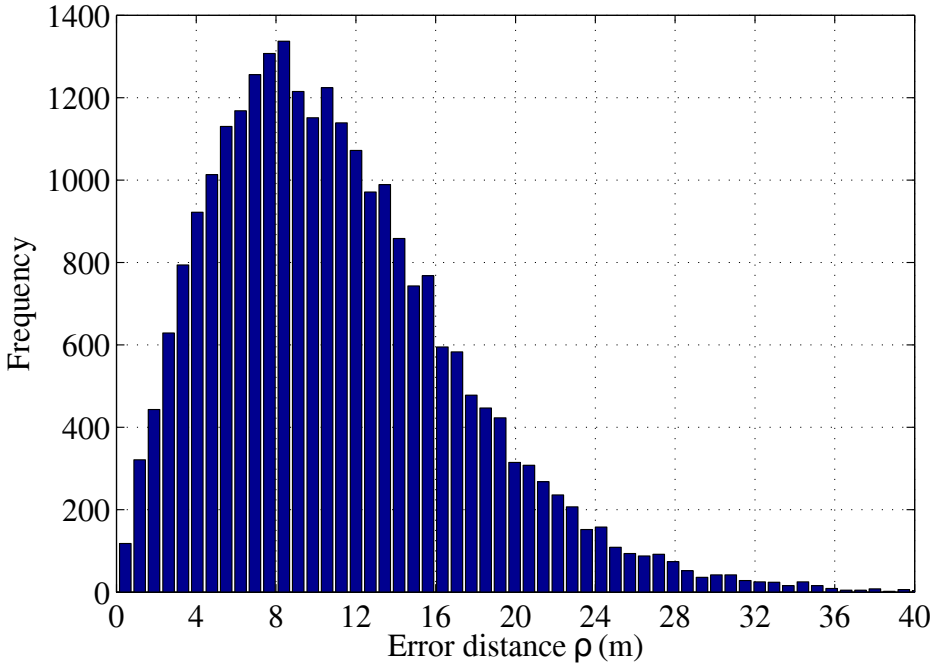

Figure 4.8: Error distance distribution for the IEKF in case of 6 anchor nodes.

For comparison purpose, the histogram distributions of the popular EKF are depicted in figures 4.9, 4.10, and 4.11. Figure 4.10 shows the results for the case of 3 anchor nodes with 60 % of the error distance values are below 20 m. The largest probability is achieved at the distance of 12 m. Figure. 4.11 depects the distribution with a probability of 67 % for distances below 20 m for the case of 4 anchor nodes. The largest probability exists at the distance of 8 m. Figure 4.10 which shows the results for 6 anchor nodes, achieves the probability of 77 % at error distance of 20 m. The largest error probability occurs at a distance of error of 6 m.

From the simulation results above as well as the values of Table 4.2, it can be seen clearly that the IEKF has substantial improvement in estimation accuracy compared with the popular EKF approach in all the testing conditions.

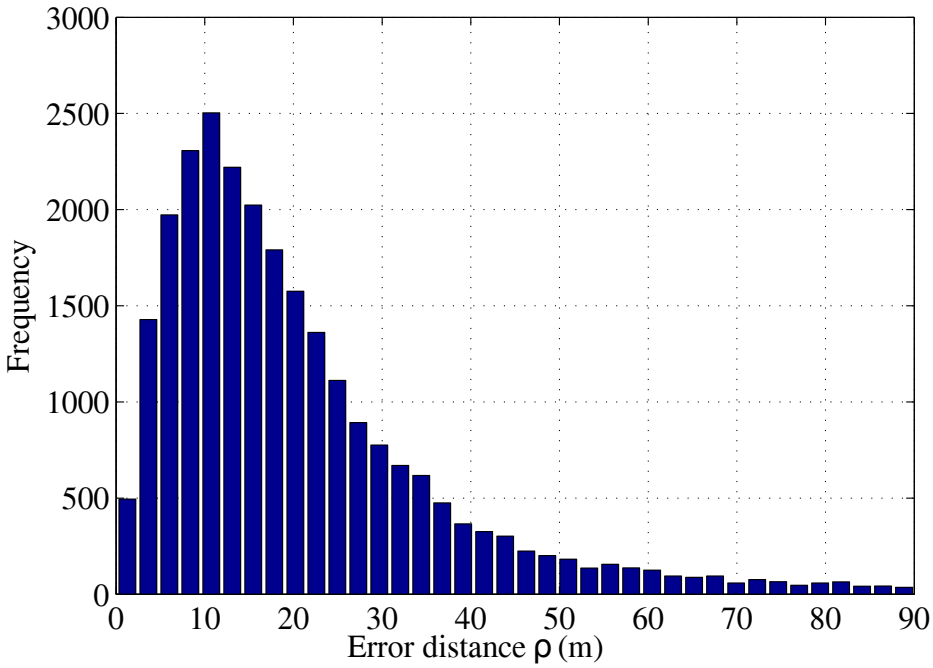

Figure 4.9: EKF error distance distribution for 3 anchor nodes.

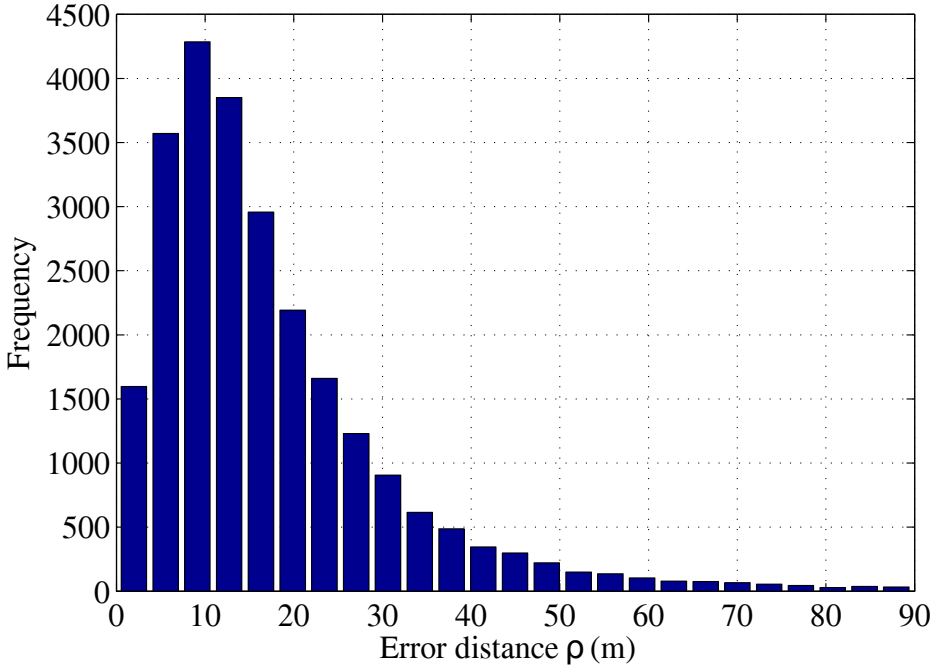

Figure 4.10: EKF error distance distribution for 4 anchor nodes.

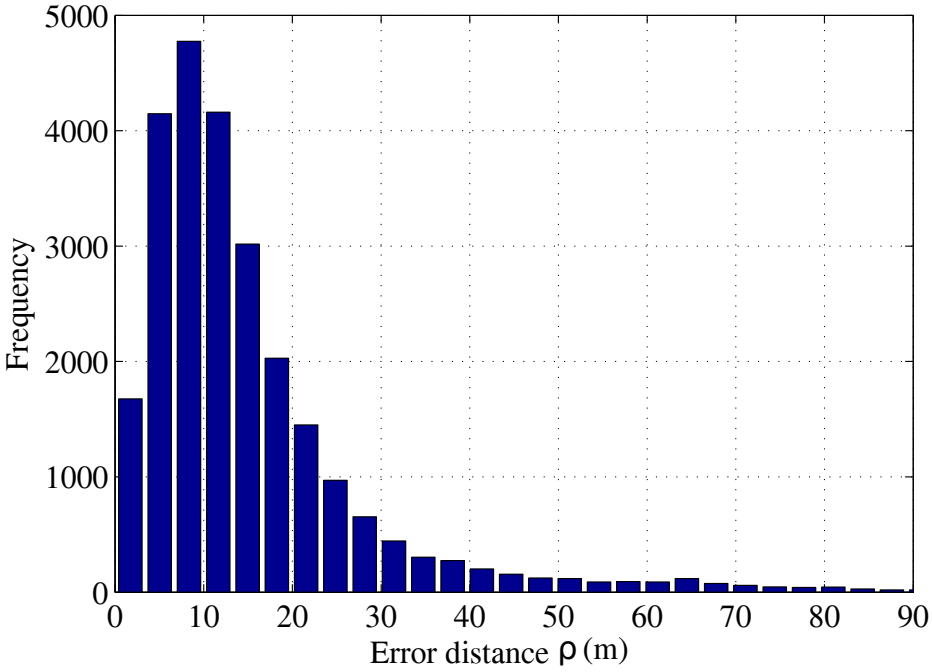

Figure 4.11: EKF error distance distribution for 6 anchor nodes.

5 SPKFs for RSSI-Based WLAN IEEE 802.11n Positioning and Tracking

5.1 Introduction

The EKF applies the non-linear equations to the KF by linearizing the non-linearity which exists in the models of (2.19) and (2.20) so that the traditional KF can be adapted. However, the use of EKF has several drawbacks as pointed out earlier in section 1.3.2.

To address those drawbacks, several approaches have been developed and proposed to deal with the non-linear system models. Among those approaches is the sigma-point sampling approach. This approach uses a deterministic sampling framework to predict the mean and covariance of non-linear models [Van04]. *Unscented Transformation* (UT) techniques are examples of the sigma-point approach. Unlike the EKF which requires the derivation of particular matrices which are called the Jacobian derivatives, this approach does not require analytic derivatives of the non-linear system equations [PW09]. The implementation of different techniques of the sigma-point approach to the KF resulting in what is called the family of the *Sigma Point Kalman Filter* (SPKF) [PW09].

To deal with the non-linearity available in the positioning problem, the author proposes the *Scaled Unscented Transformation* (SUT) which can be implemented with the KF. In the beginning, the SUT is designed to address the positioning problem. Then, the implementation of this transformation to the KF is given. The author calls this implementation as the *Scaled Unscented Kalman Filter* (SUKF). The algorithmic implementation of this filter is presented. The author proposes the resulting filter for the positioning and tracking application. Comparative results of the implementation are illustrated.

Moreover in this chapter, the author proposes the *Spherical Simplex Unscented Transformation* (SSUT) treating the non-linearity that exists in the positioning problem. Accordingly, the SSUT is designed to address the positioning problem. The implementation of the algorithm to the KF is then given and discussed. The resulting filter from the implementation is called the *Spherical Simplex Unscented Kalman Filter* (SSUKF) [Loz+08]. The author proposes the resulting filter for indoor positioning and tracking application. Comparative results of filter implementations are presented. This chapter encompasses the research published in [KJ15a; KJ15b].

5.2 SUKF for RSSI-based WLAN IEEE 802.11n Positioning and Tracking

In this section, the author proposes the SUKF for indoor positioning and tracking based on the WLAN IEEE 802.11n to overcome the limitation of the EKF. Unlike the EKF which uses a first order truncated Taylor series expansion of the non-linear function, SUT guarantees second order and partially incorporate higher order terms into the estimates [Jul02]. In addition, SUT does not require the calculation of particular matrices called the Jacobian matrices, which makes SUT easier to implement compared to EKF [Jul02].

In the beginning, the SUT is designed according to the positioning problem. Then, the application of this transformation into the KF is presented. The resulting filter is tested and the simulation procedure of the implementation of the filter is given. Finally, comparative results and discussion are presented.

5.2.1 The Scaled Unscented Transformation Design

In this section, the SUT [Jul02] is presented in its general form for a general overview. Then, the SUT is designed to deal with the non-linear measurement function $\mathbf{h}(\cdot)$ of (4.8) for the designed state-space models of the KF.

The SUT is a method for calculating the statistics of a random variable which undergoes a non-linear transformation instead of linearizing the transformation. SUT is based on the intuition that "*with a fixed number of parameters it should be easier to approximate a distribution (not necessarily Gaussian) than it is to approximate an arbitrary non-linear function/transformation*" [Jul02].

In this approach, a random variable is specified by a set of deterministically determined *sample points*. These sample points, or so called *sigma points*, capture the mean and the covariance of the random variable and allow direct propagation of the information through an arbitrary set of non-linear equations. The mean and covariance of the transformed ensemble can be computed as the estimation of the non-linear transformation of the original distribution. This method guarantees second order accuracy of Taylor series expansion in the mean and covariance. More importantly, this method can partially incorporate higher order term information into the estimates.

To accomplish the SUT objectives, a discrete distribution having the same first and second order moments is generated and then scaled, where each point in this distribution can be directly transformed. The mean and covariance of the transformed information can be computed as the estimate of the non-linear transformations.

Given an n-dimensional vector random variable $\mathbf{x}$ with mean $\bar{\mathbf{x}}$ and covariance $\mathbf{P}_x$, where

$$\mathbf{P}_x = \mathrm{E}\{(\mathbf{x} - \bar{\mathbf{x}})(\mathbf{x} - \bar{\mathbf{x}})^T\}. \tag{5.1}$$

It is desired to predict the mean $\bar{\mathbf{y}}$ and the covariance $\mathbf{P}_\mathrm{y}$ of a m-dimensional vector random variable $\mathbf{y}$, where

$$\mathbf{P}_y = \mathrm{E}\{(\mathbf{y} - \bar{\mathbf{y}})(\mathbf{y} - \bar{\mathbf{y}})^T\}, \tag{5.2}$$

and $\mathbf{y}$ is related to $\mathbf{x}$ by the non-linear function

$$\mathbf{y} = \mathbf{g}(\mathbf{x}). \tag{5.3}$$

The discrete distribution of the SUT can be obtained by generating a set $\mathbf{S}$ of points and their weights as

$$\mathbf{S} = \{\chi_i, W_i; i = 0, 1, \ldots, 2n\}, \tag{5.4}$$

where χ_i is the the i-th sigma point and W_i is i-th associated weight. The generated sigma points have the same mean and covariance as the random variable $\mathbf{x}$. The generated sigma points and their weights are then scaled according to a procedure given in [Jul02].

Combining the sigma points generation and scaling schemes in one step is presented in [Van04] as an attempt to reduce the number of calculations. According to this procedure, the sigma points are calculated as

$$\begin{aligned}
\chi_i &= \bar{\mathbf{x}} && i = 0 \\
\chi_i &= \bar{\mathbf{x}} + (\sqrt{(n+\lambda)\mathbf{P}_\mathrm{x}})_i && i = 1, \ldots, n \\
\chi_i &= \bar{\mathbf{x}} - (\sqrt{(n+\lambda)\mathbf{P}_\mathrm{x}})_{i-n} && i = n+1, \ldots, 2n
\end{aligned} \tag{5.5}$$

where $(\sqrt{(n+\lambda)\mathbf{P}_x})_i$ is the ith column of the matrix square root $\sqrt{(n+\lambda)\mathbf{P}_x}$. λ

is calculated as

$$\lambda = \alpha^2(n + \kappa) - n, \tag{5.6}$$

where α is a positive scaling parameter which arbitrarily can be chosen as

$$0 \leq \alpha \leq 1, \tag{5.7}$$

to be small to minimize the higher order effects and κ is selected to guarantee positive semidefinite covariance matrix according to

$$\kappa \geq 0. \tag{5.8}$$

However, the κ scales the sigma points from the mean $\bar{\mathbf{x}}$ and the nearest points to the mean happened when $\kappa = 1$ [Van04]. While the n is equal to 4 throughout this dissertation, the parameters α and κ are selected for tuning purpose and they will be assigned later in this section. Nevertheless, the selection values for α and κ that satisfy (5.7) and (5.8) guarantee second order accuracy of Taylor series expansion in the mean and covariance and incorporate partially higher order terms information. As such, the tuning affects the incorporation of the higher order terms information into the estimates. The weights are calculated as

$$\begin{aligned} W_0^{(m)} &= \frac{\lambda}{(n+\lambda)} && i = 0 \\ W_0^{(c)} &= \frac{\lambda}{n+\lambda} + (1 - \alpha^2 + \beta) && i = 0 \\ W_i^{(m)} &= W_i^c = \frac{1}{2(n+\lambda)} && i = 1, 2, \ldots, 2n \end{aligned} \tag{5.9}$$

where the superscripts m and c refer to the weights associated with the mean and covariance respectively. β is a weighting factor that participate in including partial higher order information of the fourth order term in the Taylor series expansion of the covariance. Under the assumption that $\mathbf{x}$ has Gaussian distribution, error in the forth order term of the Taylor series expansion of the covariance of $\mathbf{x}$ is minimized when $\beta = 2$ [Jul02].

Once the set of the *scaled points* are obtained, a transformed set of the points is evaluated by means of the non-linear function of the system

$$\boldsymbol{\xi}_i = \mathbf{g}(\boldsymbol{\chi}_i) \qquad i = \{0, 1, \ldots, 2n\}. \tag{5.10}$$

Finally, the predicted mean is calculated and covariance as follows

$$\bar{\mathbf{y}} = \sum_{i=0}^{2n} W_i^{(m)} \boldsymbol{\xi}_i, \tag{5.11}$$

and the predicted covariance is calculated as follows

$$\mathbf{P}_{\mathrm{y}} = \sum_{i=0}^{2n} W_i^{(c)} [\boldsymbol{\xi}_i - \bar{\mathbf{y}}][\boldsymbol{\xi}_i - \bar{\mathbf{y}}]^T. \tag{5.12}$$

The designing of the SUT starts by assigning the parameters α and κ. The author of this dissertation assumes

$$\alpha = 0.1, \tag{5.13}$$

and

$$\kappa = 0, \tag{5.14}$$

to satisfy (5.7) and (5.8) respectively. The value of κ is chosen here so that the sigma points stay near the mean as given in [Van04]. The author of this dissertation found through simulations that the SUT is not much sensitive to the selection of those values. However, the selection of the values α and κ to achieve the best results is still an open topic and will be left to future work. The author of this dissertation assumes that the random variable $\mathbf{x}$ has a Gaussian distribution and therefore β is equal to 2.

By considering the measurement function $\mathbf{h}(\cdot)$ of (4.9) for the designed state-space models which is presented in Section 4.2, equation (5.3) is then written

as

$$\mathbf{g}(\mathbf{x}) = \mathbf{h}(\hat{\mathbf{x}}_k^-) = \begin{bmatrix} \sqrt{(x_{\mathrm{BS}_1} - \hat{x}_k^-)^2 + (y_{\mathrm{BS}_1} - \hat{y}_k^-)^2} \\ \vdots \\ \sqrt{(x_{\mathrm{BS}_N} - \hat{x}_k^-)^2 + (y_{\mathrm{BS}_N} - \hat{y}_k^-)^2} \end{bmatrix} = \begin{bmatrix} \tilde{z}_k^1 \\ \vdots \\ \tilde{z}_k^N \end{bmatrix}, \tag{5.15}$$

where

$$\hat{\mathbf{x}}_k^- = \begin{bmatrix} \hat{x}_k^- \\ \hat{y}_k^- \\ \hat{v}_k^{x-} \\ \hat{v}_k^{y-} \end{bmatrix}. \tag{5.16}$$

To select the method to calculate the square root matrix, the selection conditions of this matrix should be considered. The SUT gives the freedom to select the calculation method of the square roots including selecting non-square matrix roots calculation methods. Furthermore, the transformation is not restricted to using orthogonal or symmetric matrix square roots, which have implementation complexity.

A recent study as in [Rhu+12] showed that the Cholesky decomposition method is considered the best overall matrix square root calculation method for UT in terms of performance and execution time. Based on that study, the author of this dissertation proposes the Cholesky decomposition method [GV12] for calculating the square root matrix. The Cholesky method decomposes a matrix into a product of a lower triangular matrix $\mathbf{L}$ and its transpose [Rhu+12]. As such, the matrix $(n+\lambda)\mathbf{P}_{k-1}$ can be expressed as

$$(n+\lambda)\mathbf{P}_{k-1} = \mathbf{L}\mathbf{L}^T, \tag{5.17}$$

where $\mathbf{L}$ is the square root matrix. By considering that the square root matrix $\mathbf{L}$ of the matrix $(n+\lambda)\mathbf{P}_k^-$ has the dimension 4×4 based on the the design of the state-space models given in section 4.2, the elements of the matrix $\mathbf{L}$ can be found

by solving, from [Rhu+12; GV12], the following:

$$(n+\kappa)\mathbf{P}_k^- = \begin{bmatrix} P_{11} & P_{12} & P_{13} & P_{14} \\ P_{21} & P_{22} & P_{23} & P_{24} \\ P_{31} & P_{32} & P_{33} & P_{34} \\ P_{41} & P_{42} & P_{43} & P_{44} \end{bmatrix} = \begin{bmatrix} L_{11} & 0 & 0 & 0 \\ L_{21} & L_{22} & 0 & 0 \\ L_{31} & L_{32} & L_{32} & 0 \\ L_{41} & L_{42} & L_{43} & L_{44} \end{bmatrix} \begin{bmatrix} L_{11} & 0 & 0 & 0 \\ L_{21} & L_{22} & 0 & 0 \\ L_{31} & L_{32} & L_{32} & 0 \\ L_{41} & L_{42} & L_{43} & L_{44} \end{bmatrix}^T . \tag{5.18}$$

By considering that the noise of (4.9) has zero mean value, the sigma points calculation of (5.5) is then written as

$$\begin{aligned} \boldsymbol{\chi}_i &= \hat{\mathbf{x}}_k^- && i = 0 \\ \boldsymbol{\chi}_i &= \hat{\mathbf{x}}_k^- + \mathbf{L}(:, i) && i = 1, 2, 3, 4 \\ \boldsymbol{\chi}_i &= \hat{\mathbf{x}}_k^- - \mathbf{L}(:, i-4) && i = 5, 6, 7, 8 \end{aligned} \tag{5.19}$$

The obtained sigma points from the *a priori* state estimate $\hat{\mathbf{x}}_k^- \in \mathbb{R}^4$ and the associated estimation error matrix $\mathbf{P}_k^- \in \mathbb{R}^{4\times4}$ are then transformed using (5.15) to produce the approximated measurement $\tilde{\mathbf{z}}_k \in \mathbb{R}^N$ and the associated covariance matrix $\mathbf{P}_z \in \mathbb{R}^{4\times4}$. As such, equation (5.15) is rewritten as

$$\boldsymbol{\xi}_i = \mathbf{h}(\boldsymbol{\chi}_i) = \begin{bmatrix} \sqrt{(x_{\mathrm{BS}_1} - \chi_i(1))^2 + (y_{\mathrm{BS}_1} - \chi_i(2))^2} \\ \vdots \\ \sqrt{(x_{\mathrm{BS}_N} - \chi_i(1))^2 + (y_{\mathrm{BS}_N} - \chi_i(2))^2} \end{bmatrix}, \tag{5.20}$$

where

$$\boldsymbol{\chi}_i = \begin{bmatrix} \chi_i(1) \\ \chi_i(2) \\ \chi_i(3) \\ \chi_i(4) \end{bmatrix}. \tag{5.21}$$

The transformed sigma points are then used to calculate the aproximate measurement $\tilde{\mathbf{z}}_k$. This can be done by writing (5.11) as

$$\tilde{\mathbf{z}}_k = \sum_{i=0}^{8} W_i^{(m)} \boldsymbol{\xi}_i. \tag{5.22}$$

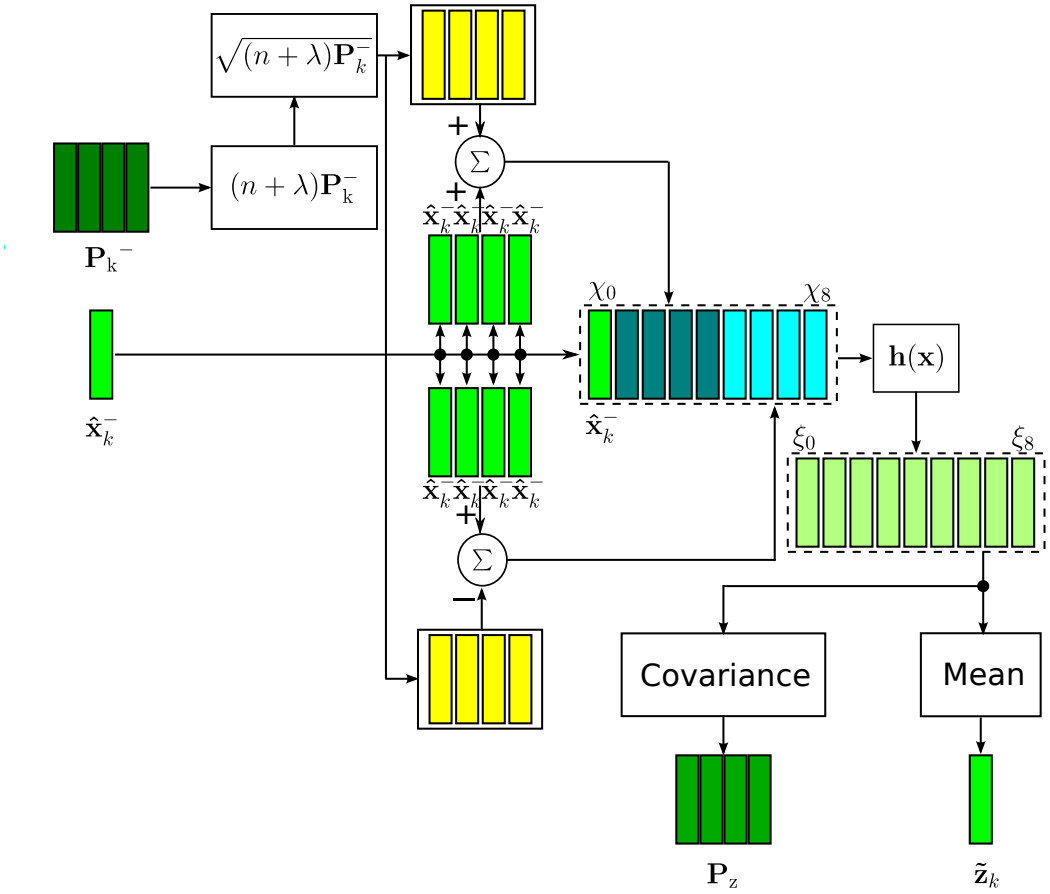

Figure 5.1: Block diagram of the 4-dimensional variable $\hat{\mathbf{x}}_k$ that undergoes the SUT to produce the measurement approximation $\tilde{\mathbf{z}}_k$. Inspired by [Van04].

Then, the associated covariance matrix $\mathbf{P}_z$ can be computed by writing (5.12) as

$$\mathbf{P}_z = \sum_{i=0}^{8} W_i^{(c)} [\boldsymbol{\xi}_i - \tilde{\mathbf{z}}_k][\boldsymbol{\xi}_i - \tilde{\mathbf{z}}_k]^T. \tag{5.23}$$

The complete design of the SUT algorithm for measurements to state function of the designed model of (4.9) of the positioning problem of section 2.2 is summarized in Algorithm 5.1. In addition, a block diagram that summarizes the SUT is given in Figure 5.1.

Algorithm 5.1 Scaled Unscented Transformation Algorithm Design for Measurements to State Function

1: Obtain the parameter λ from (5.6);
2: Obtain the weights of the sigma points from (5.9);
3: Compute the square root matrix $\mathbf{L}$ of the matrix $(n+\lambda)\mathbf{P}_k^-$ as in (5.18).;
4: **for** $i = 0$ to $i = 4$ **do**
5: Compute the Sigma point χ_i as in (5.19);
6: Obtain the transformed sigma point ξ_i as in (5.20);
7: **end for**
8: Compute the the approximated measurements $\tilde{\mathbf{z}}$ as in (5.22).
9: Compute the covariance matrix $\mathbf{P}_z$ as in (5.23);

5.2.2 Scaled Unscented Kalman Filter Implementation

The introduction of the SUT to the KF is firstly proposed by [CM03]. The filter is called unscented filter. A different introduction of the SUT to the KF is proposed by [V+04]. The resulting filter is called Unscented Kalman Filter (UKF). The author of this dissertation compares the performance of the Unscented filter and the UKF with the EKF. Based on this comparison, the UKF showed to lag behind the EKF.

A different application for the UT techniques to the KF is recently proposed by [GA11]. Based on the application, the author of this dissertation calls the resulting filter as the *Scaled Unscented Kalman Filter* (SUKF).

For the operation of the SUKF, the filter noise covariances $\mathbf{Q} \in \mathbb{R}^{4\times4}$ and $\mathbf{R} \in \mathbb{R}^{4\times4}$ need to be determined, which can be done according to the procedure given in section 4.3. The error covariance matrix $\mathbf{P}_{k-1}$ can be initialized for $k = 1$ as

$$\mathbf{P}_{k-1} = \mathbf{Q}, \tag{5.24}$$

and the system state $\hat{\mathbf{x}}_{k-1}$ for $k = 1$ is initialized as

$$\hat{\mathbf{x}}_{k-1} = \begin{bmatrix} \hat{\mathbf{x}}_{\text{tr}} \\ 0 \\ 0 \end{bmatrix}, \tag{5.25}$$

where $\hat{\mathbf{x}}_{\text{tr}}$ is the estimated position obtained from Algorithm 3.1 and the velocities v_k^x and v_k^y of the *zeroth* state $\hat{\mathbf{x}}_0$ are assumed to be zero.

By recalling the state-space models design given in section 4.2, the *a priori* state estimate $\hat{\mathbf{x}}_k^-$ is obtained as

$$\hat{\mathbf{x}}_k^- = \hat{\mathbf{x}}_{k-1} + \mathbf{B}\mathbf{u}_{k-1}. \tag{5.26}$$

The *a priori* estimation error matrix $\mathbf{P}_k^-$ is obtained from

$$\mathbf{P}_k^- = \mathbf{P}_{k-1} + \mathbf{Q}. \tag{5.27}$$

The standard Kalman gain of (2.44) is applied only for linear system. However, the term $\mathbf{P}_k^-\mathbf{H}_k^T$ of (2.44) is expressed, from [GA11], as

$$\mathbf{P}_k^-\mathbf{H}_k^T \approx \mathbf{P}_{\text{xz}}, \tag{5.28}$$

where $\mathbf{P}_{\text{xz}}$ is the cross covariance matrix which is calculated from

$$\mathbf{P}_{\text{xz}} = \sum_{i=0}^{8} W_i^{(m)}[\boldsymbol{\xi}_i - \hat{\mathbf{x}}_k^-][\boldsymbol{\xi}_i - \tilde{\mathbf{z}}_k]^T. \tag{5.29}$$

In addition, the term $\mathbf{H}_k\mathbf{P}_k^-\mathbf{H}_k^T$ of (2.44) can be expressed, from [GA11], as

$$\mathbf{H}_k\mathbf{P}_k^-\mathbf{H}_k^T = \mathbf{P}_z, \tag{5.30}$$

where the matrix $\mathbf{P}_{\text{z}}$ is obtained according to Algorithm 5.1. The Kalman gain of (2.44) is then written as

$$\mathbf{K}_k = \mathbf{P}_{\text{xz}}[\mathbf{P}_{\text{z}} + \mathbf{R}]^{-1}. \tag{5.31}$$

The measurements $\mathbf{z}$ and the *approximated* measurement $\tilde{\mathbf{z}}$, which is obtained from Algorithm 5.1, are then used to produce the *a posteriori* state estimation as

$$\hat{\mathbf{x}}_k = \hat{\mathbf{x}}_k^- + \mathbf{K}_k(\mathbf{z}_k - \tilde{\mathbf{z}}_k). \tag{5.32}$$

Algorithm 5.2 Scaled Unscented Kalman Filter Algorithm

procedure INITIALIZATION
    Obtain the location of the anchor nodes $\mathbf{P}_{BS_i}$.
    Initialize the measurement noise matrix $\mathbf{R}$ as in section 4.3.
    Initialize and tune the process noise matrix $\mathbf{Q}$ as in section 4.3.
    Initialize the error estimation covariance $\mathbf{P}_0$ as in (5.24).
    Initialize the estimated position $\hat{\mathbf{x}}_0$ as in (5.25).
    Initialize κ, α, β;
end procedure
for $k = 1$ to ∞ **do**
    Obtain the measurements $\mathbf{z}_k$;
    Obtain the *a priori* state estimate $\hat{\mathbf{x}}_k^-$ as in (5.26).
    Compute the *a priori* estimation error matrix $\mathbf{P}_k^-$ as in (5.27);
    Obtain $\tilde{\mathbf{z}}_k$ and $\mathbf{P}_z$ from Algorithm 5.1;
    Compute the cross covariance matrix $\mathbf{P}_{xz}$ as in (5.29);
    Compute the Kalman gain $\mathbf{K}_k$ from (5.31);
    Compute *a posteriori* state estimate $\hat{\mathbf{x}}_k$ from (5.32);
    Compute the *a posteriori* estimation error covariance $\mathbf{P}_k$ from (5.33);
    Obtain the estimated position $\hat{\mathbf{p}}_k = \hat{\mathbf{x}}_k$;
end for

The *a posteriori* estimation error covariance matrix is then obtained as

$$\mathbf{P}_k = \mathbf{P}_k^- - \mathbf{K}_k \mathbf{P}_{xz}^T. \tag{5.33}$$

The position coordinates $\hat{x}_k$ and $\hat{y}_k$ are then extracted from (5.32). Once new measurements are available, the SUKF is implemented for an update position $\hat{\mathbf{p}}_k$. The complete implementation algorithm of the SUKF to the L&T problem is presented in Algorithm 5.2.

5.2.3 Simulation Procedure

The SUKF is tested based on the model presented in section 3.2. The simulation steps are carried out according to the following

1. The simulation steps 1-8 of the simulation procedure given in section 3.7 are implemented to obtain an initial system state $\hat{\mathbf{x}}_0$.

2. SUKF is used for location estimation and tracking. Here, the system measurements hold the estimated distance $\hat{d}_i$ and the system state holds the position estimation $\hat{\mathbf{p}}$.
3. The estimated position $\hat{\mathbf{p}}$ is extracted from the the system state $\hat{\mathbf{x}}$.
4. The distance error ρ is calculated as given in (3.64).
5. The simulation steps 1-4 are conducted for different traces according to the performance evaluation model presented in section 3.2.
6. The simulation steps 1-5 are repeated for 100 iterations to simulate different noise conditions.
7. The mean distance error $E(\Delta\rho)$ is conducted by averaging all the obtained values of the distance error ρ.
8. The simulation steps 1-7 are repeated for different anchor node numbers $N \in \{3, 4, 6\}$.

5.2.4 Results

In this section, the results are obtained based on the performance evaluation model of section 3.2 and the simulation procedure of section 5.2.3.

The error distance ρ for distance d form the network center of coordinate $(0, 0)$ are depicted in Figs 5.2, 5.3, and 5.4 using $3, 4$ and 6 anchor nodes respectively. In the figures, the SUKF results are presented in comparison with the EKF. The error distance ρ is obtained using the difference between the estimated position $\hat{\mathbf{p}}$ and the real position $\mathbf{p}$ of the mobile node as given in (3.65). The error distance ρ is calculated for all the positions of the movement traces generated according to section 3.2. The distance d is the measurement between the network's center of coordinate $(0, 0)$ and the maximum radius of 75 m which represent the half of the diameter of the *circle of trust* which explained in earlier section 2.2.

Unlike the EKF which shows divergence in in some cases, the SUKF did not show the divergences resulting in lower error distance estimation compared with the EKF as depicted in Figs 5.2, 5.3, 5.4.

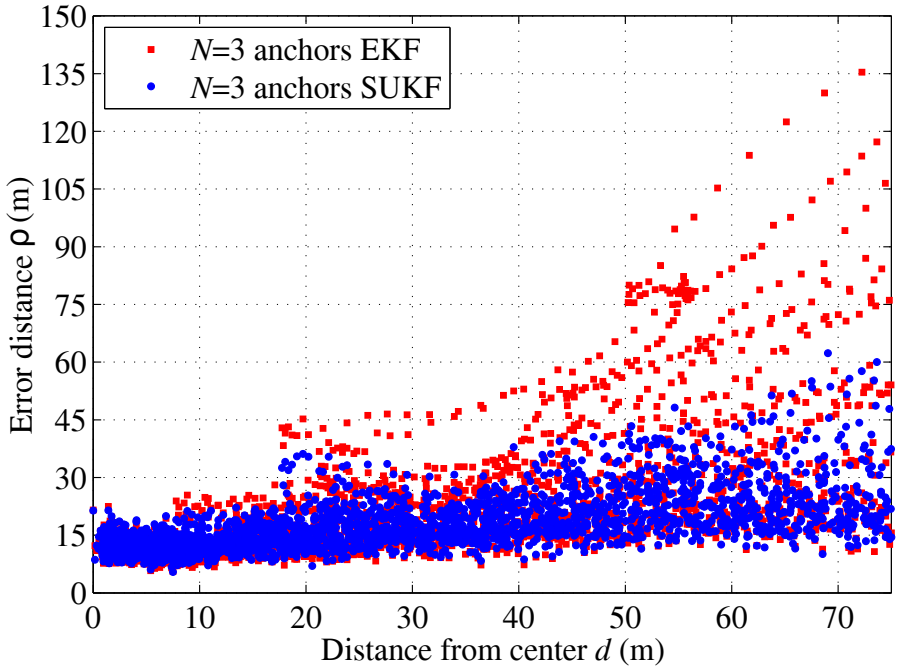

Figure 5.2: Error distance ρ according to distances d for the SUKF compared with the EKF using 3 anchor nodes.

In order to compare the SUKF with other techniques, the estimated mean error distance$\mathrm{E}[\Delta\rho]$ values of the SUKF are calculated by averaging all the obtained error distance ρ values for $3, 4$ and 6 anchor nodes. The resulting values are 18.00 m, 15.52 m, 12.66 m for $3, 4, 6$ anchor nodes respectively. Compared with the EKF, the SUKF shows $17,84\,\%$, $23,20\,\%$, $23,59\,\%$ improvement for $3, 4, 6$ anchor nodes respectively.

The distribution of error distance values of the SUKF over the distance d is depicted in figures 5.5, 5.6 and 5.7. Figure 5.5 depicts the distribution with $67\,\%$ of the error distance values are below 20 m for the case of 3 anchor nodes. The largest probability occurs at the error distance of 11 m. By considering Fig. 5.6 in which distances below 20 m has a probability of $76\,\%$ for the case of 4 anchor nodes, the largest probability occurs at the error distance of 10 m. Figure 5.7 which shows the results for 6 anchor nodes and has a probability of $84\,\%$ for distances below 20 m, the largest probability occurs at the distance of 7 m. Based on the presented results of Figs. 5.2, 5.3, 5.4, and the mean error distance val-

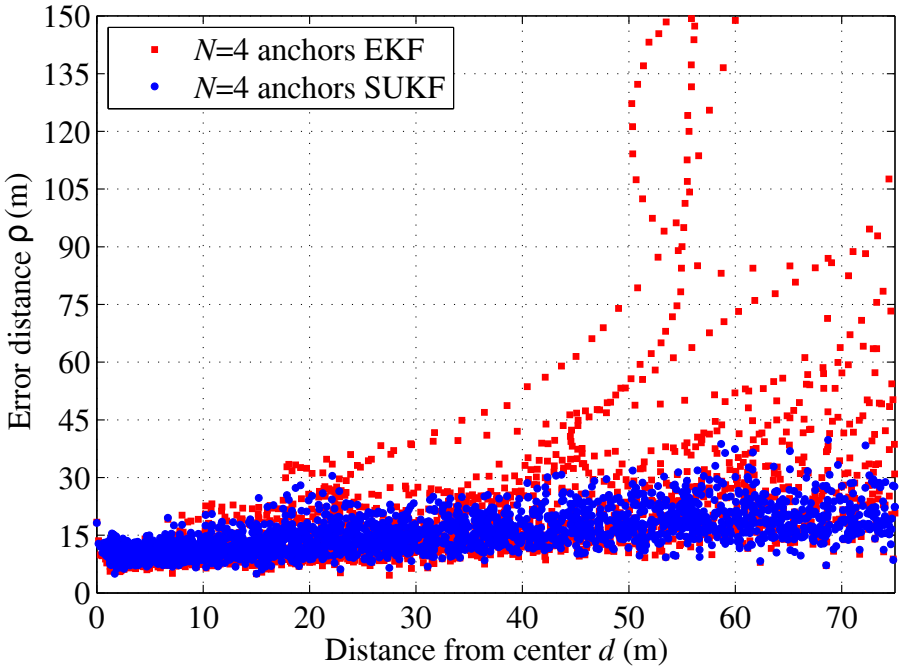

Figure 5.3: Error distance ρ according to distances d for the SUKF compared with the EKF using 4 anchor nodes.

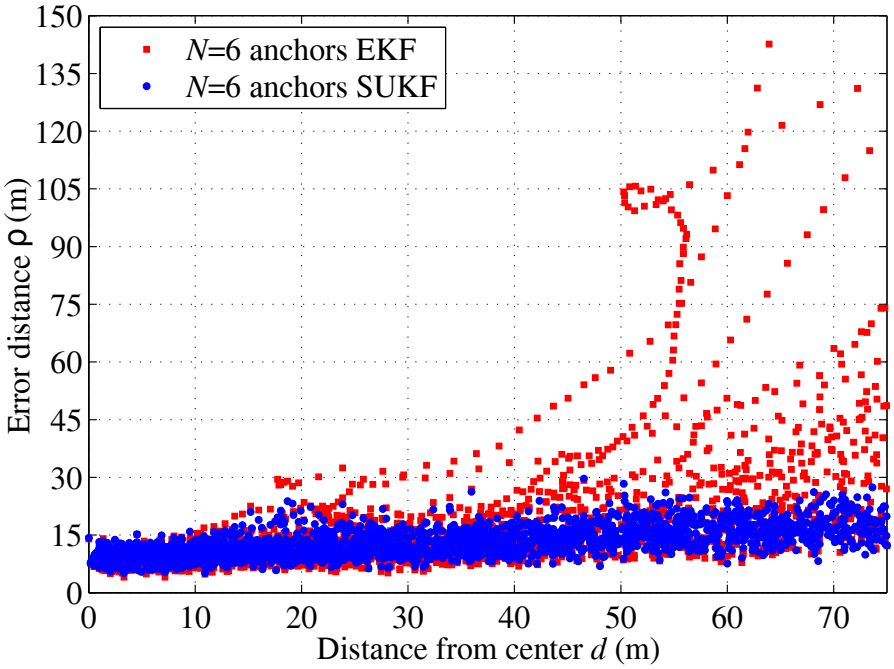

Figure 5.4: Error distance ρ according to distances d for the SUKF compared with the EKF using 6 anchor nodes.

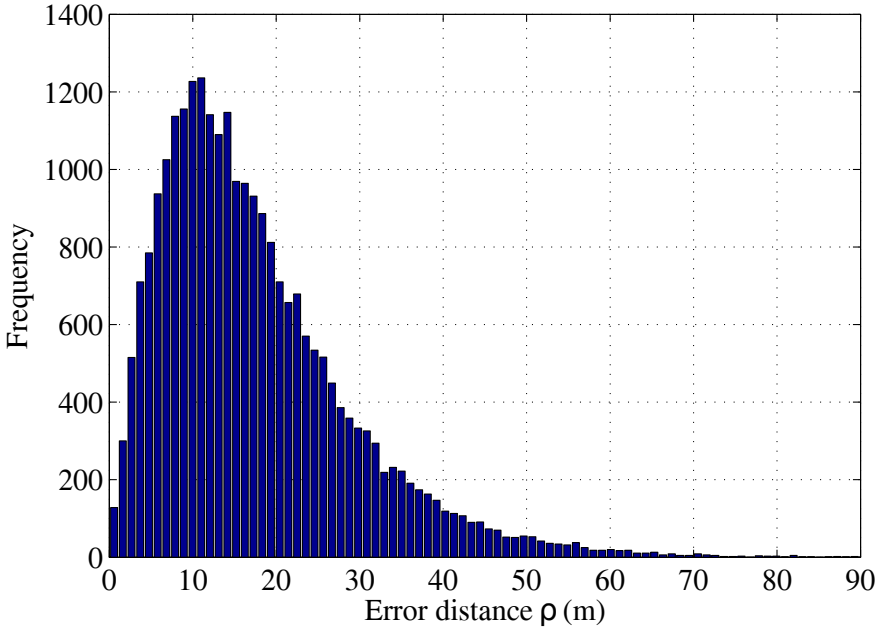

Figure 5.5: SUKF error distance ρ distribution for distances d using 3 anchor nodes.

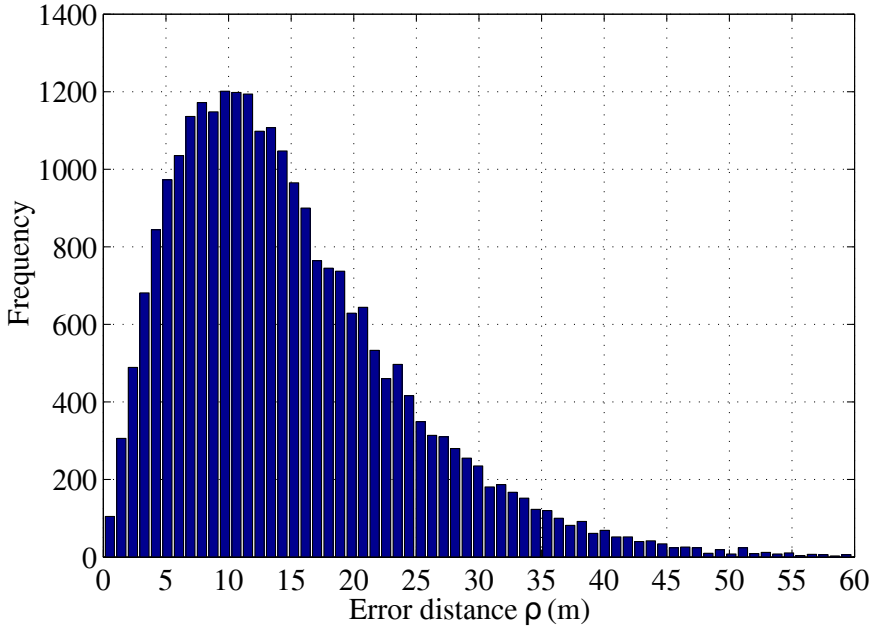

Figure 5.6: SUKF error distance ρ distribution for distances d using 4 anchor nodes.

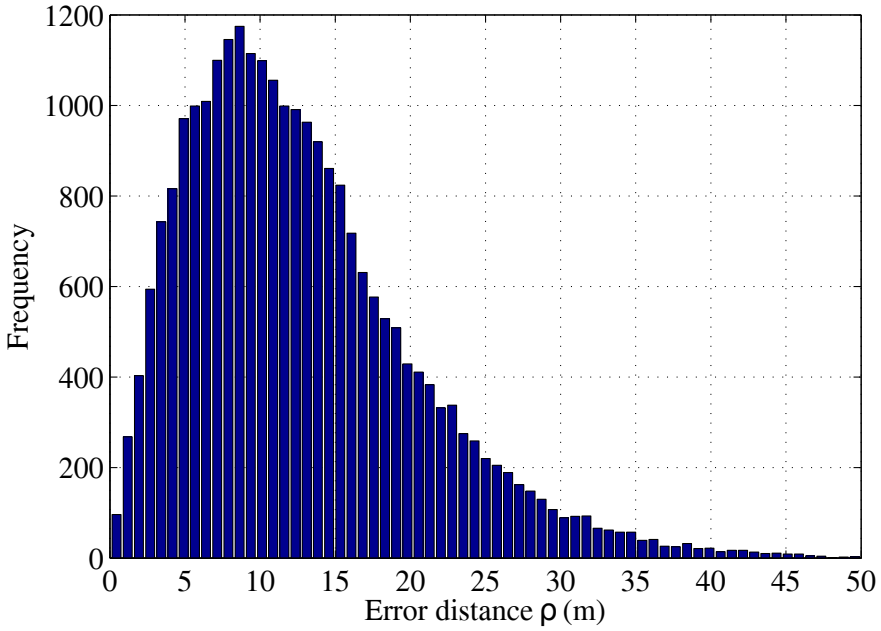

Figure 5.7: SUKF error distance ρ distribution for distances d using 6 anchor nodes.

Table 5.1: Mean error distance for SUKF compared with EKF.

Method	Mean error distance E[$\Delta\rho$] (m)		
	3 Anchor nodes	4 Anchor nodes	6 Anchor nodes
SUKF	18.00	15.52	12.66
EKF	21.915	20.21	16.57

ues of Table 5.1, it can be concluded that the SUKF has substantial better results compared to the EKF in all of the testing conditions.

5.3 SSUT for RSSI-Based WLAN IEEE 802.11n Positioning and Tracking

In this section, the author proposes the SSUKF for indoor positioning and tracking by utilizing the widly deployed WLAN IEEE 802.11n to overcome the limita-

tion of the EKF. Unlike the EKF which uses a first order truncated Taylor series expansion of the non-linear function, SSUT guarantees second order in the mean and covariance [Jul03] of the estimates. Unlike the EKF, the SSUT does not require the calculation of particular matrices such as the Jacobian matrices which makes SUT easier to implement compared to the non-linear approach used by the EKF [Jul03] .

In what follows in this section, the SUT is designed according to the positioning problem. Then, the application of this transformation into the KF is presented. The testing scenario of this filter including the simulation procedure is given. Finally, comparative results and discussion are presented.

5.3.1 The Spherical Simplex Unscented Transformation Design

The SSUT [Jul03] is a method for calculating the mean and covariance of a random variable that undergoes a non-linear function instead of linearizing that function. Similar to the SUT which is presented in section 5.2.1, the SSUT is based on the intuition that "*it is easier to approximate a distribution (not necessarily Gaussian) than it is to approximate an arbitrary non-linear function or transformation*" [Jul03].

This method is proposed in an attempt to minimize the number of sigma points used by the SUT. Instead of $2n+1$ points used by the SUT, the SSUT uses a set of a reduced number of $n+2$ sigma points for an n-dimensional state. This selection strategy defines a simplex of points that lie on hypersphere. In particular, $n+1$ of the points lie on a hypersphere whose radius is proportional to $\sqrt{n}$. The radius which bounds the points is proportional to $\sqrt{n}$ and the weight applied to each point is proportional to $1/n$.

In this method, a random variable $\mathbf{x} \in \mathbb{R}^n$ with mean $\bar{\mathbf{x}}$ and covariance $\mathbf{P}_x$, where

$$\mathbf{P}_x = \mathrm{E}\{(\mathbf{x}-\bar{\mathbf{x}})(\mathbf{x}-\bar{\mathbf{x}})^T\}, \tag{5.34}$$

which undergoes the non-linear transformation

$$\mathbf{y} = \mathbf{g}(\mathbf{x}), \tag{5.35}$$

is represented by a set of sigma points that are deterministically determined and capture the mean and the covariance of the random variable. The sigma points then transform through the non-linear transformation. The mean $\bar{\mathbf{y}} \in \mathbb{R}^m$ and the covariance $\mathbf{P}_\mathrm{y}$, where

$$\mathbf{P}_y = \mathrm{E}\{(\mathbf{y} - \bar{\mathbf{y}})(\mathbf{y} - \bar{\mathbf{y}})^T\}, \tag{5.36}$$

of the transformed points represent the estimation of the non-linear transformation of the original random variable distribution. Similar to the SUT, this method perceive second order accuracy of Taylor series expansion in the mean and covariance.

The distribution of the SSUT is obtained by determining a set S of points and their associated weights as

$$\mathbf{S} = \{\chi_i, Wi; i = 0, \ldots, n+1\}, \tag{5.37}$$

where χ_i is the i-th sigma point and Wi is the i-th weight. The generated sigma points have the same mean and the same covariance as the random variable $\mathbf{x}$. The sigma points selection that meet the objectives of this method is done according to the following:

$$\chi_i = \bar{\mathbf{x}} + \sqrt{\mathbf{P}_\mathrm{x}}\mathbf{Z}_i \qquad i = 0, \ldots, n+1, \tag{5.38}$$

where $\sqrt{\mathbf{P}_\mathrm{x}}$ is the square root matrix of the covariance matrix $\mathbf{P}_\mathrm{x}$ and $\mathbf{Z}_i$ is the i-th column of the spherical simplex sigma point matrix $\mathbf{Z} \in \mathbb{R}^{n \times n+2}$ which can be calculated by constructing the one-dimensional vector $\mathbf{Z}_i^j$ for $j = 1$ as

$$\mathbf{Z}_0^1 = \begin{bmatrix} 0 \end{bmatrix}, \quad \mathbf{Z}_1^1 = \begin{bmatrix} \frac{-1}{\sqrt{2W_1}} \end{bmatrix}, \quad \mathbf{Z}_2^1 = \begin{bmatrix} \frac{1}{\sqrt{2W_1}} \end{bmatrix}, \tag{5.39}$$

and then expand the vector $\mathbf{Z}_i^j$ for $j = 2, \ldots, n$ according to

$$\mathbf{Z}_i^j = \begin{cases} \begin{bmatrix} \mathbf{Z}_0^{j-1} \\ 0 \end{bmatrix} & i = 0 \\ \begin{bmatrix} \mathbf{Z}_i^{j-1} \\ \frac{-1}{\sqrt{j(j+1)W_1}} \end{bmatrix} & i = 1, \ldots, j \\ \begin{bmatrix} 0_{j-1} \\ \frac{j}{\sqrt{j(j+1)W_1}} \end{bmatrix} & i = j+1 \end{cases} \tag{5.40}$$

to construct the spherical simplex sigma point matrix $\mathbf{Z}$.

The weights of the sigma points that meet the objectives of this method is calculated by assigning an arbitrary value, for tuning purpose, for the zeroth weight W_0

$$0 \leq W_0 \leq 1. \tag{5.41}$$

It should be mentioned that the selected values for W_0 that satisfy (5.41) guarantee second order accuracy of Taylor series expansion in the mean and covariance. The tuning affects the incorporation of the forth and higher order terms information into the estimates. The remaining weight sequence are calculated as follows

$$W_i = (1 - W_0)/(n+1) \qquad i = 1, \ldots, n+1. \tag{5.42}$$

Once the sigma points have been calculated, they are transformed through the non-linear function $\mathbf{g}(\cdot)$ as given

$$\boldsymbol{\xi}_i = \mathbf{g}(\boldsymbol{\chi}_i) \qquad i = 0, \ldots, n+1. \tag{5.43}$$

The predicted mean is then calculated as

$$\bar{\mathbf{y}} = \sum_{i=0}^{n+1} W_i \boldsymbol{\xi}_i, \tag{5.44}$$

and the predicted covariance is calculated as

$$\mathbf{P}_{\mathrm{y}} = \sum_{i=0}^{n+1} W_i \{\boldsymbol{\xi}_i - \bar{\mathbf{y}}\}\{\boldsymbol{\xi}_i - \bar{\mathbf{y}}\}^T. \tag{5.45}$$

The design of the SSUT begins by assuming that

$$W_0 = 0.1, \tag{5.46}$$

to satisfy (5.41). The author of this dissertation found through simulation that the SSUT is not much sensitive to the selection value of the weight W_0. However, the selection of a value to achieve the optimal results is still an open topic and will be left to future work.

By referring to the measurement function $\mathbf{H}(\cdot)$ of (4.9), equation (5.35) is then written as

$$\mathbf{g}(\mathbf{x}) = \mathbf{h}(\hat{\mathbf{x}}_k^-) = \begin{bmatrix} \sqrt{(x_{\mathrm{BS}_1} - \hat{x}_k^-)^2 + (y_{\mathrm{BS}_1} - \hat{y}_k^-)^2} \\ \vdots \\ \sqrt{(x_{\mathrm{BS}_N} - \hat{x}_k^-)^2 + (y_{\mathrm{BS}_N} - \hat{y}_k^-)^2} \end{bmatrix} = \begin{bmatrix} \tilde{z}_k^1 \\ \vdots \\ \tilde{z}_k^N \end{bmatrix}, \tag{5.47}$$

where

$$\hat{\mathbf{x}}_k^- = \begin{bmatrix} \hat{x}_k^- \\ \hat{y}_k^- \\ \hat{v}_k^{x-} \\ \hat{v}_k^{y-} \end{bmatrix} \tag{5.48}$$

To select the method to calculate the square root matrix needed for this transformation, the selection conditions of this matrix should be considered. Similar to the SUT, this transformation gives the freedom to select the method that calculates the square root matrix.

Based on the recent study presented in [Rhu+12] which showed that the Cholesky decomposition method is the best overall matrix square root calculation method

for UT in terms of performance and execution time. Based on the study, the author of this dissertation proposes the Cholesky decomposition [GV12] method for calculating the square root matrix.

Based on Cholesky decomposition, a matrix $\mathbf{P}_{k-1}$ can be decomposed into a product of a lower triangular matrix $\mathbf{L}$ and its transpose [Rhu+12]. As such, the matrix $\mathbf{P}_{k-1}$ can be expressed as

$$\mathbf{P}_{k-1} = \mathbf{L}\mathbf{L}^T, \tag{5.49}$$

where $\mathbf{L}$ is the Cholesky decomposition matrix and represents the square root matrix.

Since the matrix $\mathbf{P}_k^-$ has the dimension 4×4 based on the design of the state-space models given in section 4.2, the elements of the matrix $\mathbf{L}$ then can be found,from [Rhu+12; GV12], by solving

$$\mathbf{P}_k^- = \begin{bmatrix} P_{11} & P_{12} & P_{13} & P_{14} \\ P_{21} & P_{22} & P_{23} & P_{24} \\ P_{31} & P_{32} & P_{33} & P_{34} \\ P_{41} & P_{42} & P_{43} & P_{44} \end{bmatrix} = \begin{bmatrix} L_{11} & 0 & 0 & 0 \\ L_{21} & L_{22} & 0 & 0 \\ L_{31} & L_{32} & L_{32} & 0 \\ L_{41} & L_{42} & L_{43} & L_{44} \end{bmatrix} \begin{bmatrix} L_{11} & 0 & 0 & 0 \\ L_{21} & L_{22} & 0 & 0 \\ L_{31} & L_{32} & L_{32} & 0 \\ L_{41} & L_{42} & L_{43} & L_{44} \end{bmatrix}^T. \tag{5.50}$$

By considering that the *a priori* state estimate $\hat{\mathbf{x}}_k^-$ is used to generate the sigma points, equation (5.38) is then written as

$$\boldsymbol{\chi}_i = \hat{\mathbf{x}}_k^- + \mathbf{L}\mathbf{Z}_i \qquad i = 0, \ldots, 5, \tag{5.51}$$

By considering that the obtained sigma points are transferred using (5.47) to obtain the points $\boldsymbol{\xi}_i$, equation (5.47) is then written as

$$\boldsymbol{\xi}_i = \begin{bmatrix} \sqrt{(x_{\mathrm{BS}_1} - \chi_i(1))^2 + (y_{\mathrm{BS}_1} - \chi_i(2))^2} \\ \vdots \\ \sqrt{(x_{\mathrm{BS}_N} - \chi_i(1))^2 + (y_{\mathrm{BS}_N} - \chi_i(2))^2} \end{bmatrix} \qquad i = 0, \ldots, 5, \tag{5.52}$$

Algorithm 5.3 Spherical Simplex Unscented Transformation Algorithm Design for Measurement Function $\mathbf{h}(\cdot)$ of the Positioning Problem

1: Compute the zeroth weight W_0 as in (5.41).
2: **for** $i = 1$ to $i = 5$ **do**
3: Compute the weight W_i as in (5.42).
4: **end for**
5: Compute the vector sequence $\mathbf{Z}$ as in (5.39) and (5.39);
6: Compute the square root matrix $\mathbf{L}$ by solving (5.50) using Cholesky decomposition;
7: **for** $i = 0$ to $i = 5$ **do**
8: Calculate the Sigma points χ_i as in (5.51);
9: Obtain the transformed sigma point ξ_i as in (5.52);
10: **end for**
11: Compute the *approximated* measurements $\tilde{\mathbf{z}}$ as in (5.54).
12: Compute the covariance $\mathbf{P}_z$ as in (5.55).

where

$$\chi_i = \begin{bmatrix} \chi_i(1) \\ \chi_i(2) \\ \chi_i(3) \\ \chi_i(4) \end{bmatrix}. \tag{5.53}$$

The transferred sigma points are then used calculate the *approximate* measurements $\tilde{\mathbf{z}}$. This is done by writing (5.44) as

$$\tilde{\mathbf{z}}_k = \sum_{i=0}^{5} W_i \xi_i, \tag{5.54}$$

and the associated covariance is calculated by writing (5.45) as

$$\mathbf{P}_z = \sum_{i=0}^{5} W_i [\xi_i - \tilde{\mathbf{z}}_k][\xi_i - \tilde{\mathbf{z}}_k]^T. \tag{5.55}$$

The complete design of the SSUT for the designed measurement function $\mathbf{h}(\cdot)$ of (4.9) of the positioning problem is summarized in Algorithm 5.3. Furthermore, a block diagram that depicts the SSUT is given in Fig. 5.8.

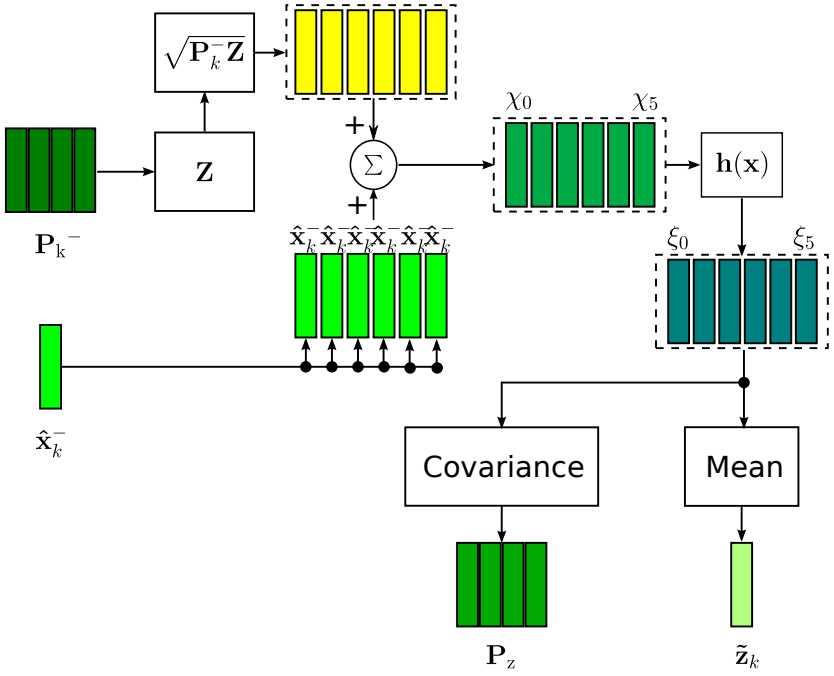

Figure 5.8: Block diagram of the 4-dimensional variable $\hat{\mathbf{x}}_k$ that undergoes the SSUT to produce the measurement approximation $\tilde{\mathbf{z}}_k$.

5.3.2 Spherical Simplex Unscented Kalman Filter Implementation

The SSUT is firstly introduced into KF by [Loz+08] and the resulting filter is called Spherical Simplex-Unscented Kalman Filter (SS-UKF).

A different application for different UT techniques into the KF is proposed recently by [GA11]. The author of this dissertation calls the application of the SSUT into the KF as the Spherical Simplex Unscented Kalman Filter (SSUKF) which performs better than the first implementation by [Loz+08].

The design of the SSUT based to the designed state-space models of section 4.2 is considered the core of SSUKF.

Determining the noise covariances of designed state-space models of section 4.2 allows the SSUKF to be operable. The determination of the noise covariances can be done according to the procedure given in section 4.3. By following the section, the process noise covariance $\mathbf{Q} \in \mathbb{R}^{4\times4}$ and the measurement noise covariance

$\mathbf{R} \in \mathbb{R}^{4\times4}$ are obtained. The error covariance matrix $\mathbf{P}_{k-1}$ can be initialized for $k = 1$ as

$$\mathbf{P}_{k-1} = \mathbf{Q} \tag{5.56}$$

and the system state $\hat{\mathbf{x}}_{k-1}$ is initialized for $k = 1$ as

$$\hat{\mathbf{x}}_{k-1} = \begin{bmatrix} \hat{\mathbf{x}}_{\text{tr}} \\ 0 \\ 0 \end{bmatrix}, \tag{5.57}$$

where $\hat{\mathbf{x}}_{\text{tr}}$ is the estimated position obtained from Algorithm 3.1 and the velocities v_k^x and v_k^y of the *zeroth* state $\hat{\mathbf{x}}_0$ are assumed to be zero.

Based on the state-space models design given in section 4.2, the *a priori* state estimate $\hat{\mathbf{x}}_k^-$ is obtained as

$$\hat{\mathbf{x}}_k^- = \hat{\mathbf{x}}_{k-1} + \mathbf{B}\mathbf{u}_{k-1}. \tag{5.58}$$

The *a priori* error matrix $\mathbf{P}_k^-$ is calculate as

$$\mathbf{P}_k^- = \mathbf{P}_{k-1} + \mathbf{Q}. \tag{5.59}$$

The *a priori* state $\hat{\mathbf{x}}_k^-$ and the error matrix $\mathbf{P}_k^-$ are then used by the designed algorithm 5.3 of section 5.3.1 to compute the approximated measurements $\tilde{\mathbf{z}}_k$ and the corresponding matrix $\mathbf{P}_z$.

Based on the the following equivalent, from [GA11]

$$\mathbf{P}_z = \mathbf{H}_k \mathbf{P}_k^- \mathbf{H}_k^T, \tag{5.60}$$

and the approximation presented by [GA11]

$$\mathbf{P}_{xz} \approx \mathbf{P}_k^- \mathbf{H}_k^T, \tag{5.61}$$

where $\mathbf{P}_{xz}$ is the cross covariance matrix which can be calculated from

$$\mathbf{P}_{xz} = \sum_{i=0}^{3} W_i[\boldsymbol{\xi}_i - \hat{\mathbf{x}}_k^-][\boldsymbol{\xi}_i - \tilde{\mathbf{z}}_k]^T, \tag{5.62}$$

the Kalman gain of the standard KF of (2.44) is then computed as

$$\mathbf{K}_k = \mathbf{P}_{xz}[\mathbf{P}_z + \mathbf{R}]^{-1}. \tag{5.63}$$

The *a posteriori* state estimate is computed by using the measurements $\mathbf{z}$ and the *approximated* measurements $\tilde{\mathbf{z}}$ as

$$\hat{\mathbf{x}}_k = \hat{\mathbf{x}}_k^- + \mathbf{K}_k(\mathbf{z}_k - \tilde{\mathbf{z}}_k) \tag{5.64}$$

The *a posteriori* estimation error covariance is computed as

$$\mathbf{P}_k = \mathbf{P}_k^- - \mathbf{K}_k\mathbf{P}_{xz}^T. \tag{5.65}$$

The position coordinates $\hat{x}_k$ and $\hat{y}_k$ are then extracted from (5.64). The SUKF is implemented for an update position $\hat{\mathbf{p}}_k$ once new measurements are obtained. The complete implementation of the SSUKF to the positioning problem is summarized in Algorithm 5.4.

5.3.3 Simulation Procedure

The SSUKF is evaluated based on the model presented in section 3.2. The simulation procedure is carried out according to the following

1. The step 1-8 of the simulation procedure which presented in section 3.7 are executed for system state $\hat{\mathbf{x}}_0$ initialization.
2. SSUKF is used for location estimation and tracking. In this filter, the system measurements are the estimated distance $\hat{d}_i$ and the system state is the position estimation $\hat{\mathbf{p}}$.

Algorithm 5.4 Spherical Simplex Unscented Kalman Filter Algorithm

procedure INITIALIZATION
  Obtain the location of the anchor nodes $\mathbf{P}_{BS_i}$.
  Initialize the measurement noise matrix $\mathbf{R}$ as in section 4.3.
  Initialize and tune the process noise matrix $\mathbf{Q}$ as in section 4.3.
  Initialize the error estimation covariance $\mathbf{P}_0$ as in (5.56).
  Initialize the estimated position $\hat{\mathbf{x}}_0$ as in (5.57).
end procedure
for $k = 1$ to ∞ **do**
  Obtain the measurements $\mathbf{z}_k$;
  Compute the *a priori* state $\mathbf{x}_k^-$ as in 5.58;
  Compute the *a priori* estimation error matrix $\mathbf{P}_k^-$ as in (5.59);
  Compute the approximated measurements $\tilde{\mathbf{z}}_k$, the covariance matrix $\mathbf{P}_z$ and the cross covariance matrix $\mathbf{P}_{xz}$ from Algorithm 5.3;
  Compute the cross covariance $\mathbf{P}_{xz}$ as in (5.62);
  Compute the Kalman gain $\mathbf{K}_k$ as in (5.63);
  Compute the *a posteriori* state estimation $\hat{\mathbf{x}}_k$ as in (5.64);
  Compute the *a posteriori* estimation covariance matrix $\mathbf{P}_k$ as in (5.65);
  Obtain the estimated position $\hat{\mathbf{p}}_k = \hat{\mathbf{x}}_k$
end for

3. The estimated position $\hat{\mathbf{p}}$ is extracted from the system state $\hat{\mathbf{x}}$.
4. The distance error ρ is calculated according to (3.64).
5. The simulation steps 1-4 are carried out for different traces according to the performance evaluation model presented in section 3.2.
6. The simulation steps 1-5 are repeated for 100 iterations to have different noise conditions.
7. The mean distance error $E(\Delta\rho)$ is calculated by averaging all the obtained values of the distance error ρ.
8. The simulation steps 1-7 are repeated to test the different anchor nodes values $N \in \{3, 4, 6\}$.

5.3.4 Results and Discussion

The results given here in this section are accomplished according to the performance evaluation model presented in section 3.2 and the simulation procedure

presented in section 5.3.3.

Figures 5.9, 5.10, and 5.11 show the error distance ρ based on different distances d to the network's center of coordinate $(0, 0)$ for $3, 4$ and 6 anchor nodes respectively as a comparison between SSUKF and EKF. The error distance ρ is calculated according to (3.65), and is obtained based on the performance evaluation model of section 3.2. In this section, 100 traces are generated from the network's center of coordinate $(0, 0)$ towards the maximum radius of the *circle of trust*. In addition, each trace is repeated 100 times to simulate different noise conditions on each trace. As a result, the total traces become 10000. Each estimated position $\hat{\mathbf{p}}$ of all the traces is recorded in order to obtain the error distance ρ values. The distance d is calculated from the network's center to the half of the diameter of the *circle of trust* which has 150 m diameter.

As can be seen from Figs. 5.9, 5.10, 5.11, the SSUKF did not diverge as the SSUKF. This results in lower error distance estimation compared with the EKF.

For comparison purpose, the estimated mean error distance $\mathrm{E}[\Delta\rho]$ values for $3, 4$ and 6 anchor nodes are calculated. The SSUKF has mean error distance of 17.62 m, 15.19 m and 12.70 m for $3, 4$ and 6 anchor nodes respectively. The mean error distance for both SSUKF and EKF are given in Table. 5.2. Comparing to the EKF, the SSUKF performs better with improvement of $19,58\%$, $24,83\%$ and $23,35\%$ for $3, 4$ and 6 anchor nodes respectively.

To demonstrate the distribution of the error distance values of the SSUKF according to distance d, figures 5.12, 5.13 and 5.14 are given. Figure 5.12 depicts the results with a probability of 66 % for distances below 20 m for the case of 3 anchor nodes. The largest probability occurs at the distance of 11 m. From Fig. 5.13 that has a probability of 73 % for distances below 20 m for 4 anchor nodes, the largest error probability occurs at the distance of 10 m. Figure 5.14 which shows the results for 6 anchor nodes and brings a probability of 85 % for distances below 20 m, achieves the largest probability at the distance of 9 m.

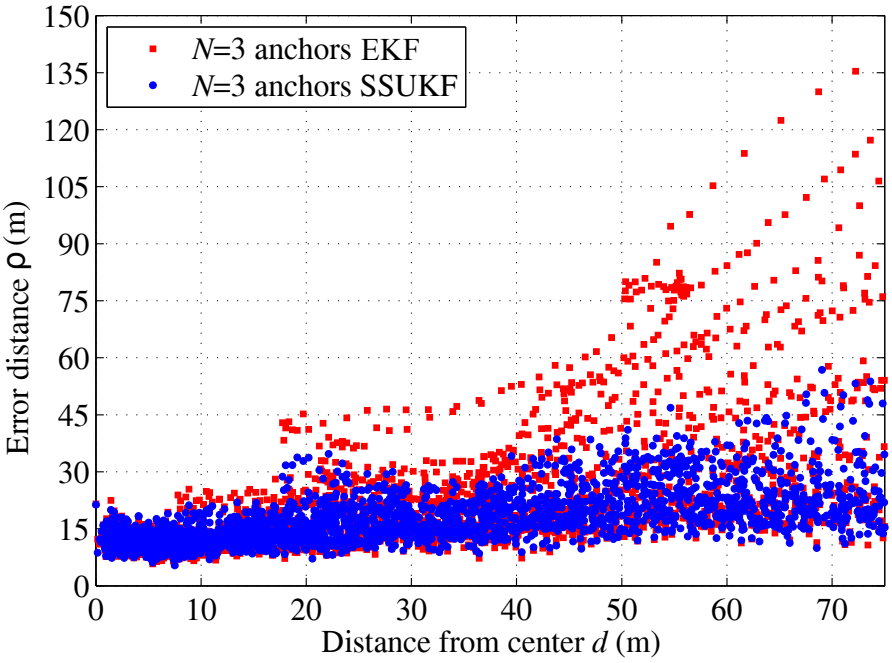

Figure 5.9: Simulated error distance ρ according to distance d for the SSUKF compared with the EKF using 3 anchor nodes.

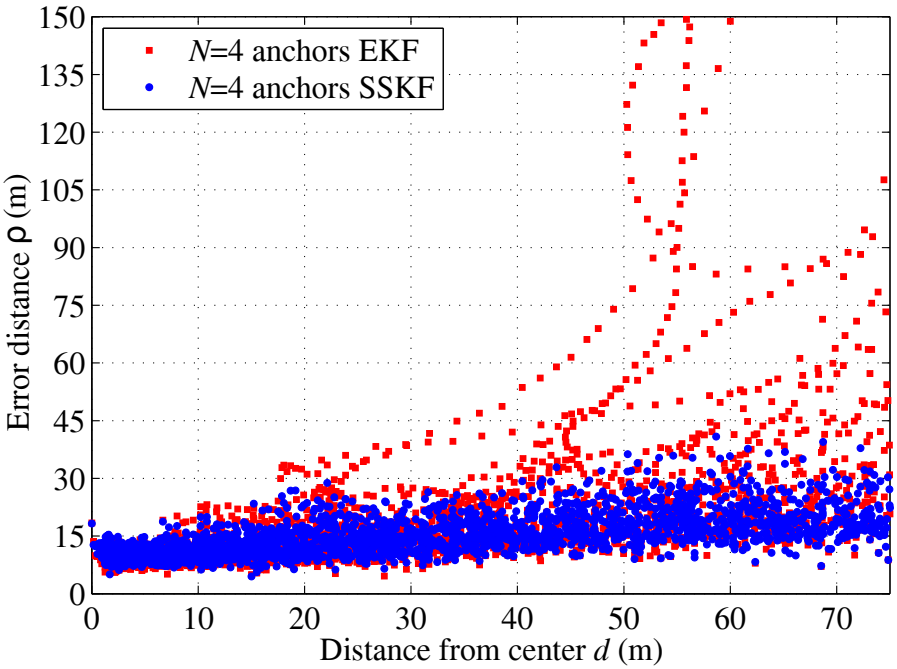

Figure 5.10: Simulated error distance ρ according to distance d for the SSUKF compared with the EKF using 4 anchor nodes.

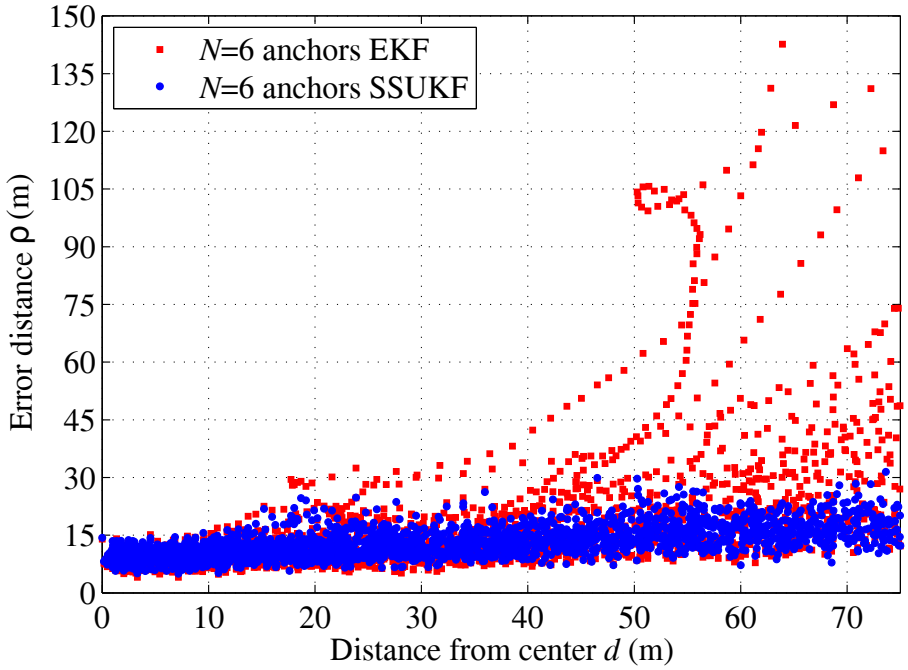

Figure 5.11: Simulated error distance ρ according to distance d for the SSUKF compared with the EKF using 6 anchor nodes.

Table 5.2: Mean error distance for SSUKF compared with EKF.

Method	Mean error distance E[$\Delta\rho$] (m)		
	3 Anchor nodes	4 Anchor nodes	6 Anchor nodes
SSUKF	17.62	15.19	12.70
EKF	21.915	20.21	16.57

Finally, it can be concluded from the presented figures as well as the results of the mean error values of Table 5.2 that the proposed SSUKF outperforms the popular EKF in terms of the positioning accuracy.

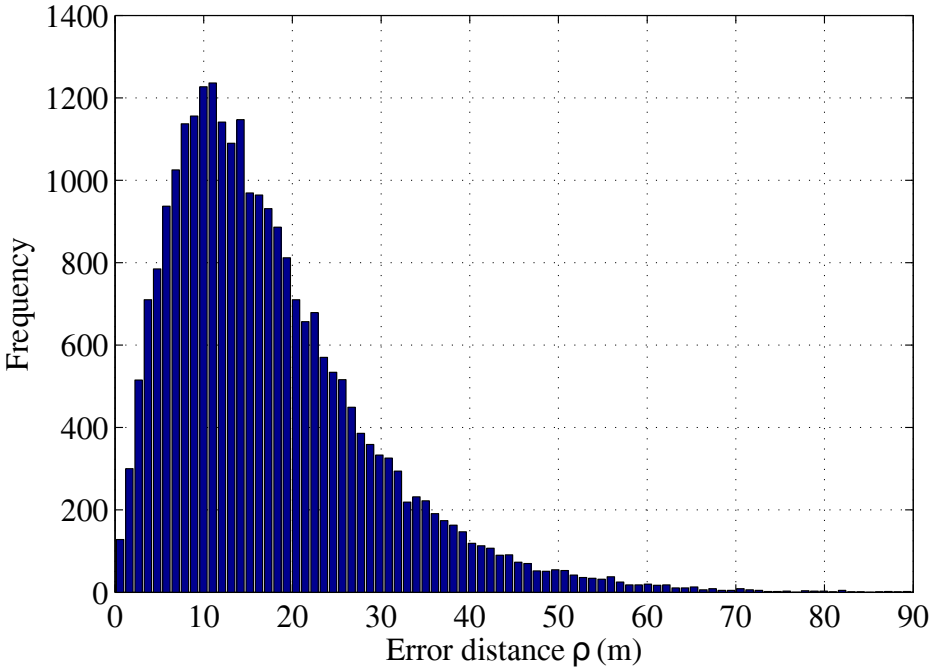

Figure 5.12: Error distance distribution for SSUKF in case of 3 anchor nodes.

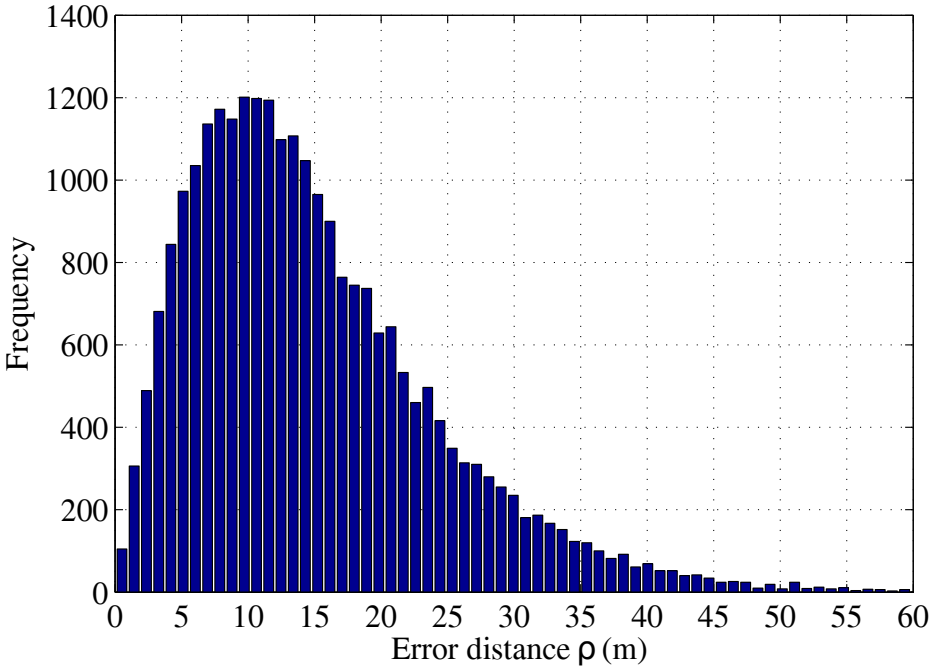

Figure 5.13: Error distance distribution for SSUKF in case of 4 anchor nodes.

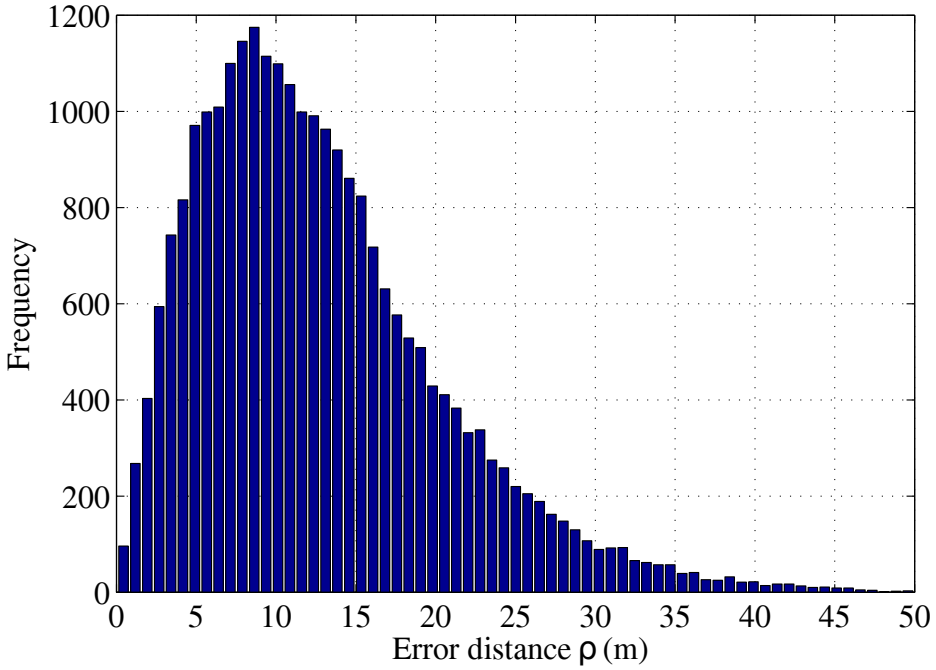

Figure 5.14: Error distance distribution for SSUKF in case of 6 anchor nodes.

6 Conclusion and Future Work

In this chapter, the conclusions achieved throughout this dissertation are summarized as well as the future work.

6.1 Conclusion

In this dissertation, the author deals with the interesting and challenging problem of indoor positioning and tracking based on RSSI for WLAN IEEE 802.11n. In particular, the author designs Location and Tracking (L&T) solutions that aim to overcome the limitations of the state of the art techniques.

The relative high positioning errors are due to the high standard deviation of the path loss model. The worst case value of 6 dB among other models that proposed by the TGn has been chosen. The selected model is intended for large environment with the highest standard deviation representing the worst case for the transmitter/receiver surroundings configuration. Selecting other models intended for large or small environment with smaller standard deviation noise shall reduce the positioning errors almost to the half according to the simulation. It is anticipated that the errors can be further reduced upon adapting deterministic path loss model which is obtained from measurements for a specific environment. In addition, the wide coverage area which represents a circle of 150 m diameter contributes to the positioning errors. Despite the positioning errors, the proposed

solutions brings the advantages: the ease of implementation, reliability and the improved positioning accuracy compared with the popular approach EKF.

In Chapter 3, the author focuses on designing a positioning framework that is transparent to accuracy improvement technologies. In addition, the KF is proposed for ease of implementation so that it does not require the calculation of particular matrices called the Jacobian matrices. The simulation results show that this implementation improves the accuracy significantly in all areas of the test scenario.

In Chapter 4, the author proposes a L&T solution based on the IEKF. IEKF is designed to utilize the RSSI measurements and the locations of the anchor nodes for L&T. The proposed technique is evaluated by numerical simulation under testing different conditions. The simulation results show that the positioning accuracy is significantly improved over the EKF for all of the testing conditions.

In Chapter 5, the author considers proposing two L&T solutions that overcome the limitations of the common non-linear KF known as the EKF. For this purpose, two non-linear transformations that are applicable to the KF are considered. The applications of those transformations to the KF results in two different non-linear filters.

The author calls the first non-linear filter Scaled Unscented Kalman Filter (SUKF). SUKF is proposed for indoor L&T. The SUKF is designed to exploit the RSSI measurements and the information about the location of the anchor nodes for L&T. This filter does not require the derivation of the Jacobian matrices and therefore brings the ease of implementation. In addition, the filter maintains the first two moments during the non-linear transformation. As such, this filter is more reliable compared with the EKF which might be unstable due to the linearizaion issues. The proposed solution is tested by numerical simulations under different conditions. The accuracy of the positioning information is significantly improved over the EKF for all of the testing conditions as the simulation results relieved.

The author calls the second non-linear filter Spherical Simplex Unscented Kalman Filter (SSUKF). The author proposes SSUKF for indoor L&T. The SSUKF is designed to exploit the RSSI and the anchor nodes's locations for L&T. This filter does not require the calculation of the Jabobian matrices and therefore provides ease of implementation. Moreover, this filter inherits the properties of the SSUT so that the mean and covariance of the data undergoes non-linear transformation are maintained during the transformation. As a result, this filter has more reliability compared with the EKF which linearizes about the first order Taylor series expansion. Numerical simulation for the purpose of the filter evaluation is used. The simulation results show that the SSUKF achieves substantially better than the performance of the EKF.

Based on the results presented in this dissertation, it is recommended to adopt the IEKF due to the reduced error results compared with other filters presented in this dissertation if the Jacobian matrices are obtainable from the non-linear system equation. If the Jacobian matrices are hard to obtain, it is recommended to adopt either the SUKF or SSUKF since they both have similar results and both share the second best filter out of this dissertation.

Finally, for systems that do not have access to the distance measurements and provide only position estimates, the implementation presented in Chapter 3 is recommended.

6.2 Future Work

This section presents some future research in the following tracks.

1. RSSI-based L&T is only considered through this dissertation. Recent work on indoor L&T as in [FA13] involve switching between different positioning technologies upon availability for ubiquitous service. Therefore, extension to involve different positioning technologies is a promising future research topic.

2. Recent work on hybrid localization as in [FKW09] combines measurements from the cellular radio network and GPS. As such, extension to include the measurements from the cellular radio network and GPS combined with the WLAN is a promising future direction for this work.

3. In chapter 5, the scaling and tuning parameters are chosen to meet the criteria of the SUT and the SSUT. As such, it is anticipated that further tuning of those parameters may increase the accuracy especially in the case of the SSUKF.

Bibliography

[03] *Commission pushes for rapid deployment of location enhanced 112 emergency services*. "europa.eu/rapid/press-release_IP-03-1122_en.pdf". [Online; accessed 25-August-2015]. 2003.

[09] *Wi-Fi CERTIFIED™ n:What Retailers Need to Know*. "http://www.wi-fi.org/download.php?file=/sites/default/files/private/11nbasics_Retailer_Training_Deck.pdf". [Online; accessed 23-March-2015]. WiFi Alliance, 2009.

[12] *802.11 n*. "http://www.tech-faq.com/80211n.html". [Online; accessed 23-March-2015]. 2012.

[13a] *IEEE 802.11ac:What Does it Mean for Test?* "http://litepoint.com/whitepaper/80211ac_Whitepaper.pdf". [Online; accessed 23-March-2015]. 2013.

[13b] *Wireless Communication Technology Is Rapidly Growing Computer Science Essay.* "http://www.ukessays.com/essays/computer-science/wireless-communication-technology-is-rapidly-growing-computer-science-essay.php?cref=1". [Online; accessed 21-December-2015]. 2013.

[14] *Mobile Location-Based Services - 9th Edition*. Tech. rep. Market Research Report - 224223, BERG Insight, 2014.

[AH15] Abusara, A. and Hassan, M. "Enhanced fingerprinting in WLAN-based indoor positioning using hybrid search techniques". In: *International Conference on Communications, Signal Processing, and their Applications (ICCSPA)*. IEEE. 2015, pp. 1–6.

[AM79] Anderson, B. D. and Moore, J. B. *Optimal Filtering*. 1979.

[Ant05] Antonini, G. "A Discrete Choice Modeling Framework For Pedestrian Walking Behavior With Application To Human Tracking In Video Sequence". In: *Thase EPFL* 3382 (2005).

[AS72] Alspach, D. L. and Sorenson, H. W. "Nonlinear Bayesian estimation using Gaussian sum approximations". In: *IEEE Transactions on Automatic Control* 17.4 (1972), pp. 439–448.

[Ati+15] Atia, M. M., Liu, S., Nematallah, H., Karamat, T. B., and Noureldin, A. "Integrated Indoor Navigation System for Ground Vehicles With Automatic 3-D Alignment and Position Initialization". In: *IEEE Transactions on Vehicular Technology* 64.4 (2015), pp. 1279–1292.

[Bar+08] Barva, M., Uhercik, M., Mari, J. M., Kybic, J., Duhamel, J. R., Liebgott, H., Hlavác, V., and Cachard, C. "Parallel integral projection transform for straight electrode localization in 3-D ultrasound images". In: *IEEE Transactions on Ultrasonics, Ferroelectrics, and Frequency Control* 55.7 (2008), pp. 1559–1569.

[Bel07] Belanger, P. *802.11n Delivers Better Range*. "`http://www.wi-fiplanet.com/tutorials/article.php/3680781`". [Online; accessed 23-March-2015]. 2007.

[Ben81] Beneš, V. "Exact finite-dimensional filters for certain diffusions with nonlinear drift". In: *Stochastics: An International Journal of Probability and Stochastic Processes* 5.1-2 (1981), pp. 65–92.

[BH12] Brown, R. G. and Hwang, P. Y. "Introduction to random signals and applied Kalman filtering". In: (2012).

[BP00] Bahl, P. and Padmanabhan, V. N. "RADAR: An in-building RF-based user location and tracking system". In: *Proceedings of Nineteenth Annual Joint Conference of the IEEE Computer and Communications Societies*. Vol. 2. IEEE. 2000, pp. 775–784.

[BT10] Bilik, I. and Tabrikian, J. "Maneuvering target tracking in the presence of glint using the nonlinear Gaussian mixture Kalman filter". In: *IEEE Transactions on Aerospace and Electronic Systems* 46.1 (2010), pp. 246–262.

[Cha+15] Chang, H.-C., Lin, C.-T., Wu, Y.-w. A., and Chiang, W.-L. "Methods for estimating spacecraft inertia Tensor". In: *2015 IEEE Aerospace Conference*. IEEE. 2015, pp. 1–12.

[Cho14] Choppala, P. B. "Bayesian multiple target tracking". In: (2014).

[CKV11] Clark, J. M., Kountouriotis, P.-A., and Vinter, R. B. "A Gaussian mixture filter for range-only tracking". In: *Automatic Control, IEEE Transactions on* 56.3 (2011), pp. 602–613.

[CM03] Crassidis, J. L. and Markley, F. L. "Unscented filtering for spacecraft attitude estimation". In: *Journal of guidance, control, and dynamics* 26.4 (2003), pp. 536–542.

[Com+01] Commission, F. C. et al. "FCC wireless 911 requirements". In: *Fact Sheet, Jan* (2001).

[Com+99] Commission, F. C. et al. "FCC acts to promote competition and public safety in enhanced wireless 911 services". In: *Press Release, Sept* 15 (1999), p. 1999.

[Dau95] Daum, F. E. "Beyond Kalman filters: practical design of nonlinear filters". In: *SPIE's 1995 International Symposium on Optical Science, Engineering, and Instrumentation*. International Society for Optics and Photonics. 1995, pp. 252–262.

[Des12] Destino, G. "Positioning in Wireless Networks: Noncooperative and Cooperative Algorithms". In: *University of Oulu* (2012).

[Erc04] Erceg, V. "TGn channel models". In: *IEEE 802.11 document 03/940r4* (2004).

[FA13] Ficco, M. and Aversa, R. "Hybrid Localization for Ubiquitous Services". In: *10th International Conference on Ubiquitous Intelligence and Computing and 10th International Conference on Autonomic and Trusted Computing (UIC/ATC)*. IEEE. 2013, pp. 1–8.

[Fan90] Fang, B. T. "Simple solutions for hyperbolic and related position fixes". In: *Aerospace and Electronic Systems, IEEE Transactions on* 26.5 (1990), pp. 748–753.

[FF11] Figueiras, J. and Frattasi, S. *Mobile positioning and tracking: From conventional to cooperative techniques*. John Wiley & Sons, 2011.

[FKW09] Fritsche, C., Klein, A., and Würtz, D. "Hybrid GPS/GSM localization of mobile terminals using the extended Kalman filter". In: *6th Workshop on Positioning, Navigation and Communication WPNC 2009 (WPNC´09)*. IEEE. 2009, pp. 189–194.

[GA11] Grewal, M. S. and Andrews, A. P. *Kalman filtering: theory and practice using MATLAB*. John Wiley & Sons, 2011.

[Gel74] Gelb, A. *Applied optimal estimation*. MIT press, 1974.

[GH00] Ghahramani, Z. and Hinton, G. E. "Variational learning for switching state-space models". In: *Neural computation* 12.4 (2000), pp. 831–864.

[Gil+09] Gilboa, I. et al. *Theory of decision under uncertainty*. Vol. 1. Cambridge university press Cambridge, 2009.

[Gol05] Goldsmith, A. *Wireless communications*. Cambridge university press, 2005.

[Gre15] Greicius, T. *Three Years on Mars*. "`http://www.nasa.gov/jpl/three-years-on-mars`". [Online; accessed 05-August-2015]. 2015.

[GV12] Golub, G. H. and Van Loan, C. F. *Matrix computations*. Vol. 3. JHU Press, 2012.

[Ham94] Hamilton, J. D. *Time series analysis*. Vol. 2. Princeton university press Princeton, 1994.

[Hau05] Haug, A. "A tutorial on Bayesian estimation and tracking techniques applicable to nonlinear and non-Gaussian processes". In: *MITRE Corporation, McLean* (2005).

[Hel+13] Hellmers, H., Norrdine, A., Blankenbach, J., and Eichhorn, A. "An IMU/magnetometer-based Indoor positioning system using Kalman filtering". In: *Indoor Positioning and Indoor Navigation (IPIN), 2013 International Conference on*. IEEE. 2013, pp. 1–9.

[HH13] Hlavacs, H. and Hummel, K. "Cooperative positioning when using local position information: theoretical framework and error analysis". In: *IEEE Transactions on Mobile Computing* 12.10 (2013), pp. 2091–2104.

[HLW07] Hofmann-Wellenhof, B., Lichtenegger, H., and Wasle, E. *GNSS–global navigation satellite systems: GPS, GLONASS, Galileo, and more*. Springer Science & Business Media, 2007.

[Hoa63] Hoag, D. *Apollo Guidance and Navigation //Considerations of Apollo IMU Gimbal Lock //MIT Instrumentation Laboratory Document E-1344*. "`http://www.hq.nasa.gov/office/pao/History/alsj/e-1344.htm`". [Online; accessed 22-August-2015]. 1963.

[Hon+09] Honkavirta, V., Perälä, T., Ali-Löytty, S., and Piché, R. "A comparative survey of WLAN location fingerprinting methods". In: *6th Workshop on Positioning, Navigation and Communication 2009 (WPNC´09)*. IEEE. 2009, pp. 243–251.

[Jel97] Jelinek, F. *Statistical methods for speech recognition*. MIT press, 1997.

[Jo+14] Jo, K., Kim, J., Kim, D., Jang, C., and Sunwoo, M. "Development of autonomous car—part I: distributed system architecture and development process". In: *Industrial Electronics, IEEE Transactions on* 61.12 (2014), pp. 7131–7140.

[JU97] Julier, S. J. and Uhlmann, J. K. "A new extension of the Kalman filter to nonlinear systems". In: *Int. symp. aerospace/defense sensing, simul. and controls*. Vol. 3. 26. Orlando, FL. 1997, pp. 3–2.

[JUD95] Julier, S. J., Uhlmann, J. K., and Durrant-Whyte, H. F. "A new approach for filtering nonlinear systems". In: *American Control Conference, Proceedings of the 1995*. Vol. 3. IEEE. 1995, pp. 1628–1632.

[Jul02] Julier, S. J. "The scaled unscented transformation". In: *Proceedings of the 2002 American Control Conference, 2002.* Vol. 6. IEEE. 2002, pp. 4555–4559.

[Jul03] Julier, S. J. "The spherical simplex unscented transformation". In: *Proceedings of the 2003 American Control Conference, 2003.* Vol. 3. IEEE. 2003, pp. 2430–2434.

[Kha+14] Khalil, L., Waadt, A., Bruck, G., and Jung, P. "Positioning framework for WLAN 802.11 n utilizing Kalman filter on received signal strength". In: *International Wireless Communications and Mobile Computing Conference (IWCMC)*. IEEE. 2014, pp. 1172–1176.

[KJ15a] Khalil, L. and Jung, P. "Scaled Unscented Kalman Filter for RSSI-Based Indoor Positioning and Tracking". In: *9th International Conference on Next Generation Mobile Applications, Services and Technologies (NGMAST)*. IEEE. 2015, pp. 132–137.

[KJ15b] Khalil, L. and Jung, P. "Spherical Simplex Unscented Kalman Filter for RSSI-Based Indoor Positioning and Tracking". In: *IEEE 26th International Symposium on Personal Indoor and Mobile Radio Communications (PIMRC)*. IEEE. 2015, pp. 2284–2288.

[Kot+03] Kotanen, A., Hannikainen, M., Leppakoski, H., and Hamalainen, T. D. "Experiments on local positioning with Bluetooth". In: *Information Technology: Coding and Computing [Computers and Communications], 2003. Proceedings. ITCC 2003. International Conference on*. IEEE. 2003, pp. 297–303.

[KPV10] Kushki, A., Plataniotis, K. N., and Venetsanopoulos, A. N. "Intelligent dynamic radio tracking in indoor wireless local area networks". In: *IEEE Transactions on Mobile Computing* 9.3 (2010), pp. 405–419.

[Kuh+10] Kuhn, M. J., Turnmire, J., Mahfouz, M. R., and Fathy, A. E. "Adaptive leading-edge detection in UWB indoor localization". In: *Radio and Wireless Symposium (RWS), 2010 IEEE*. IEEE. 2010, pp. 268–271.

[Lac] Lacey, T. "Tutorial: The kalman filter". In: *Georgia Institute of Technology* ().

[Leu+14] Leutenegger, S., Melzer, A., Alexis, K., and Siegwart, R. "Robust state estimation for small unmanned airplanes". In: *Control Applications (CCA), 2014 IEEE Conference on*. IEEE. 2014, pp. 1003–1010.

[LH13] Lin, C.-M. and Hsueh, C.-S. "Adaptive EKF-CMAC-based multisensor data fusion for maneuvering target". In: *IEEE Transactions on Instrumentation and Measurement* 62.7 (2013), pp. 2058–2066.

[Li+09] Li, K., Wang, Q., Zhang, Q., and Zhao, C. "Vision Autonomous Relative Navigation Algorithm for Distributed Micro/Nano Satellite Earth Observation System Based on Motor Algebra". In: *Environmental Science and Information Application Technology, 2009. ESIAT 2009. International Conference on*. Vol. 3. IEEE. 2009, pp. 470–473.

[Liu+07] Liu, H., Darabi, H., Banerjee, P., and Liu, J. "Survey of wireless indoor positioning techniques and systems". In: *IEEE Transactions on Systems, Man, and Cybernetics, Part C: Applications and Reviews* 37.6 (2007), pp. 1067–1080.

[Low11] Lowe, D. *Networking For Dummies*. John Wiley & Sons, 2011.

[Loz+08] Lozano, J. G. C., Carrillo, L. R. G., Dzul, A., and Lozano, R. "Spherical simplex sigma-point Kalman filters: a comparison in the inertial navigation of a terrestrial vehicle". In: *American Control Conference*. IEEE. 2008, pp. 3536–3541.

[LTC12] Laskar, M. N. U., Tawhid, M. N. A., and Chung, T. "Extended Kalman Filter (EKF) and K-means clustering approach for state space decomposition of autonomous mobile robots". In: *Electrical & Computer Engineering (ICECE), 2012 7th International Conference on*. IEEE. 2012, pp. 113–116.

[M+09] Meca, M., Galilea, L., Monzu, S., et al. "Error corrections in phase-shift measurement for robot infrared localization in intelligent spaces". In: *2009 IEEE International Workshop on Robotic and Sensors Environments*. 2009, pp. 92–97.

[Mac12] Macagnano, D. "Multitarget localization and tracking". PhD thesis. UNIVERSITY OF OULU GRADUATE SCHOOL, 2012.

[Mac14] Mackenzie, M. *M2M device connections and revenue: worldwide forecast 2014–2024*.
"`http://www.analysysmason.com/M2M-forecast-2014`". [Online; accessed 05-August-2015]. 2014.

[Mas06] Masiero, R. "RSSI Based Tracking Algorithms for Wireless Sensor Networks: Theoretical Aspects and Performance Evaluation". MA thesis. University of Padova, 2006.

[May82] Maybeck, P. S. *Stochastic models, estimation, and control*. Vol. 3. Academic press, 1982.

[McC+00] McCrady, D. D., Doyle, L., Forstrom, H., Dempsey, T., and Martorana, M. "Mobile ranging using low-accuracy clocks". In: *IEEE Transactions on Microwave Theory and Techniques* 48.6 (2000), pp. 951–958.

[McC96] McCallum, A. K. "Reinforcement learning with selective perception and hidden state". PhD thesis. University of Rochester, 1996.

[MCH02] Meek, C., Chickering, D. M., and Heckerman, D. "Autoregressive Tree Models for Time-Series Analysis." In: *SDM*. SIAM. 2002, pp. 229–244.

[MFA07] Mao, G., Fidan, B., and Anderson, B. D. "Wireless sensor network localization techniques". In: *Computer networks* 51.10 (2007), pp. 2529–2553.

[MH95] Murphy, W. and Hereman, W. "Determination of a position in three dimensions using trilateration and approximate distances". In: *Department of Mathematical and Computer Sciences, Colorado School of Mines, Golden, Colorado, MCS-95-07* 19 (1995).

[MH99] Murphy, W. and Hereman, W. "Determination of a position in three dimensions using trilateration and approximate distances". In: (1999).

[MKH06] Modsching, M., Kramer, R., and Hagen, K. ten. "Field trial on GPS Accuracy in a medium size city: The influence of built-up". In: *3rd Workshop on Positioning, Navigation and Communication 2006 (WPNC´06)*. 2006, pp. 209–218.

[MLM13] Machado, L., Larrat, M., and Monteiro, D. "Performance Evaluation of Lateration, KNN and Artificial Neural Networks Techniques Applied to Real Indoor Localization in WSN". In: *INNOV 2013, The Second International Conference on Communications, Computation, Networks and Technologies*. 2013, pp. 34–40.

[MLV10] Meng, L., Li, L., and Veres, S. "Aerodynamic parameter estimation of an unmanned aerial vehicle based on extended kalman filter and its higher order approach". In: *2010 2nd International Conference on Advanced Computer Control (ICACC)*. Vol. 5. IEEE. 2010, pp. 526–531.

[Mor14] Morin, D. J. *Problems and Solutions in Introductory Mechanics*. 2014.

[MR07] Masiero, R. and Rossi, M. "Rssi Based Tracking Algorithms For Wireless Sensor Networks: Theoretical Aspects And Performance Evaluation". In: *Corso di Laurea Specialistica in Ingegneria delle Telecomunicazioni AA* (2007).

[Mur02] Murphy, K. P. "Dynamic bayesian networks: representation, inference and learning". PhD thesis. University of California, Berkeley, 2002.

[NPR00] NøRgaard, M., Poulsen, N. K., and Ravn, O. "New developments in state estimation for nonlinear systems". In: *Automatica* 36.11 (2000), pp. 1627–1638.

[Ots+05] Otsason, V., Varshavsky, A., LaMarca, A., and De Lara, E. "Accurate GSM indoor localization". In: *UbiComp 2005: Ubiquitous Computing*. Springer, 2005, pp. 141–158.

[Pet08] Pettinari, M. "Context detection and abstraction in smart environments". In: (2008).

[PO08] Paul, T. and Ogunfunmi, T. "Wireless LAN comes of age: Understanding the IEEE 802.11 n amendment". In: *Circuits and Systems Magazine, IEEE* 8.1 (2008), pp. 28–54.

[Pro98] Proakis, J. G. *Digital Communications Fourth Edition, 2001*. 1998.

[PW08] Paul, A. S. and Wan, E. A. "Wi-Fi based indoor localization and tracking using sigma-point Kalman filtering methods". In: *IEEE/ION Position Location and Navigation Symposium Position, Location and Navigation Symposium*. IEEE. 2008, pp. 646–659.

[PW09] Paul, A. S. and Wan, E. A. "RSSI-based indoor localization and tracking using sigma-point kalman smoothers". In: *IEEE Journal of Selected Topics in Signal Processing* 3.5 (2009), pp. 860–873.

[RAG04] Ristic, B., Arulampalam, S., and Gordon, N. J. *Beyond the Kalman filter: Particle filters for tracking applications*. Artech house, 2004.

[Rap02] Rappaport, T. S. "Wireless communications: principles and practice". In: (2002).

[RH05] Rice, A. and Harle, R. "Evaluating lateration-based positioning algorithms for fine-grained tracking". In: *Proceedings of the 2005 joint workshop on Foundations of mobile computing*. ACM. 2005, pp. 54–61.

[Rhu+12] Rhudy, M., Gu, Y., Gross, J., and Napolitano, M. R. "Evaluation of matrix square root operations for UKF within a UAV GPS/INS sensor fusion application". In: *International Journal of Navigation and Observation* 2011 (2012).

[Rib04] Ribeiro, M. I. "Kalman and extended kalman filters: Concept, derivation and properties". In: *Institute for Systems and Robotics* 43 (2004).

[RST96] Ron, D., Singer, Y., and Tishby, N. "The power of amnesia: Learning probabilistic automata with variable memory length". In: *Machine learning* 25.2-3 (1996), pp. 117–149.

[Sim96] Simon, H. "Adaptive filter theory". In: (1996).

[Smi+13] Smith, A., Doucet, A., Freitas, N. de, and Gordon, N. *Sequential Monte Carlo methods in practice*. Springer Science & Business Media, 2013.

[Sor+15] Sorour, S., Lostanlen, Y., Valaee, S., and Majeed, K. "Joint indoor localization and radio map construction with limited deployment load". In: *IEEE Transactions on Mobile Computing* 14.5 (2015), pp. 1031–1043.

[Sta10] Stanway, M. J. "Delayed-state sigma point Kalman filters for underwater navigation". In: *IEEE/OES Autonomous Underwater Vehicles (AUV)*. IEEE. 2010, pp. 1–9.

[Sun+05] Sun, G., Chen, J., Guo, W., and Liu, K. "Signal processing techniques in network-aided positioning: a survey of state-of-the-art positioning designs". In: *IEEE Signal Processing Magazine* 22.4 (2005), pp. 12–23.

[Tao+15] Tao, S., Kudo, M., Pei, B.-N., Nonaka, H., and Toyama, J. "Multiperson Locating and Their Soft Tracking in a Binary Infrared Sensor Network". In: *IEEE Transactions on Human-Machine Systems* 45.5 (2015), pp. 550–561.

[TM10] Tilch, S. and Mautz, R. "Current investigations at the ETH Zurich in optical indoor positioning". In: *7th Workshop on Positioning Navigation and Communication 2010 (WPNC´10)*. IEEE. 2010, pp. 174–178.

[TM11] Tilch, S. and Mautz, R. "CLIPS proceedings." In: *IPIN*. 2011, pp. 1–6.

[V+04] Van Der Merwe, R., Wan, E. A., Julier, S., et al. "Sigma-point Kalman filters for nonlinear estimation and sensor-fusion: Applications to integrated navigation". In: *Proceedings of the AIAA Guidance, Navigation & Control Conference*. 2004, pp. 16–19.

[Van04] Van Der Merwe, R. "Sigma-point Kalman filters for probabilistic inference in dynamic state-space models". PhD thesis. Oregon Health & Science University, 2004.

[VF13] Vermesan, O. and Friess, P. *Internet of things: converging technologies for smart environments and integrated ecosystems*. River Publishers, 2013.

[Vij10] Vij, V. *Wireless Communication*. Laxmi Publications, Ltd., 2010.

[Waa+10a] Waadt, A. E., Kocks, C., Wang, S., Bruck, G. H., and Jung, P. "Maximum likelihood localization estimation based on received signal strength". In: *2010 3rd International Symposium on Applied Sciences in Biomedical and Communication Technologies (ISABEL)*. IEEE. 2010, pp. 1–5.

[Waa+10b] Waadt, A., Burnic, A., Xu, D., Kocks, C., Wang, S., and Jung, P. "Analysis of RSSI based positioning with multiband OFDM UWB". In: *Future Network and Mobile Summit, 2010*. IEEE. 2010, pp. 1–8.

[Wal12] Wall, M. *Touchdown! Huge NASA Rover Lands on Mars*. "`http://www.space.com/16932-mars-rover-curiosity-landing-success.html`". [Online; accessed 05-August-2015]. 2012.

[WB] Welch, G. and Bishop, G. "An Introduction to the Kalman Filter. 2006". In: *University of North Carolina: Chapel Hill, North Carolina, US* ().

[WHT10] Weir, M. D., Hass, J., and Thomas, G. B. "Thomas\'calculus". In: (2010).

[WLW09] Wymeersch, H., Lien, J., and Win, M. Z. "Cooperative localization in wireless networks". In: *Proceedings of the IEEE* 97.2 (2009), pp. 427–450.

[Yan+13] Yang, P., Wu, W., Moniri, M., and Chibelushi, C. C. "Efficient object localization using sparsely distributed passive RFID tags". In: *IEEE Transactions on Industrial Electronics* 60.12 (2013), pp. 5914–5924.

[ZJ14] Zhang, Y. and Ji, H. "Clustering Gaussian mixture reduction algorithm based on fuzzy adaptive resonance theory for extended target tracking". In: *Radar, Sonar Navigation, IET* 8.5 (June 2014), pp. 536–546.

Publications of the Author

[Kha+14] Khalil, L., Waadt, A., Bruck, G., and Jung, P. "Positioning framework for WLAN 802.11 n utilizing Kalman filter on received signal strength". In: *International Wireless Communications and Mobile Computing Conference (IWCMC)*. IEEE. 2014, pp. 1172–1176.

[KJ15a] Khalil, L. and Jung, P. "Scaled Unscented Kalman Filter for RSSI-Based Indoor Positioning and Tracking". In: *9th International Conference on Next Generation Mobile Applications, Services and Technologies (NGMAST)*. IEEE. 2015, pp. 132–137.

[KJ15b] Khalil, L. and Jung, P. "Spherical Simplex Unscented Kalman Filter for RSSI-Based Indoor Positioning and Tracking". In: *IEEE 26th International Symposium on Personal Indoor and Mobile Radio Communications (PIMRC)*. IEEE. 2015, pp. 2284–2288.